CONTROL AND DYNAMICS OF
INVERTER-FED INDUCTION MOTOR


Krishnan Ramu


A Thesis

in

/The Department

of

Electrical Engineering


Presented in Partial Fulfillment of the Requirements
for the degree of Doctor of Philosophy at
Concordia University
Montreal, Quebec, Canada

.March 1982

## ABSTRACT

## CONTROL AND DYNAMICS OF INVERTER-FED
## INDUCTION MOTOR

Krishnan Ramu, Ph.D.

Concordia University, 1982

Three predominant fast response strategies for the control of inverter-fed induction motor drive are:

(i)    Angle control scheme

(ii)   Synchronous control scheme

(iii)  Field-oriented control scheme

The unifying aspect of all the three schemes is identified. This is the simultaneous control of torque angle and magnitude of current phasor in the drive and is known as "frequency compensation".

It is proved that the response to a load torque disturbance or to a change in frequency is accompanied by a change in the speed of the magnetizing current phasor and hence the torque angle. The control of torque angle needs a knowledge of the characteristics of torque angle. It is proved that the incremental torque angle is a linear combination of drive electrical states only. The control consequence of torque angle feedback in a drive scheme is examined. It is shown that torque angle feedback alone

cannot stabilize a current source inverter-fed induction motor drive system. Feedback of torque angle and rotor speed has the effect of feeding all the system states in a scheme.

A generalized control concept of electric motor drives is developed to evaluate the different drive schemes from the control and the pole-zero assignment point of view. A comparison of the three drive schemes is given.

The role of drive inputs on the performance of an inverter-fed induction motor drive is investigated. The superiority of frequency input over voltage/current (magnitude) input is demonstrated. From the response of drive output signals, the suitability of some of them for feedback control purposes is evaluated. It is found that rotor speed is the best feedback signal for load torque disturbance and torque angle for frequency reference change.

An analysis and a step-by-step design of an angle controlled current source inverter-fed induction motor drive is presented. The design procedure is supported by the experimental results. The commutation delay in the current source inverter is modelled as a second order Padé transfer function. The effect of commutation delay on drive dynamics is evaluated.

## ACKNOWLEDGEMENTS

## TABLE OF CONTENTS

## LIST OF TABLES

# LIST OF FIGURES

## NOMENCLATURE

| | | |
|---|---|---|
| $A,B,C,D,K$ | - | Matrices |
| $a_p$ | - | Sum of the poles |
| C | - | Commutation capacitance per leg |
| $\underline{d}$ | - | Disturbance vector |
| f | - | Friction coefficient of the machine |
| $G_1(s)$ | - | Transfer function of the speed controller |
| $G_2(s)$ | - | Transfer function of the real component of stator current controller |
| $G_3(s)$ | - | Transfer function of link current controller |
| $G_5(s)$ | - | Transfer function of the slip speed controller |
| $G_D(s)$ | - | Transfer function of the current source inverter commutation delay |
| $G_{dc}(s)$ | - | Transfer function of the front-end controlled rectifier delay |
| $G_\ell(s)$ | - | Transfer function of the equivalent link filter and induction motor stator |
| $G_{d\ell}(s)$ | - | $G_\ell(s) \cdot G_{dc}(s)$ |
| $H_1(s)$ | - | Transfer function of the current feedback block |
| $i_a$ | - | Armature current of D.C. machine |
| $i_{as}, i_{bs}, i_{cs}$ | - | Stator phase currents |
| $I_d$ | - | D.C. link current |

$I_s$ — Steady-state stator current

$I_r$ — Steady-state real component of stator current

$I_m$ — Steady-state magnetizing component of stator current

$\underline{i}_s$ — Stator current space phasor

$\underline{i}_r$ — Rotor current space phasor

$\underline{i}_m$ — Magnetizing current space phasor

$i_{S1}$ — Component of stator current space phasor along stator reference axis

$i_{S2}$ — Component of stator current space phasor in quadrature to stator reference axis

$i_{SD}$ — Component of stator current space phasor along the field axis

$i_{SQ}$ — Component of stator current space phasor in quadrature to the field axis

$i_r$ — Rotor current magnitude in synchronously rotating reference frame

$i_{dr}$ — d-axis rotor current in synchronously rotating reference frame

$i_{qr}$ — q-axis rotor current in synchronously rotating reference frame

$J$ — Moment of inertia of the machine

$K_b$ — Back emf constant in d.c. machine

$K_t$ — Torque constant

| | | |
|---|---|---|
| $L_a$ | $-$ | Armature inductance of the D.C. machine |
| $L_F$ | $-$ | D.C. link filter inductance |
| $L_\ell$ | $-$ | Sum of the stator and rotor leakage inductances per phase |
| $L_{\ell r}$ | $-$ | Rotor leakage inductance per phase, referred to stator |
| $L_{\ell s}$ | $-$ | Stator leakage inductance per phase |
| $L_m$ | $-$ | Mutual inductance per phase |
| $L_r$ | $-$ | Rotor self-inductance per phase, referred to stator |
| $L_s$ | $-$ | Stator self-inductance per phase |
| n | $-$ | Pairs of poles |
| $R_F$ | $-$ | D.C. link filter resistance |
| $R_r$ | $-$ | Stator referred rotor resistance per phase |
| $R_s$ | $-$ | Stator resistance per phase |
| p | $-$ | Differential operator |
| s | $-$ | Slip, Laplace operator |
| $s_o$ | $-$ | Slip at an operating point |
| $s_s$ | $-$ | Slip speed |
| $T_e$ | $-$ | Electromagnetic torque |
| $T_L$ | $-$ | Load torque |
| $T_r$ | $-$ | Rotor time constant |
| $\underline{U}$ | $-$ | Input vector |
| $V_d$ | $-$ | Output voltage of the controlled rectifier |

$V_{ds}$ — Stator d-axis voltage in synchronously rotating reference frame

$V_{qs}$ — Stator q-axis voltage in synchronously rotating reference frame

$V_I$ — Inverter input voltage

$\omega_b$ — Base angular frequency

$\omega_e$ — Stator electrical angular frequency

$\omega_m$ — Rotor mechanical speed

$\omega_r$ — Rotor electrical speed

$\omega_{sl}$ — Angular slip frequency

$\underline{X}$ — State-vector

$X_{lr}$ — Rotor leakage reactance per phase, referred to stator

$X_{ls}$ — Stator leakage reactance per phase

$X_m$ — Mutual reactance per phase

$X_r$ — Rotor self-reactance per phase, referred to stator

$X_s$ — Stator self-reactance per phase

$y$ — Output variable

$\sigma_r$ — Rotor leakage coefficient

$\lambda$ — Eigenvalue

$\psi$ — Air-gap flux

$\theta$ — Torque angle

$\theta_1$ — $\tan^{-1}\left(\dfrac{|i_{dro}|}{|i_{qso}|}\right)$

$\phi$ — Power factor angle

$\phi_s$    -    Field angle referred to stator reference frame

$\epsilon$    -    Rotor angle referred to stator reference frame

$\epsilon_s$    -    Stator current space phasor angle referred to stator reference frame

$\delta$    -    Used with a variable to denote its incremental value

Subscript 'o'    -    Denotes the steady-state operating point value

Superscript 't'    -    Denotes the transpose of a vector, a matrix

# CHAPTER 1.

## INTRODUCTION

### 1.1 Introduction

Speed and torque control of electric machines are the basis of industrial automation, quality control in production, increase in productivity and of energy saving in the present times. With the advent of thyristors and consequently a wide range of electronic power converters, the control of electric machines is now achieved with high efficiency and good system response.

Separately excited D.C. motor drives have found wide industrial application for the following reasons:

(i)  The control task is made simple as the field and armature are independently controlled, leading to an all-purpose drive.

(ii) Mostly natural commutation can be used in the power converters thereby simplifying the power and control circuitry and providing a robust power conversion equipment.

To mention a few, they have the disadvantages of arcing at the commutator demanding frequent maintenance, larger rotor inertia causing a poor dynamic response, higher cost compared to the induction motor and problems of torque ripples at low speed operation.

The induction motor is inexpensive, robust, relatively light weight and capable of operation in hazardous environmental conditions.   Driven from a variable frequency source, a wide speed variation is possible.   The variable frequency is obtained either through direct conversion from the mains supply or through a D.C. power link.   The direct frequency changer involves a large number of thyristor devices, a limited output frequency variation from the standard mains and the advantageous natural commutation process.   The D.C. power link frequency converters provide a large frequency variation but rely on forced commutation.   The D.C. link frequency converters are broadly classified into voltage and current source types.   The Voltage Source Inverter-fed Induction Motor drive (hereafter referred to as VSIM drive) needs an additional controlled bridge converter for regeneration and is shown in Figure 1.1.   The Current Source Inverter-fed Induction Motor drive shown in Figure 1.2 (hereafter referred to as CSIM drive) has four quadrant operation with twelve thyristors, the same number required for a four quadrant D.C. motor drive.   The electromagnetic torque of the induction motor is directly controlled by the stator currents rather than the voltages and this fact has placed the CSIM in the forefront over the VSIM drive.   CSIM drives have the advantages of:

(i)     Inherent four quadrant operation without extra power switches.
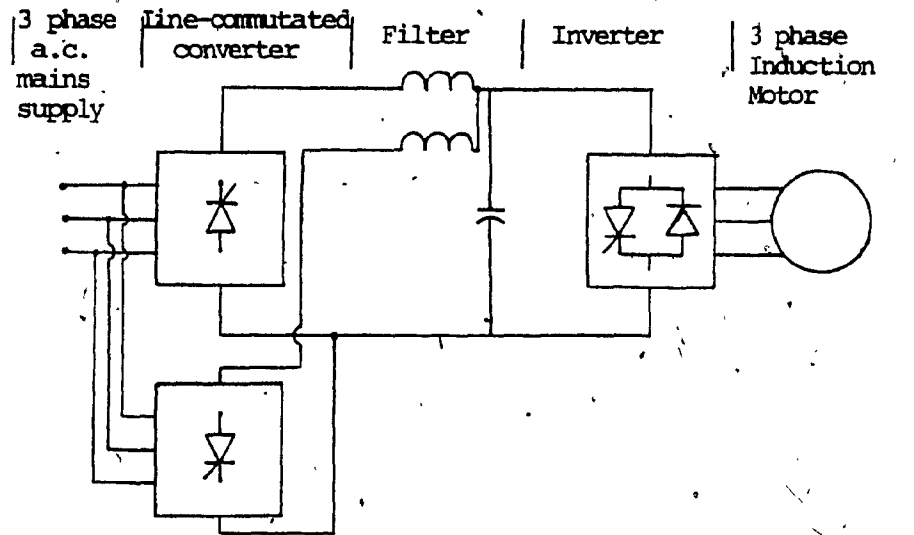
Figure 1.1    Voltage Source Inverter-fed Induction Motor
Drive
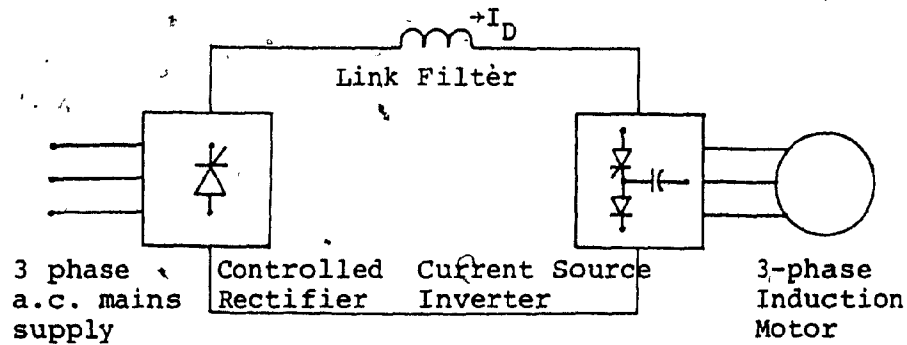


Figure 1.2    Current Source Inverter-fed Induction Motor
Drive

(ii)    Converter grade thyristors are used in the inverter part.

(iii)  Provides a high impedance to misfiring of inverter thyristors.

(iv)   Has a wide range of speed variation, meeting all-purpose drive requirements.

The CSIM drives are used extensively in fans, pumps, extruders, paper and pulp mills, machine tools etc.

## 1.2 Review of Previous Work

In this section the development of variable-speed drives using thyristor circuits is traced. The advantages of frequency control in induction motor drives over other control methods are discussed. The steady-state perfor-mance and dynamic control problems of these drives and the existing solutions to them are described.

## 1.2.1 Methods for speed control of induction motor

The following methods are used to obtain the speed control of induction motors:

(i)    Phase control

(ii)   Integral cycle control

(iii)  Rotor chopper control

(iv)   Slip-power recovery control

(v)    Variable frequency control

Brief descriptions of the above control methods are given in the following paragraphs.

Phase control: Applied voltage to the motor armature is varied by controlling the triggering angle of thyristors connected to the sinusoidal mains supply [1], [2]. The speed control range is very small. Efficiency of the drive is nearly equal to (1.0-slip) and therefore it is poor at low speeds.

Integral-cycle control: An integer number of cycles of the sinusoidal supply voltage is switched on and off to give an effective variation of applied voltage to the machine [3]. It has basically the same characteristics of phase controlled induction motors.

Rotor-chopper control: Rotor voltage is rectified and the rotor windings are shorted on and off using a chopper. Rotor current is varied and hence torque and speed control are obtained. The speed control range is much greater than the phase control and integral-cycle control methods but the efficiency remains poor [4]. A slip-ring induction motor is needed for this form of control.

Slip-power recovery control: The slip-power in the rotor is recovered and transferred back to the supply mains thereby increasing the efficiency of the drive. The speed control region in practice is limited from 0.5 p.u. to 1 p.u. The overall power factor is low [5], [6] when line commutated converters are used.

speed. The overall power factor is low [5], [6].

Variable frequency control: The interrelationship
between the stator supply frequency and the synchronous
speed of the induction motor indicates that frequency is a
strong candidate for speed control of that machine. Due
to the fact that rotor speed is always close to synchronous
speed of the machine the efficiency is high. Availability
of solid-state frequency converters with precise control
of frequency has made possible variable speed induction
motor drives with high efficiency and a wide speed range,
hitherto not obtained with the previous methods [7].

## 1.2.2   Development of variable frequency drives

D.C. link converters of voltage and current source
types are considered in this section. Though one of the
current source inverters was invented as early as 1934
[8], impulse commutated voltage source inverters and na-
turally commutated cycloconverters were favoured during
the first stages of variable frequency induction motor
drives development. Therefore various problems of VSIM
were investigated first and the problems of CSIM came
later to the attention of researchers.

## 1.2.3   Steady-state analysis

Steady-state analysis of the six-stepped voltage fed
variable frequency induction motor was attempted in a

state-space formulation of the machine equations with the
symmetry of currents as constraints to find the initial
steady-state vector [9], [10], [11], [12], [13]. The
direct evaluation of this vector spared the tedious compu-
tational effort of going through all the starting transients,
to find the steady-state of the machine. Switching func-
tion [14], with space-phasor representation of the machine
is one of the techniques to evaluate the steady-state
performance of inverter-fed machines [15], [16]. These
solutions are analytical and hence an insight into the
influence of machine parameters and other variables on
instantaneous electromagnetic torque and various losses is
obtained, whereas the state-variable methods do not provide
such insight though they are computationally elegant.
Classical harmonic equivalent circuits are also used to
find the steady-state of the inverter-fed induction motor
[17], [18]. This method has the advantage of identifying
the effects due to harmonics. To eliminate such effects
requires the suppression of the corresponding input
harmonic voltages. The only disadvantage of the harmonic
analysis method is that a significant number of harmonics
has to be considered for reasonable accuracy.

Introduction of current source inverter-fed drives
[19], [20], [21], [22], [23] posed the question of evalua-
tion of steady-state performance for application purposes.
State-space methods provided an elegant solution procedure

including current harmonics and avoided the problem of find-
ing the derivatives of stator current either by redefining
the states [24] or using the rotor flux linkages for states
[25]. The space-phasor approach yielded analytical closed
form solutions and for small slips, the solution is simple
[15]. Harmonic analysis [23] similar to the VSIM drives
provided results of comparable accuracy. Though use of
symmetrical componetns for steady-state evaluation of the
CSIM drive [26] is computationally tedious, the saturation
effect is taken into account.

### 1.2.4 Losses

Harmonic equivalent circuits are extensively used to
separate the various losses that occur in inverter-fed
induction machines [27], [28], [29] and the losses are
invariably greater in comparison to themachine with a
pure sinusoidal input. Reduction of losses lies in the
direction of reducing the harmonic content of the input
waveforms and hence the need for pulse-width modulated
inverters. CSIM drives are slightly better in efficiency
than VSIM drives [23], [30] up to the rated torque opera-
tion, but above this load the opposite is true. All
induction machines have to be derated for application
considerations to account for increased losses due to
non-sinusoidal excitation.

## 1.2.5 Inverter-motor interaction

The interaction of an induction motor with the D.C. link consisting of energy storage elements is modelled on the basis that no reactive power is supplied by the D.C. link. The reactive power is obtained by the switching of the inverter itself. A stator referred equivalent circuit for steady-state analysis [31] for fundamental component relationships is of use when the source impedance has to be taken into account in the analysis. In the steady-state, the D.C. link constrains the quality of input current and voltage waveforms and its resistance lowers the maximum torque significantly.

Dynamic study of the inverter-fed induction motor involves the machine model in a synchronously rotating reference frame and the D.C. link is incorporated in the above model considering only the fundamental component of voltages and currents [32]. From the power relationship, the stator current is written in terms of the link current in the VSIM and stator voltage is given in terms of the inverter input voltage in the CSIM drives. An analog computer study of inverter-fed induction motor drive [33], [34] does not involve any approximation in the input voltage/current waveform and the only disadvantage of this method is that it does not lend itself to analytical design.

The CSIM drive model has the D.C. link incorporated along the same basis [35] and its analog computer representation with [36] and without [37] approximations are available.

### 1.2.6 Pulsating torques

Introduction of fifth and seventh harmonic currents with fundamental flux produces resultant sixth harmonic pulsating torque. The other higher order pulsating torques can be neglected in comparison to the sixth harmonic pulsating torque. They have the undesirable effect of producing speed oscillations and hence low frequency operation becomes difficult [38], [39]. Their magnitudes are comparable to the fundamental electromagnetic torque and hence they are of real concern at low loads, particularly at no load. In VSIM drives, the torque pulsations are reduced by eliminating the fifth and seventh harmonic voltages by suitable pulse-width modulation of the input voltage. They can also be minimized by a modified design of induction motor [40].

CSIM drives have a similar sixth harmonic pulsating torque [41]. Elimination of it is achieved by one of the following methods:

    (i)    Programming the D.C. link current in response to the operating point [42], [43].

    (ii)    Current pulse-width modulation [43], [44], [45].

(iii)   Employment of twelve-step waveforms and twenty four-stepped waveforms [46], [47].

(iv)    Feedback control through an electromagnetic torque loop [48].

(v)     Modifying machine parameters such as magnetizing inductance and rotor resistance [41], [49].

## 1.2.7 Stability

VSIM drives have exhibited instability on open loop in the 10 to 50 percent of base speed region and in the 0 to 60 percent of rated torque operation [50]. Machine constants and filter parameters influence the region of instability. CSIM drives are normally unstable on open loop [51], [52]. The methods used to stabilize the inverter-fed drives can be broadly classified into the following categories:

(i)    Design of feedback control loops.

(ii)   Machine modification.

Stabilitization using feedback loops [52], [53] has the advantage of utilizing the standard available machine since the loops incorporated are external to the machine and are easy to implement. Also they do not deteriorate the steady-state charactertics.

Machine modification has proceeded on the lines of:

(i)    Change in machine constants

(ii)   Altogether new machine design

While the change in machine constants calls for change in steady-state characteristics, the new machine may not have this disadvantage and it provides leading reactive power for commutation of the thyristors. But feedback loops are still required. Details are given in Reference [54].

## 1.3 Scope of the Thesis

High performance and fast response drive strategies such as the angle control scheme [58], synchronous control scheme [59] and field-oriented control scheme [60] contributed to the development and widespread use of inverter-fed induction motor drives. In the literature, these schemes are posed as independent of each other. Each scheme is analysed in its isolation but there is no method to make a relative comparison of the drive schemes. The crucial role of the torque angle in the control of drive dynamics has not been investigated. The present thesis is concerned with the control and dynamics of inverter-fed induction motor drives and in particular that of the CSIM drives. The following aspects of them are studied:

(i)     Unification of the three existing high performance drive control strategies.

(ii)    The generalized control concept of inverter-fed induction motor drives.

(iii)   A comparison of the drive schemes.

(iv)  Torque angle characteristics and their role in drive dynamics.

(v)   Assessment of the role of drive inputs and relative suitability of the possible feedback signals.

(vi)  Modelling of the current source inverter commutation delay.

(vii) Analysis and design of the angle controlled CSIM drive.

## CHAPTER 2

## FAST RESPONSE DRIVE STRATEGIES AND THEIR BASIS

### 2.1 Introduction

The development of variable frequency induction motor drives are associated with three strategies at first:

(i)    Constant slip control [55].

(ii)    Constant volts per Hertz control [56],

(iii)    Constant air-gap flux control [57].

They have differences not only in steady-state operation but also their dynamic performance is entirely different from each other [57]. The precise dynamic control of electromagnetic torque, speed and flux over most of the speed range is not satisfactory in that they are oscillatory [58]. The constant power operation or flux weakening mode is difficult to stabilize with front-end controlled rectifier fully phased on [59]. Three prominent control schemes emerged to overcome the above problems and they are:

(i)    Angle control scheme [58].

(ii)    Synchronous control scheme [59].

(iii)    Field-oriented control scheme [60].

Though the first two schemes are for the CSIM drives, it will be subsequently seen that they are also applicable to the VSIM drives.

Brief descriptions of these control schemes as applied to the CSIM drives and their salient features are given in this chapter. From the discussion emerges the basic underlying factor of all these schemes. The schemes are taken up in the order of their complexity, from the simplest to the most complex.

## 2.2 Angle Control Scheme

Figure 2.1 shows the block diagram of the CSIM drive with its power circuit. The front-end rectifier is fully controllable and capable of handling reversed power flow. The link filter with a fast acting current loop constitutes the current source. The current in the link is varied by changing the current reference not shown in the figure. The inverter is an auto-sequential commutated inverter delivering three phase currents to the stator of the induction motor. The frequency of the output currents is one sixth of the switching frequency of the inverter. This basic power circuit is considered throughout this study.

Fig. 2.2 shows the angle control scheme and Appendix-V lists the transfer function of the controllers. The drive has five loops, namely, unity speed feedback loop, slip speed loop, angle loop, inner current loop and an outer speed loop. The unity gain speed feedback loop consits of the inverter, motor, $G_{12}$, $G_{11}$, $G_{10}$, $G_7$, $G_n$ and is to basically run the
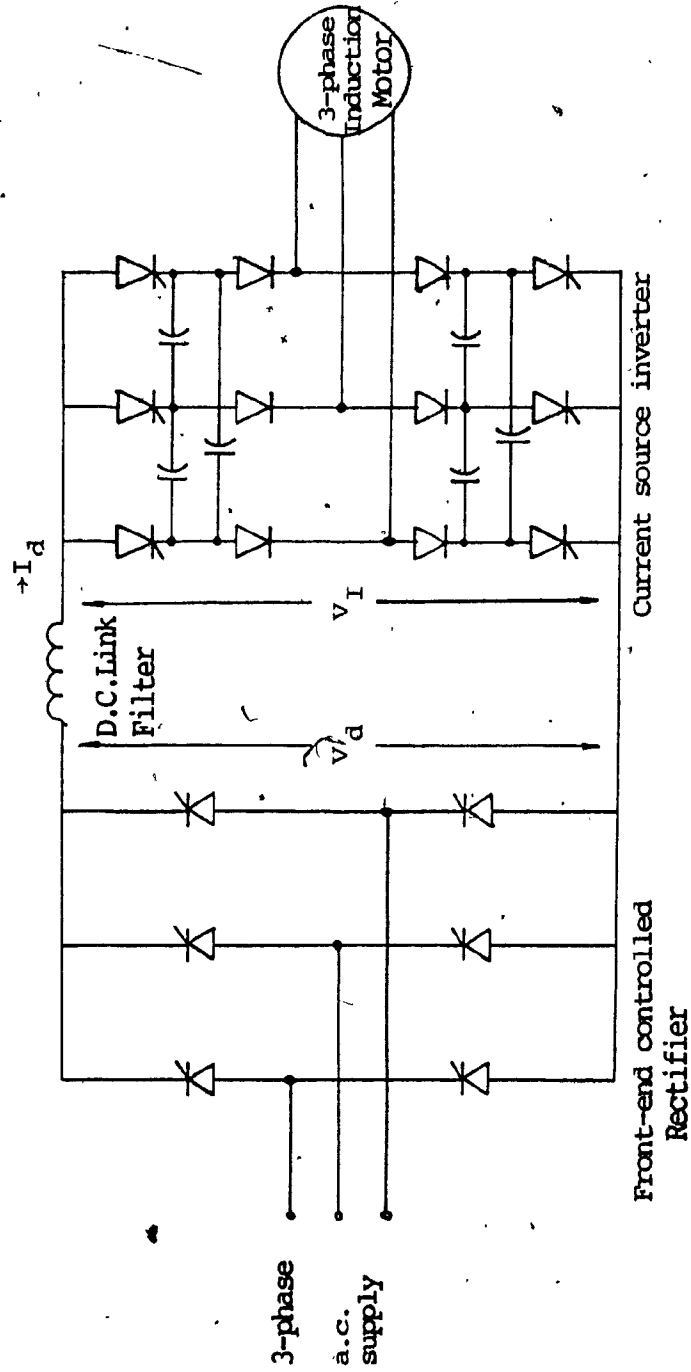
Figure 2.1. Current Source Induction Motor Drive
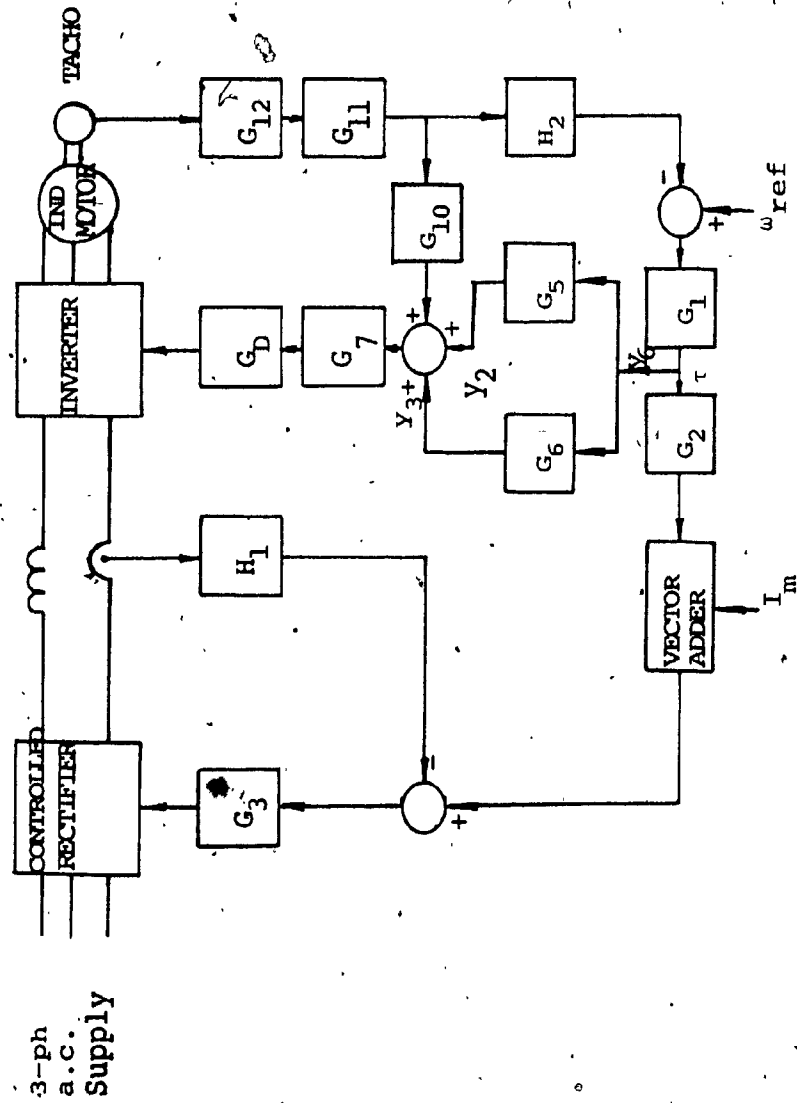
Figure 2.2   Block Diagram of Angle Controlled CSIM Drive

the inverter to give an output frequency corresponding to the speed of the rotor. $G_D$ is the block represen- ting the commutation delay in the current-source inverter. The path via $H_2$, $G_1$, and $G_5$ gives the slip speed sig- nal corresponding to the load whereas the loop consisting of $H_2$, $G_1$, and $G_6$ is to provide angle control during the load torque disturbance and reference frequency change. The point $y_6$ decides the torque reference and the gain block $G_2$ is used to obtain the rotor current reference. The phasor sum of rotor current reference and the excita- tion current forms the stator current reference. The inner current loop is made up of $G_3$, controlled rectifier, link filter, current feedback gain $H_1$. This loop is to regulate the link current in a fast manner. The outer speed loop consists of controlled rectifier, link, inver- ter, $G_{12}$, $G_{11}$, $H_2$, $G_1$ and $G_2$.

For better utilization of the drive, it is necessary to get maximum torque per ampere. The electromagnetic torque is determined by the slip and the magnitude of the rotor current. Therefore the slip signal block $G_5$ and the rotor current reference gain block $G_2$ are to be co- ordinated to achieve the objective of maximum torque per ampere. The angle controller decides the torque angle input for corresponding load torque. The load torque is indicated by the torque reference. There is a definite relationship between torque and torque angle and between slip and torque. From this a relationship can be found

between torque reference and torque angle. This torque
angle has to be fed to the inverter in the form of frequency.
The rate of change of load is proportional to rate of
change of torque angle and this is the frequency compensa-
tion to be applied to the induction motor during a load
torque disturbance. The incremental frequency obtained is
added to the slip frequency and rotational frequency to
make up the stator frequency. The gain of the angle con-
troller block $G_6$ has to be non-linear because the rela-
tionship between torque reference and torque angle is
non-linear and also due to the fact that the commutation
time in the inverter is both load and frequency dependent.
The design of the drive is treated later in detail.

## 2.3  Synchronous Control Scheme

The synchronous control scheme for its implementation
counts on the actual or calculated values of electromagne-
tic torque and torque angle. The relationship between
electromagnetic torque and slip frequency can be correlated
to the relationship between torque angle and slip frequency,
and hence slip frequency can be obtained either through
electromagnetic torque or torque angle. The scheme is
mainly concerned with maintaining synchronism between motor
flux and stator currents or in other words maintaining
the synchronous speed of the flux phasor in the face of
load disturbances.

The scheme is shown in Figure 2.3. The torque reference may be generated either through the slip speed signal or in a torque regulated drive it could be an external reference. It is assumed (but not shown in the Figure 2.3) that the drive has a current loop, flux loop and an outer speed loop interfacing the torque reference and current loop. Requested and actual values of torque set the demanded value of the sine of the torque angle. This is compared with the actual value of the sine of the torque angle to generate the needed slip frequency which in turn is added to the rotor mechanical speed to obtain the stator current frequency. Because of the comparison with measured values and the calculated values of the torque and torque angle, the scheme takes into account the effects of machine nonlinearities and parameter sensitivity of the machine. The speed of response of the torque angle loop is fast due to the absence of time constants in its path. The commutation delay is countered by the fast acting angle loop. An important feature of the scheme is that the angle is independent of rotor speed and hence operation at and near zero speed becomes possible.

It is found that the torque angle calculated from stator current and air-gap flux is double-valued with reference to slip frequency. To avoid this situation, a modified torque angle between rotor flux and stator current is utilized for feedback in the angle loop. The
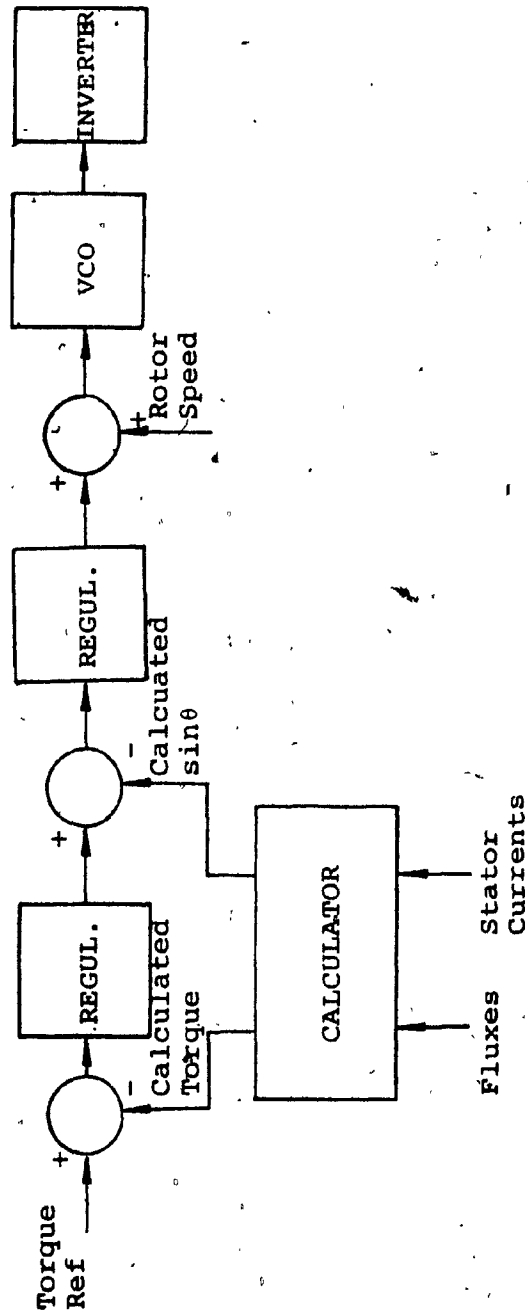
Figure 2.3 Synchronous Control Scheme

calculation circuit for electromagnetic torque and torque angle is given in [59].

A robust drive mostly based on synchronous control but with the additional feature of regulation of power factor is described in [44]. A variable flux program with the torque angle kept at its optimum above a certain load is implemented to obtain the high performance drive. Except at low speeds, keeping the torque angle constant amounts to having a constant power factor. The drive is an all-purpose one as it has a torque loop, current and voltage loops, angle loop, unity gain speed loop, an outer speed loop and an inner preprogrammed flux loop both to act upon the torque loop as well as on the angle loop.

## 2.4 Field-Oriented Control Scheme

A current space phasor is defined as

$$\underline{i}_s(t) = i_{as}(t) + i_{bs}(t) e^{j2\pi/3} + i_{cs}(t) e^{-j2\pi/3} \qquad (2.1)$$

and for sinusoidal three phase quantities, it becomes

$$\underline{i}_s(t) = i_s e^{j\epsilon_s(t)} \qquad (2.2)$$

and

$$\omega_e(t) = \frac{d}{dt} [\epsilon_s(t)] \qquad (2.3)$$

= electrical angular frequency of the supply currents

The machine equations in stator reference frame are:

$$R_s \underline{i}_s + L_s \frac{d}{dt}(\underline{i}_s) + L_m \frac{d}{dt}(\underline{i}_r e^{j\epsilon}) = \underline{u}_s \qquad (2.4)$$

$$R_r \underline{i}_r + L_r \frac{d}{dt}(\underline{i}_r) + L_m \frac{d}{dt}(\underline{i}_s e^{-j\epsilon}) = 0 \qquad (2.5)$$

In the case of CSIM drives, the stator currents are the inputs and they can be changed in short time by proper design of controllers in the inner current control loop. The potentially large time constant introduced by the filter inductor could be countered in the manner of pole cancellation by the addition of a zero in the controller of the inner loop. Hence the real attention could be focussed on the rotor equation. Defining,

$$\underline{i}_m(t) = i_m e^{j\phi_s} = \underline{i}_s + (1+\sigma_r)\underline{i}_r e^{j\epsilon} \qquad (2.6)$$

where

$$L_r = L_m(1+\sigma_r) \qquad (2.7)$$

Substituting equation (2.6) in (2.5) and separating out the real and imaginary equations of it into two equations, the following are obtained:

$$\underline{i}_s(t)\cos(\epsilon_s - \phi_s) = i_{SD} = T_r \frac{d}{dt} i_m + i_m \qquad (2.8)$$

$$i_s(t)\sin(\epsilon_s - \phi_s) = i_{SQ} = (\frac{d\phi_s}{dt} - \omega_m)i_m T_r \qquad (2.9)$$

and

$$T_r = \frac{L_r}{R_r}$$

$\omega_m$ = Rotor mechanical speed in rad/sec.

Electromagnetic torque,

$$T_e = \frac{2}{3} \cdot \frac{L_m}{(1+\sigma_r)} i_m i_{SQ} \qquad (2.10)$$

The phasor diagram illustrating the current components on the field axis is shown in Figure 2.4. Equation 2.8 reveals that the flux producing component of stator space current phasor, $i_{SD}$, has a time constant equal to that of the rotor and is greater than 0.5 second for machine larger than 15 h.p. The torque producing component $i_{SQ}$ is changed in little time and in CSIM drives, the commutation time decides the speed of change of $i_{SQ}$. From the above, it is appropriate to change the quadrature axis component of stator current phasor to vary the torque and hence control the drives in much faster manner. Once the two currents and their separate effects are understood and identified, then the control task is made simple. The best drive strategy follows in that the key variables $i_{SQ}$, $i_{SD}$, air-gap flux, angles $\phi_s$ and $\epsilon'_s$ are measured and compared with their demanded values. In case of
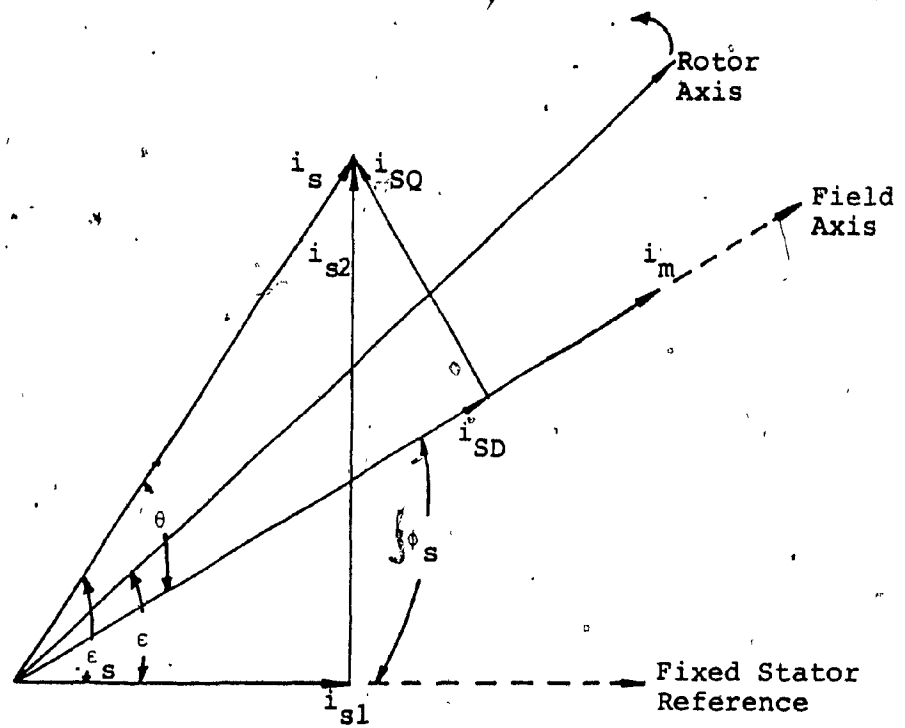
Figure 2.4   Resolution of Currents Along Field Axis

error, that particular variable which is having the error is actuated to nullify the error. This provides a desirable  non-interactive control in a highly coupled machine. The above strategy forms the basis of field-oriented control, a name derived from the fact that the control is exercised on the compoents of stator current phasor resolved along the field axis [60], [61], [62], [63].

Since the flux (i.e. field) and the torque producing components are separately controlled they resemble that of the field and armature controlled D.C. machine. It is interesting to observe that the salient differences in time constants of the field and armature control loops are carried on to the induction machine from the D.C. machine.

Above some critical load, instability can occur with this scheme. This can be overcome if rotor flux is used instead of air-gap flux for orientation of stator current components and accordingly the proper angles are taken into account [64].

The block diagram of the CSIM drive with this control strategy is shown in Figure 2.5. It could be seen that there need be no tachometer feedback for torque regulated drives. Also it is possible to reconstruct the flux and its angle signals from the instantaneous phase currents and induced voltages of the machine. But such a scheme involves the motor parameters and in case of changing
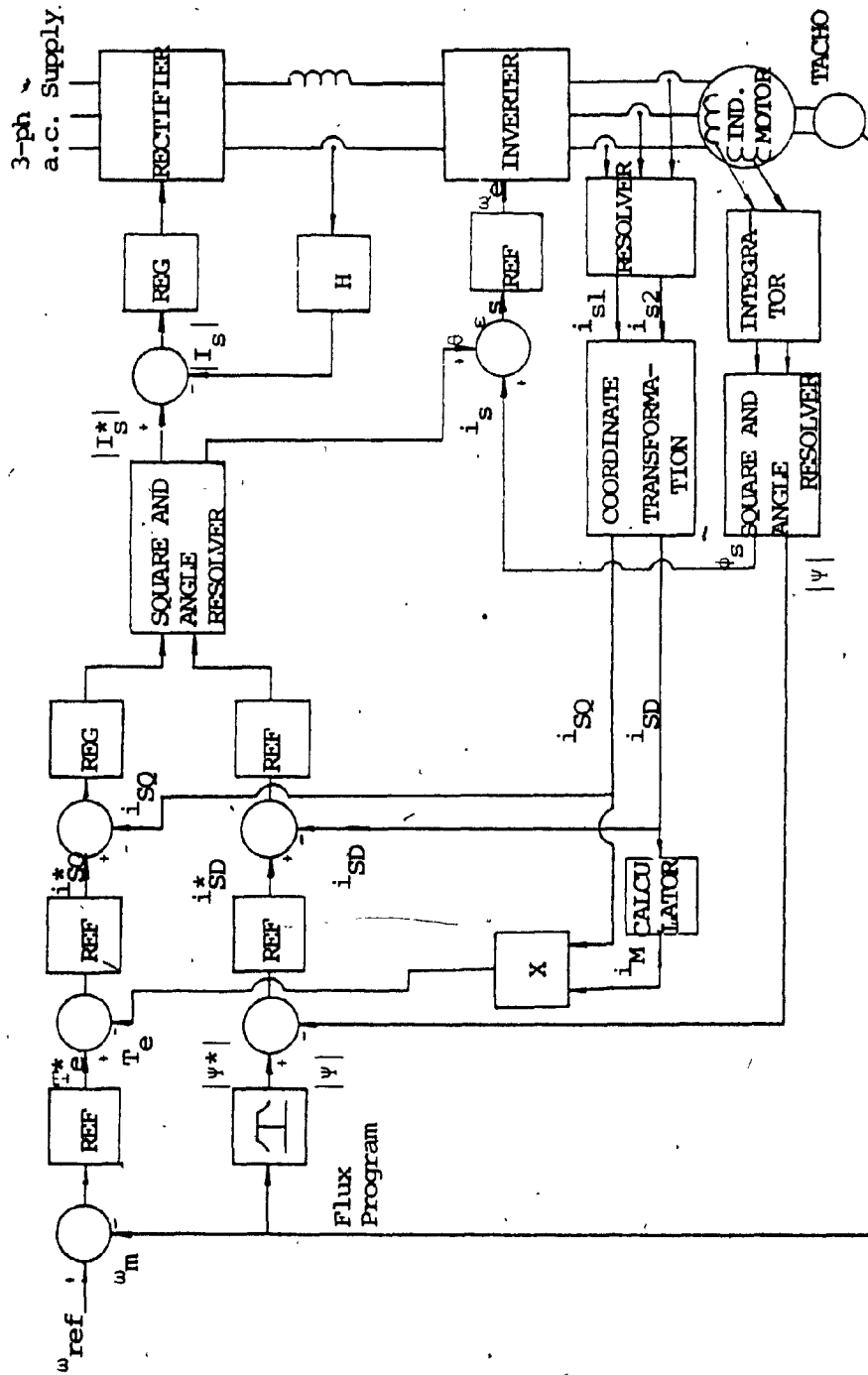
Figure 2.5  Field Oriented CSIM Drive

operating conditions proper care has to be exercised to
compensate for the variation of parameters. A scheme with
a solution to this problem is described in detail in [65],
[66]. The implementation of field-oriented control in CSIM
drives requires current feedback, air-gap flux, rotor
speed and a processor to find the angles $\phi_s$ and $\varepsilon_s$.
This information is used to create $i_{SQ}$, $i_{SD}$ through co-
ordinate transformation. Current $i_{SQ}$ is superimposed
upon the speed and torque error signal whereas the cur-
rent $i_{SD}$ is compared with the demanded field current for
the running speed. At the end point for construction of
current reference signal, no co-ordinate transformation is
necessary for obvious reason. Hence the implementation of
this strategy needs less complexity on CSIM drives than
on VSIM drives. At the same time, the tremendous task of
extracting the fundamental signals from the current sig-
nals and the induced emf signals, and also the removal
of slot harmonics from the flux deserve attention.

The strategy discussed above is based on the calcula-
tion of current components and angles with respect to the
stator reference frame. Instead, the same strategy can be
implemented with reference frames chosen on the synchro-
nously rotating reference frame [67] or in the rotor rota-
ting reference frame [68]. The major advantage of these
reference frames is that the bandwidth of the calculating
circuit can be kept constant since the signals processed
are not greater in frequency than the slip frequency, in

contrast to the stator reference frame calculator.

## 2.5  Basic Principles of the Control Schemes

All the three schemes described above have in common
the following:

(i)     Current Regulating loop which maintains
        essentially constant magnitude of the air-gap
        flux.

(ii)    Speed feedback loop determining the shaft
        speed by setting the inverter output frequency.

(iii)   Frequency compensation loop controlling the
        position of the air-gap mmf vector by tran-
        siently adjusting the inverter output frequency
        during the motor transients.

Features (i) and (ii) are commonly found in any CSIM drive
system.  The only distinguishing aspect of all the schemes,
then, lies in the frequency compensation loop.  In the
following paragraphs, the need for transient correction
of stator frequency during load and reference speed changes
is explained using a steady-state equivalent circuit of
the induction motor [69].  For the purpose of simplicity,
the following assumptions are made:

(i)     The stator impedance is neglected.  Thus the
        terminal voltage becomes equal to the air-gap
        voltage.

(ii)     Core losses are neglected.

(iii)    Magnetic hysteresis and eddy currents are neglected
         so that air-gap flux is in phase with the motor magne-
         tizing current and the frequency of the magne-
         tizing current defines the synchronous speed.

(iv)     Magnetizing current is constant during the
         load disturbance.  This presumes that the time
         constant of the magnetizing branch is suf-
         ficiently greater than the time constant of the
         current controller.

. (v)    Commutation delay is neglected.  Therefore, the
         motor input frequency can be changed instan-
         taneously.

The simplified equivalent circuit of the induction motor
is shown in Figure 2.6.  Let the induction motor operate
at synchronous speed.  The corresponding phasor diagram
is shown in Figure 2.7.  Presently, the power factor is
zero.  With a step increase in the load and no change in
motor input frequency the motor operation is represented
by Figure 2.8.  The following may be observed:

(i)      The slip speed increases thereby building up
         the rotor current.  Since the stator is
         supplied from a current source, the stator
         current remains constant.  Hence the magnetiz-
         ing current phasor is forced to part from its
         original position.
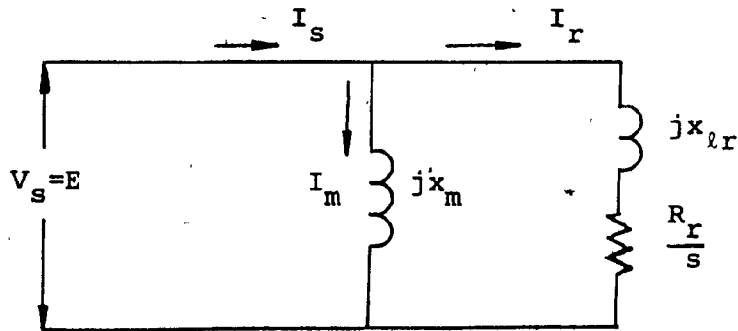
Figure 2.6   Simplified Equivalent Circuit
of Induction Motor
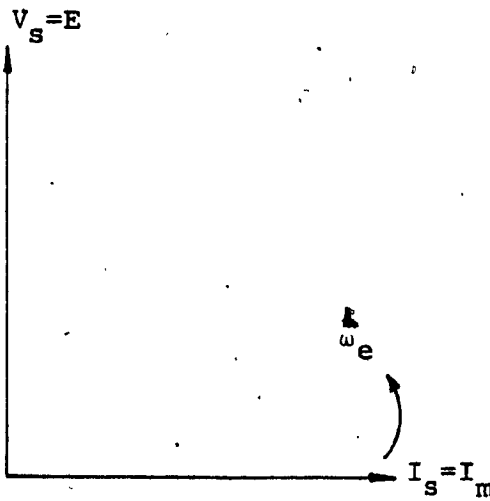


Figure 2.7   Motor at Synchronous Speed
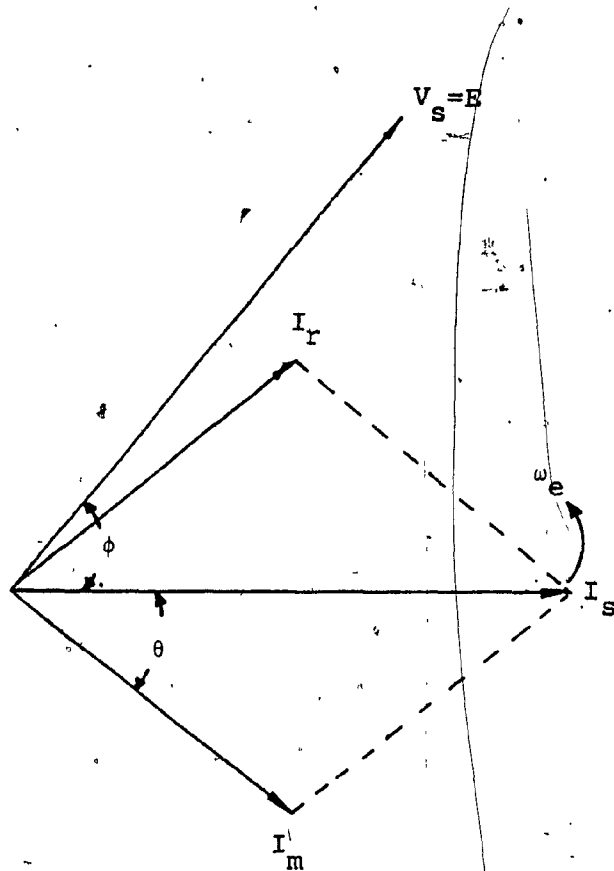
Figure 2.8  Motor After a Step Load

(ii) Magnetizing current phasor slows down decreasing the synchronous speed. The induced emf follows the magnetizing current phasor and the phase angle between stator current phasor and induced emf decreases. The power factor increases and more power is flowing into the stator.

(iii) Rotor current slowly builds up due to the increasing slip speed, even though there is reduction in induced emf due to the decrease in synchronous speed of air-gap mmf.

The cycle of events with the initiation of frequency compensation is outlined now. The inverter output frequency is transiently increased in order to keep the speed of the magnetizing current phasor constant. This involves the following:

(i) The phasor of the stator current is transiently speeded-up in order to assume a new position defined by the motor input power factor.

(ii) As the motor air-gap flux is maintained at the rated value, to meet the load, then, the stator current magnitude has to be increased to provide the necessary rotor current.

(iii) The induced emf remains constant. The rotor current and input power factor increase as the slip increases. The electromagnetic torque increases approximately in proportion to the

slip speed.

Hence, as a result of effective frequency compensation, the motor torque increases in step with the load without any oscillation giving a fast response stable drive. The frequency compensation to be applied is

$$\delta\omega_e = \frac{\delta\theta}{\delta t} \qquad (2.11)$$

where $\theta$ is the torque angle.

Alternately, from the equivalent circuit of Figure 2.6, and making a further assumption of neglecting rotor leakage inductance, the rotor current is given:

$$I_r = \frac{I_s}{(1 - j\frac{R_r}{sX_m})} \qquad (2.12)$$

$$|I_r| = \frac{|I_s|}{\sqrt{1 + (\frac{R_r}{L_m})^2 \cdot \frac{1}{s^2\omega_e^2}}} \qquad (2.13)$$

On applying a step load, rotor current increases due to increasing slip, s. Along with that if the frequency is changed, then the increase in rotor current is fast giving an enhanced electromagnetic torque. A change in inverter output frequency amounts to a change in the distribution of current in the magnetizing and rotor branches and in favour of meeting load transients. The

magnitude of stator current has to be simultaneously taken
care of to keep the air-gap flux constant through the cur-
rent channel.  The flux producing component of stator cur-
rent will undoubtedly decrease if the stator current mag-
nitude is held constant and the inverter output frequency
is increased.  Further details are taken up in Chapter 6.

CHAPTER 3

CONTROL CONSEQUENCES OF TORQUE ANGLE FEEDBACK


3.1 Introduction

Torque angle is defined as the angle between the stator current phasor and the magnetizing current phasor, where the magnetizing current phasor is the resultant of the stator and rotor current phasors. All the fast response drive strategies have within them a torque angle loop is shown in Chapter 2. Understanding the effects of the torque angle loop, through a steady-state equivalent circuit is qualitative, and for precise utilisation it needs to be put on solid quantitative grounds. The section is concerned with the evaluation of torque angle as a function of other machine variables and the assessment of its impact on the control configuration of the drive [69], [70]. Together with the speed loop, the torque angle control loop provides a complete state feedback of all machine states in the machine rotor equations. This aspect, in line with the development of other D.C. and A.C. motor drives, provides a generalized control concept of the electric motor drives. The development of the generalized control concept is helpful in the evaluation of a control scheme and its scope in relation to any other standard scheme, and leads to the realization of the optimal control of the drives.

## 3.2   Relationship of Torque Angle to Machine Variables

In order to appreciate the effect of torque angle, it
is necessary to find the constituents of the torque angle
itself.  The information is to be applied to evaluate its
impact on small-signal stability of the CSIM drive.  Hence
the machine's small-signal equations are made use of to
derive the relationship between the torque angle and other
machine variables.  The following assumptions are made in
the machine model:

(i)     Distributed windings so as to produce sinusoi-
dal mmf in stator and rotor.

(ii)    Saturation and core-looses are neglected.

(iii)   Temperature and frequency effects on machine
constants are neglected, though they can be
incorporated in the developed model when it is
necessary.

The reference frames are synchronously rotating and the
equations are given in Appendix-I [71].  The derivation
of the incremental torque angle, $\delta\theta$ , in terms of the
machine variables is given below:

A subscript ending with an 'o' denotes the steady-
state value of a variable.  The fundamental of the input
currents are only considered and alignment is so made that
the d-axis stator current is zero.  The stator and rotor
variables are denoted by the additional subscripts 's'

and 'r' along with the subscripts 'q' and 'd' for the quad-
rature and direct axes, respectively.   The phasor diagram
of the induction motor is shown in Figure 3.1  $i_{mo}$  is the
magnetizing current phasor and  $\theta$  is the torque angle.
From Figure 3.1, the following are obtained:

$$i_{ro} = \sqrt{i_{qro}^2 + i_{dro}^2} \tag{3.1}$$

$$\tan\theta_1 = \frac{|i_{dro}|}{|i_{qro}|} \tag{3.2}$$

$$\tan\theta = \frac{i_{ro}\sin\theta_1}{i_{qso} - i_{ro}\cos\theta_1} \tag{3.3}$$

Perturbing all the variables, equation (3.3) becomes

$$\tan(\theta+\delta\theta) = \frac{(i_{ro}+\delta i_r)\,\sin(\theta_1+\delta\theta_1)}{(i_{qso}+\delta i_{qs}) - (i_{ro}+\delta i_r)\cos(\theta_1+\delta\theta_1)} \tag{3.4}$$

Expanding equation (3.4) and neglecting second-order terms,
results in an equation with small-signal variables in the
form of:

$$\delta\theta = [a]\delta i_{qs} + [b]\delta i_r + [c]\delta\theta_1 \tag{3.5}$$

where
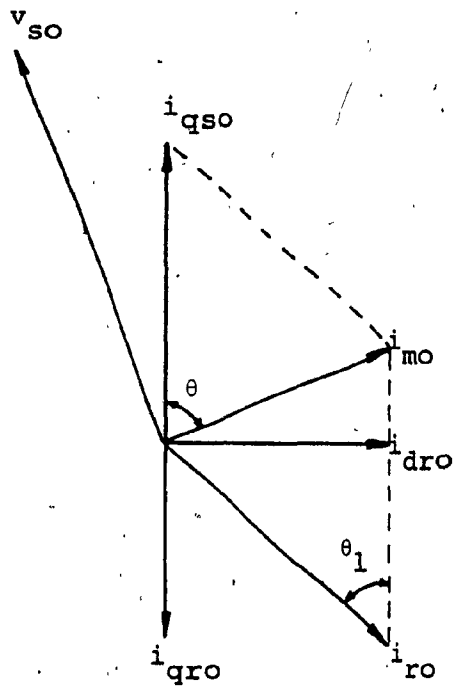
Figure 3.1 Phasor Diagram of
CSIM Drive

$$a = \frac{-\tan\theta}{h}$$

$$b = \frac{(\sin\theta_1 + \cos\theta_1 \tan\theta)}{h}$$

(3.6)

$$c = \frac{(i_{ro}\cos\theta_1 - i_{ro}\sin\theta_1 \tan\theta)}{h}$$

$$h = i_{qso} - i_{ro}\cos\theta_1 + i_{ro}\sin\theta_1 \tan\theta$$

$\delta\theta_1$ in equation (3.5) can be written in terms of other machine states and is accomplished in the following steps:

$$i_{dro} + \delta i_{dr} = (i_{ro} + \delta i_r)\sin(\theta_1 + \delta\theta_1)$$

(3.7)

$$i_{qro} + \delta i_{qr} = -(i_{ro} + \delta i_r)\cos(\theta_1 + \delta\theta_1)$$

from which

$$\delta i_{dr} = [i_{ro}\cos\theta_1]\delta\theta_1 + [\sin\theta_1]\delta i_r$$

(3.8)

$$\delta i_{qr} = [i_{ro}\sin\theta_1]\delta\theta_1 - [\cos\theta_1]\delta i_r$$

(3.9)

Combining equations (3.8) and (3.9), it is seen that

$$\delta\theta_1 = \frac{1}{i_{ro}}[\cos\theta_1 \delta i_{dr} + \sin\theta_1 \delta i_{qr}]$$

(3.10)

On substitution of equation (3.10) in (3.5), the expression
for $\delta\theta$ is obtained as

$$\delta\theta = [a]\delta i_{qs} + [b_1]\delta i_{qr} + [c_1]\delta i_{dr} \qquad (3.11)$$

where

$$b_1 = [-b\cos\theta_1 + \frac{c}{i_{r0}} \sin\theta_1] = a \qquad (3.12)$$

$$c_1 = [b\sin\theta_1 + \frac{c}{i_{ro}} \cos\theta_1] = \frac{-a}{\tan\theta} \qquad (3.13)$$

In a similar manner, the incremental torque angle
of a VSIM drive can be obtained. Even in this case, the
incremental torque angle is a function of only the electri-
cal states, i.e., the stator and rotor currents along the
quadrature and direct axes.

It is important to note that the incremental torque
angle is dependent only on electrical states and not on the
mechanical rotor speed. The use of torque angle for
electromagnetic torque control is attractive in the sense
that the generation of electromagnetic torque can be freed
from the dependence on the slip speed signal generated from
a reference and the rotor speed. At very low speeds, the
slip signal that is generated by the above means would be
inaccurate and hence the dynamic control of drives around
such speeds is very difficult. Regulating torque angle
and in turn electromagnetic torque would precisely control
the dynamic response of the drive.

### 3.3 Control Consequences of Torque Angle Feedback

The CSIM drive equations on open loop can be arranged in state-space form of:

$$\dot{\underline{X}} = A \underline{X} + B \underline{U} + \underline{d} \tag{3.14}$$

$$\underline{y} = C \underline{X} + D \underline{U} \tag{3.15}$$

where A,B,C,D are 4x4, 4x2, 1x4, 1x2 matrices, respectively, and $\underline{d}$ is the disturbance vector.

$$X = [\delta i_{qs} \ \delta i_{qr} \ \delta i_{dr} \ \delta \omega_m]^t \tag{3.16}$$

$$U = [\delta V_d \ \delta \omega_e]^t \tag{3.17}$$

$$d = [0 \ 0 \ 0 \ \delta T_L]^t \tag{3.18}$$

The matrices A and B are given in Appendix-II. Depending upon the required output, matrices C and D can be derived.

The two independent inputs of the drive, the controlled rectifier voltage, $\delta V_d$, and inverter frequency $\delta \omega_e$ are normally decided by the feedback controllers. For illustration, a simple drive configuration shown in Figure 3.2 is considered. The slip speed determines the link voltage and the sum of angle error and the reference speed determines the stator frequency of the drive. The dynamic small-signal equations of the drive inputs are given below:
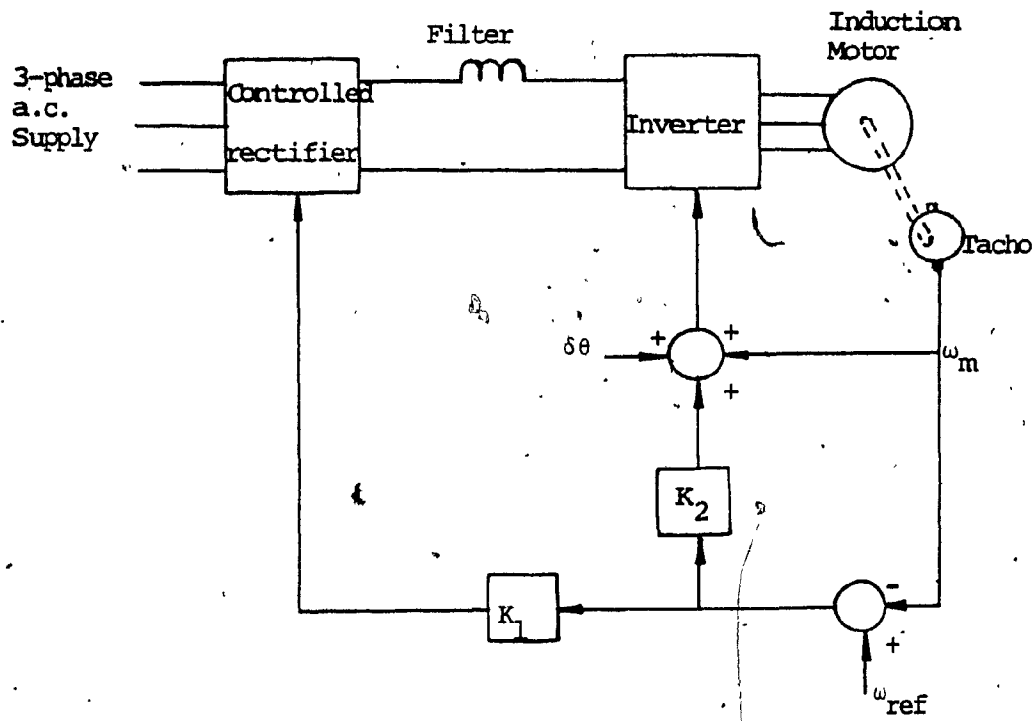
Figure 3.2  Speed and Torque Angle Feedback Scheme

$$\delta V_d = K_1 [\delta \omega_{ref} - \delta \omega_m] \tag{3.19}$$

$$\delta \omega_e = K_2 [\delta \omega_{ref} - \delta \omega_m] + \delta \omega_m + \delta \theta \tag{3.20}$$

Substituting equation (3.11) in (3.20),

$$\delta \omega_e = [a] \delta i_{qs} + [b_1] \delta i_{qr} + [c_1] \delta i_{dr} \\ + [1-K_2] \delta \omega_m + [K_2] \delta \omega_{ref} \tag{3.21}$$

$$= [a \ b_1 \ c_1 \ (1-K_2)] \begin{bmatrix} \delta i_{qs} \\ \delta i_{qr} \\ \delta i_{dr} \\ \delta \omega_m \end{bmatrix} + [K_2] \delta \omega_{ref} \tag{3.22}$$

$$= [a \ b_1 \ c_1 \ (1-K_2)] \ \underline{X} + [K_2] \delta \omega_{ref} \tag{3.23}$$

$$\delta V_d = [-K_1] \delta \omega_m + [K_1] \delta \omega_{ref} \tag{3.24}$$

$$\underline{U} = \begin{bmatrix} \delta V_d \\ \delta \omega_e \end{bmatrix} = \begin{bmatrix} 0 & 0 & 0 & -K_1 \\ a & b_1 & c_1 & (1-K_2) \end{bmatrix} \begin{bmatrix} \delta i_{qs} \\ \delta i_{qr} \\ \delta i_{dr} \\ \delta \omega_m \end{bmatrix} + \begin{bmatrix} K_1 \\ K_2 \end{bmatrix} \delta \omega_{ref} \tag{3.25}$$

$$= [K] \ \underline{X} + \begin{bmatrix} K_1 \\ K_2 \end{bmatrix} \delta\omega_{ref} \tag{3.26}$$

where matrix K is observable from equation (3.25). From equation (3.26) it is seen that the torque angle with rotor speed feedback constitutes a complete state feedback, i.e., with two signals alone a net effect of feeding four signals is obtained. Substituting equation (3.26) in (3.14) gives

$$\dot{\underline{X}} = [A+BK]\underline{X} + \underline{d} + \underline{e} \tag{3.27}$$

$$\underline{e} = [B] \begin{bmatrix} K_1 \\ K_2 \end{bmatrix} \delta\omega_{ref} \tag{3.28}$$

The relative gains of the electrical states assigned by the torque angle feedback are fixed and cannot be changed at will. In spite of this rigidity of relationship of the torque angle with drive electrical states, it is shown subsequently that this does not affect the pole-zero assignment.

## 3.4 Differences Due to Torque Angle Feedback and Speed and Current Feedback Schemes

To fully understand the significance of torque angle feedback from the pole-zero assignment point of view, it is necessary to go over the simple schemes using speed feedback only as well as schemes using both speed and current feedbacks. The differences due to the influence of

these types of feedback is explained with regard to their ability to place poles and zeros in the drive system. For purposes of conceptual clarity, the controllers are con- strained to be proportional in nature so that the system order is maintained at the minimum.

### 3.4.1 Speed feedback scheme

The CSIM drive including D.C. link filter with speed feedback, shown in Figure 3.3, is considered here. The closed-loop matrix is given by

$$[A_c] = [A+B \ K]$$

$$= \begin{bmatrix} a_{11} & a_{12} & a_{13} & a_{14}^* \\ a_{21} & a_{22} & a_{23} & a_{24}^* \\ a_{31} & a_{32} & a_{33} & a_{34}^* \\ a_{41} & a_{42} & a_{43} & a_{44} \end{bmatrix} \tag{3.29}$$

The determinant of the closed-loop matrix is given by

$$|\lambda I - A_c| = \lambda^4 + a_p \lambda^3 + b\lambda^2 + c\lambda + d \tag{3.30}$$

where $a_p$ = -(sum of the poles)

$$= -(a_{11} + a_{22} + a_{33}) \tag{3.31}$$
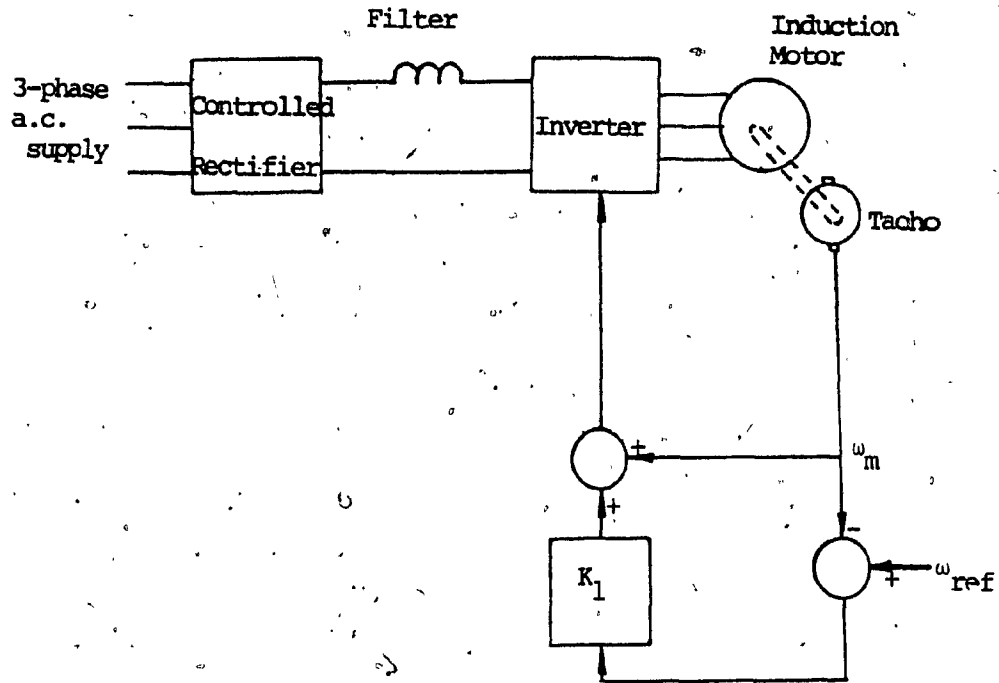
Figure 3.3   Speed Feedback Scheme

From equation (3.31), it is seen that the coefficient $a_p$ is a constant and is unaffected by the feedback. The only elements modified by the feedback are denoted by the asterisk in equation (3.29). Therefore, the placement of the poles of the system are constrained in that their sum should always be equal to that defined by equation (3.31) and this, in turn, is decided by the machine and D.C. link filter constants. For a given drive whose details are given in the Appendix-III,

$$a_p = 20.567 \qquad (3.32)$$

This demonstrates that the poles are situated near the imaginary axis, and it is not possible to move two poles farther away.so that the remaining poles determine the system damping.

For the speed-torque transfer function, the zeros are computed by deleting the mechanical equation and also the speed controller, which amounts to deleting the fourth row and column in equation (3.29) using the direct method [57]. Then it is seen that the zeros are not affected by the feedback at all. Hence the positioning of poles and zeros for good transient response is limited when only speed feedback is used.

### 3.4.2 Current and speed feedback scheme

Although the feedback of both current and speed gives much more freedom in the assignment of poles and zeros than in the case of speed feedback only, there are constraints as shown below:

The closed-loop matrix of the drive system can be denoted by $A_c$ and is given by

$$[A_c] = \begin{bmatrix} a_{11}^* & a_{12} & a_{13} & a_{14}^* \\ a_{21}^* & a_{22} & a_{23} & a_{24}^* \\ a_{31}^* & a_{32} & a_{33} & a_{34}^* \\ a_{41} & a_{42} & a_{43} & a_{44} \end{bmatrix} \qquad (3.33)$$

where the elements with the asterisk are those that are modified by the feedback. From the characteristic equation, the sum of the poles is

$$a_p = -(a_{11}^* + a_{22} + a_{33}) \qquad (3.34)$$

Equation (3.34) indicates that the poles can be varied by only one of the coefficients $a_{11}^*$ whereas the other two coefficients are fixed. Within this constraint of the sum of the poles, some pole assignment is possible. The coefficient '$a_p$' for the drive model can be written in terms of machine and feedback parameters from the Figure 3.4 and
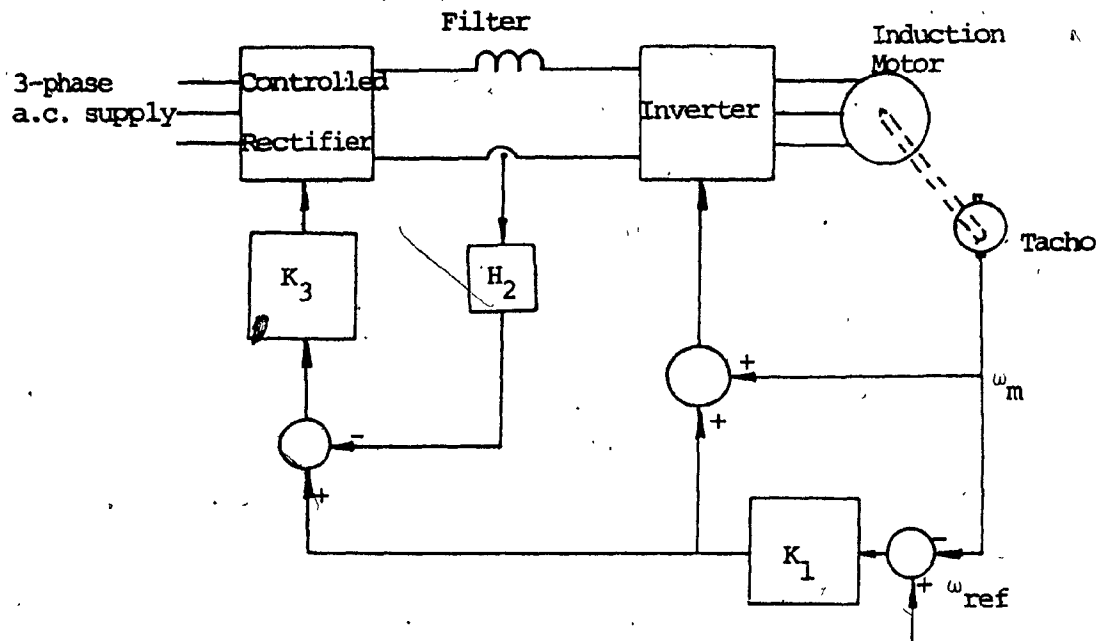
Figure 3.4  Current and Speed Feedback Scheme

the system matrices.

Link Voltage $\delta V_d = K_3 [K_1 \{ \delta \omega_{ref} - \delta \omega_m \} - H_2 \delta i_{qs}]$

$$(3.35)$$

$$a_p = -[\frac{-R_o L_r}{D_a} + \frac{L_r}{D_a} \cdot \delta V_d - \frac{L_o R_r}{D_a} - \frac{R_r}{L_r}] \qquad (3.36)$$

Substituting equation (3.35) in (3.36),

$$a_p = \frac{(R_o L_r + L_o R_r + \frac{R_r D_a}{L_r} + K_3 H_2 L_r)}{D_a} \qquad (3.37)$$

For a particular value of current feedback gain $H_2$ and current controller gain $K_3$ the poles placement is inflexible. The zeros of the speed-load torque transfer function as computed by the direct method show that the zeros are changed by the feedbacks and only the current feedback gain $H_2$ and current controller gain $K_3$ have an influence.

### 3.4.3 Torque angle feedback with current and speed feedback scheme

Finally, the case of torque angle with current and speed feedbacks, shown in Figure 3.5, is considered. In this case, the closed-loop matrix becomes
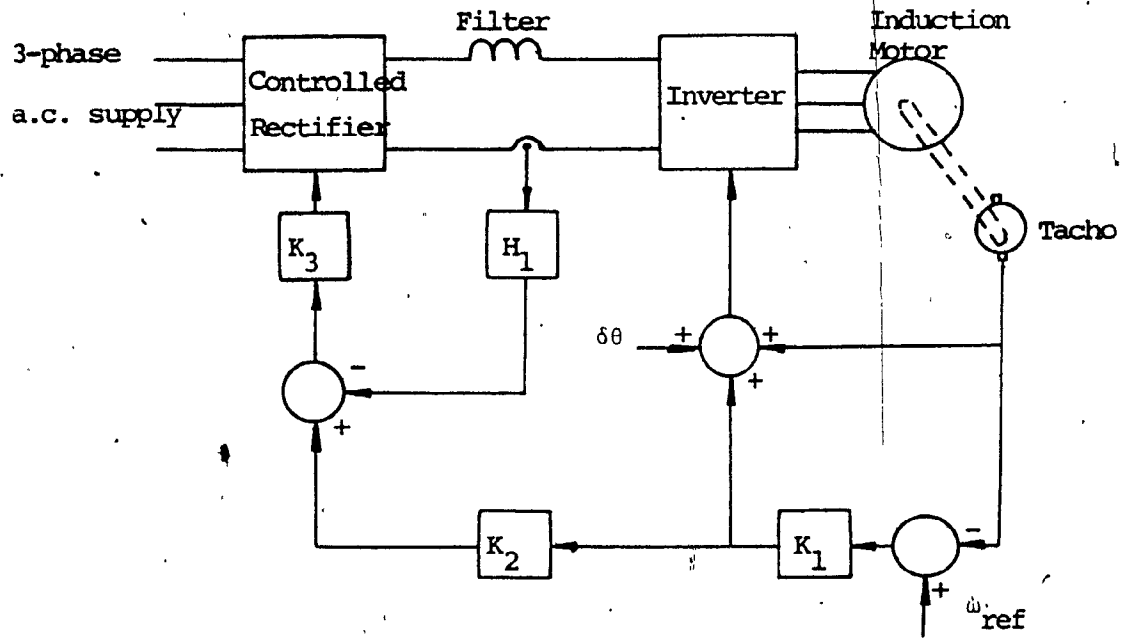
Figure 3.5.   Current, Speed and Torque Angle Feedback

$$[A_c] = \begin{bmatrix} a_{11}^* & a_{12} & a_{13} & a_{14}^* \\ a_{21}^* & a_{22}^* & a_{23}^* & a_{24}^* \\ a_{31}^* & a_{32}^* & a_{33}^* & a_{34}^* \\ a_{41} & a_{42} & a_{43} & a_{44} \end{bmatrix} \qquad (3.38)$$

where an asterisk denotes that the particular element has been modified by feedback. The sum of the poles is

$$a_p = -(a_{11}^* + a_{22}^* + a_{33}^*) \qquad (3.39)$$

All the coefficients in '$a_p$' are subject to change and depending upon the feedback gains and controller gains, a great amount of flexibility is obtained in pole placement. From the zeros of the speed-load torque transfer function, it can be seen that the zeros are assignable with enormous amount of freedom as the constituents of all the coefficients of the polynomial can be changed with feedback.

From the A matrix, it is seen that the elements of second and third column differ from each other and added with the different multiplier gains of each current in torque angle equation, the elements of the closed-loop matrix [A+BK] are uniquely determined.

## 3.5 Generalized Control Concept of Electric Motor Drives

Any drive system can be represented by

$$\dot{\underline{X}} = A\,\underline{X} + B\,\underline{U} + \underline{d} \qquad\qquad (3.40)$$

$$y = c\,\underline{X} + D\,\underline{U} \qquad\qquad (3.41)$$

and if the system is completely controllable then there exists an optimal input

$$\underline{U} = K\,\underline{X} \qquad\qquad (3.42)$$

satisfying a given system performance index. This is the well known result of optimal control theory. Note that the input becomes a linear combination of all system states. With this type of control, the closed-loop system eigenvalues are determined by the characteristic equation of the matrix [A+BK], and it is possible to assign the poles arbitrarily anywhere in the negative half of the complex plane and subsequently the zeros are also moved. This type of control not only assures the system stability requirement but also fulfils the system response requirement. Hence any system which has a complete state feedback will be superior to the one with incomplete state feedback in the above respects.

Applying this to simple D.C. drive system shown in Figure 3.6 and writing the relevant equations of the system,
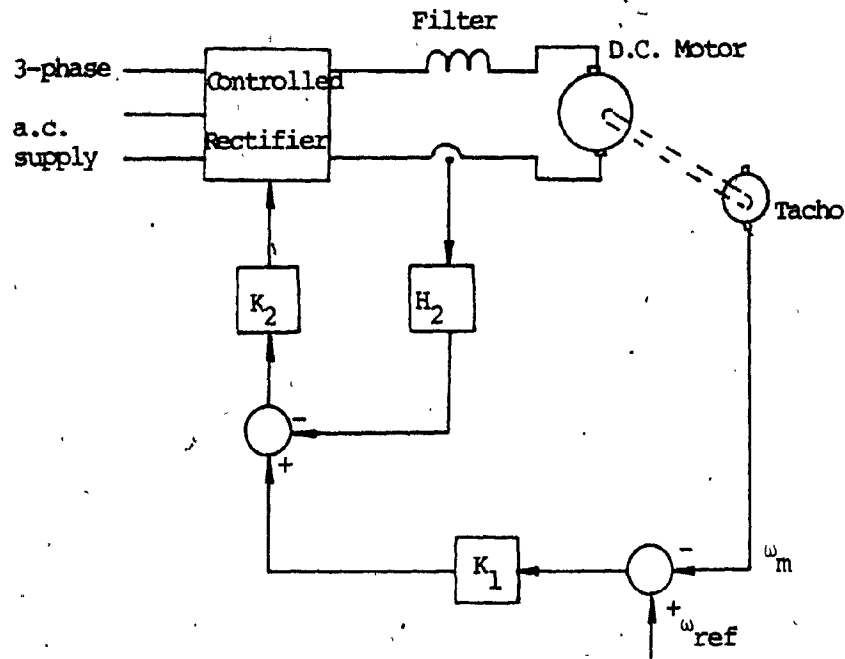
Figure 3.6    D.C. Motor Drive Scheme

the following is obtained:

$$R_a i_a + L_a \frac{di_a}{dt} + K_b \omega_m = V_d \qquad (3.43)$$

$$F\omega_m + J \frac{d\omega_m}{dt} - K_t i_a = -T_L \qquad (3.44)$$

Alternatively, in the state-space form,

$$\begin{bmatrix} \dfrac{di_a}{dt} \\[2ex] \dfrac{d\omega_m}{dt} \end{bmatrix} = \begin{bmatrix} -R_a/L_a & -K_b/L_a \\[2ex] K_t/J & -F/J \end{bmatrix} \cdot \begin{bmatrix} i_a \\[2ex] \omega_m \end{bmatrix} + \begin{bmatrix} 1/L_a \\[2ex] 0 \end{bmatrix} V_d + \begin{bmatrix} 0 \\[2ex] -T_L/J \end{bmatrix}$$

$$(3.45)$$

Controllability can be ascertained by finding the rank of
[B|AB] matrix and it is found that this matrix becomes
equal to

$$[B|AB] = \begin{bmatrix} 1/L_a & -R_a/L_a^2 \\[2ex] 0 & K_t/JL_a \end{bmatrix} \qquad (3.46)$$

and it is controllable. Taking the closed-loop equation
for the D.C. output voltage

$$V_d = K_2 [K_1 (\omega_{ref} - \omega_m) - H_2 i_a] \qquad (3.47)$$

$$= [-K_2 H_2 - K_1 K_2 H_1] \underline{X} + [K_1 K_2] \omega_{ref} \qquad (3.48)$$

It is seen that the poles and zeros can be shifted to any desired position by the feedback. Also the input is a linear combination of the system states. This is precisely one of the reasons that optimal control is in-built in such a drive system and no further extensive studies are warranted in this direction for this particular class of drive systems.

Similarly many research papers have proved beyond doubt that a complete state feedback is superior to incomplete state feedback control in synchronous machine control and in case of inaccessible states, it is necessary to reconstruct them for feedback purposes [72].

Each controlling input to the induction motor is programmed to be a function of one or more states of the drive system. Certain feedback signals contain most of the states and in combination with those missing, will constitute an all state feedback as far as an input is considered. For example, the case of speed and torque angle feedback constitutes all the drive system states. Then it would be advantageous to classify the drive systems on the basis of the nature of state feedback, i.e., whether complete state feedback or incomplete state feedback. Identification of drive systems into one of the categories and along with application of modern control theory gives a general appraisal of the drive in terms of its response, i.e., whether the scheme is optimal in a certain sense or

not.

To proceed, the controllability test is performed on
the open loop induction motor system. It is found to be
controllable. For the drive strategy given in Figure 3.5,
it can be shown that the frequency input is a linear com-
bination of all states whereas the link voltage is a func-
tion of only rotor speed and stator quadrature axis current.
Hence with regard to link voltage input, the system has an
incomplete state feedback. For a fast response and high
performance drive system, it becomes obvious that the link
voltage should also be decided by all the states. This is
achieved only in the synchronous and field-oriented schemes,
as shown later. Then in such a case, all the elements in
the closed-loop matrix $A_c$ excepting the elements $a_{41}$
and $a_{43}$ are modified by state feedback. This affords a
great deal of flexibility in the choice of combinations of
states to place the zeros and poles of the system at the
desirable locations.

## CHAPTER 4

### COMPARISON OF THE CONTROL SCHEMES.

### 4.1 Introduction

The three fast response drive schemes have as their basis the aspect of frequency compensation. Their unity in frequency compensation and diversity in the following aspects make the schemes distinct in their own right and ingenious in engineering design:

(i)     Sensing the torque angle and the method of frequency compensation

(ii)    Reference frames used for computation of machine variables

(iii)   Overcoming machine parameters' sensitivity

(iv)    Flux magnitude control

This chapter deals with the interrelationship of the schemes and their differences from the engineering implementation point of view, and their control characteristics as evaluated by the generalized control concept of the electric motor drives. A comparison of the schemes completes the chapter.

## 4.2 Interrelationship of the Drive Schemes

The theory of the control of an inverter-fed induction motor is developed in the field-oriented control scheme with the machine model in stator reference frames.  Based on this analysis and an understanding of frequency compensation, the three control schemes are considered in detail.

### 4.2.1 Angle control scheme

The angle control loop, the most crucial of the loops of the angle control scheme, shown in Figure 2.2 is considered first.  The loop consists of $G_{12}$, $G_{11}$, $H_2$, $G_1$, $G_6$, $G_7$ and $G_D$.  The output of the angle controller is $y_3$ and its input is $y_6$.  An analysis of this output for an input is given below:

The controllers have the transfer functions:

$$G_1(s) = K_1(1+T_1s)/s \tag{4.1}$$

$$G_6(s) = K_6s/(1+T_6s) \tag{4.2}$$

$G_6(s)$ is essentially a differentiator and the denominator term is to attenuate the noise at high frequencies.  For the range of frequency of interest, $T_6$ is negligible.  Therefore the cascade transfer function of the two blocks $G_1$ and $G_6$ is a proportional and differential controller.  The output $y_3$ is then,

$$Y_3 = K_1 \cdot K_6 \cdot (1+T_1 d/dt) [\omega_{ref} - \omega_m] \qquad (4.3)$$

$$= -K_1 \cdot K_6 \cdot (1+T_1 d/dt) \cdot \omega_m + K_1 \cdot K_6 (1+T_1 d/dt) \omega_{ref}$$

$$\qquad (4.4)$$

From the electromechanical equation,

$$J \cdot d\omega_m/dt = T_e - T_L \qquad (4.5)$$

and integrating equation (4.5),

$$J \cdot \omega_m = \int (T_e - T_L) dt \qquad (4.6)$$

Adding equations (4.5) and (4.6) and rearranging,

$$(1+T_1 d/dt) \cdot \omega_m = [T_e - T_L + T_1 \int (T_e - T_L) dt]/J \qquad (4.7)$$

Substituting equation (4.7) in (4.4),

$$Y_3 = - \frac{K_1 K_6}{J} [(T_e - T_L) + T_1 \int (T_e - T_L) dt] + K_1 K_6 (1+T_1 \frac{d}{dt}) \omega_{ref}$$

$$\qquad (4.8)$$

From equation (4.8), it is seen that the frequency com-
pensation is influenced by both load torque distrubance
and reference frequency change. The component of frequency
compensation due to a load torque disturbance is directly
proportional to the difference between the electromagnetic
torque and load torque and its integral. Similarly, the

component of frequency compensation due to reference frequency change is determined by the reference frequency change and its derivative. The action of the frequency compensator in coping with both load disturbance and frequency reference change is briefly described here.

(i)    Load torque disturbance: The machine is operating in steady-state and a load torque increase is initiated. Then accordingly equation (4.8) in terms of small-signal variables becomes

$$y_3 = K_1 K_6 \{ -\frac{1}{J}(\delta T_e - \delta T_L) + T_1 \int (\delta T_e - \delta T_L) dt] + (1 + T_1 \frac{d}{dt}) \delta \omega_{ref}$$

(4.9)

Let

$$\delta \omega_{ref} = 0.$$

(4.10)

Hence, the frequency compensation added is sum of the negative of acceleration torque and the integral of the same. Both these components are positive and hence the frequency of the stator currents is increased. Due to this effect, the magnetizing current phasor is left undisturbed in its position. Note that for a decrease in load torque, the stator current phasor is slowed down thereby adjusting the torque angle to correspond to load conditions.

(ii)    Reference speed change: When keeping the load torque constant, an increase in reference frequency is followed by an increasing stator current phasor speed

having two components. That directly due to reference
frequency change is given by the term

$$K_1 K_6 (1 + T_1 \frac{d}{dt}) \delta\omega_{ref}$$

At the same time any change in electromagnetic torque
beyond its steady-state level corresponding to load tor-
que is countered by subtracting the stator frequency
equivalent to a proportional change and its integral in
the electromagnetic torque given by the term

$$-K_1 K_6 [\delta T_e + T_1 \int (\delta T_e) dt]/J .$$

This balances the problem of reference speed changes in
that the torque angle is maintained constant while the
stator current phasor is speeded-up. Even during dynamic
conditions, the constancy of electromagnetic torque is
preserved for the reference speed change. For a negative
reference change, the too fast slowing down of the stator
current phasor if it affects the torque angle is instan-
taneously countered by the positive frequency compensation.
This is explained by noting that if the torque angle is
smaller than the required steady-state level, $\delta T_e$ becomes
negative and the frequency compensation term corresponding
to this becomes positive.

Herein lies the ingenuity of the angle control scheme.
Without measuring the torque angle and electromagnetic
torque of the induction motor, the stator current phasor
is positioned dynamically with the torque reference signal,
and in this case it is generated by the slip speed. While
the torque angle is dynamically corrected, the magnitude
of the current phasor also undergoes change. The components
of the current phasors are assumed to be in perfect quadra-
ture to each other and are vectorially added. Dynamically,
the torque and flux producing components are fixed by the
stator current phasor and the torque angle controller.
But in this scheme, the transient positioning of air-gap
mmf is done without reference to the actual torque angle.
There is also no feedback to help to control transiently
the air-gap flux.

Another drawback is that since the excitation current
is fixed, the air-gap flux is affected due to the magnetizing
inductance's dependence on stator current value. There
is no way to check this condition as long as there is no
feedback of air-gap flux itself. In spite of the drawbacks
mentioned, the angle control scheme is the simplest one
inherently having frequency compensation.

## 4.2.2 Synchronous control scheme

The air-gap flux-linkages are measured with the stator
currents and voltages from which electromagentic torque and torque

angle are computed. The machine parameters do not enter into such a computation in a direct form. Unlike in the angle control scheme, the reference torque is compared to the actual value of the torque angle in the machine and then frequency correction is initiated. In turn, the reference torque angle is obtained from the difference of torque reference and actual electromagnetic torque. The changes in the machine parameters are fully accounted into the drive scheme in this manner. Note that all the computations are carried out in the stator reference frame and hence no transformations are required. Air-gap flux is set at the desired level due to its comparison with the measured air-gap flux. The drive needs air-gap flux sensors and also a minimum complexity computational circuit for torque and torque angle.

## 4.2.3 Field-oriented control scheme

This incorporates perfect decoupling of the machine and each output is controlled through a non-interactive channel. The resolution of the stator current phasor into two components along the air-gap flux axis (known as field axis) and the computation of these through the measured air-gap flux-linakges and stator currents provides the basis for comparison with the respective reference values. The machine magnetizing inductance changes depending upon the stator current, and for a case of constant direct

field axis stator current reference $i_{SD}$, shown in Figure 2.4, will alter the air-gap flux. Therefore, the addition of another loop to compare the actual air-gap flux with the desired value corrects the situation. Noting that,

$$\text{Modified air-gap flux} = L_m \cdot i_m / (1 + \sigma_r) \qquad (4.11)$$

and

$$i_{SQ} = (T_r \cdot d/dt + 1) \cdot i_m \qquad (4.12)$$

It is seen from the equations (4.11) and (4.12) the air-gap flux is proportional to magnetizing current phasor magnitude $i_m$. But $i_m$ is not a simple proportion of $i_{SQ}$, as it is related through the time delay. This necessitates the flux controlling loop mentioned above.

Similarly a control loop to force the generated torque to demanded value is accomplished comparing the actual with the requested values of the electromagnetic torque. The error of this sets the reference $i_{SQ}$, which in turn is compared to the computed value. The machine parameter sensitivity is completely eliminated in this scheme. This scheme needs air-gap flux sensors and co-ordinate converters and hence results in complex control and computational circuitry.

## 4.3 Evaluation of the Control Schemes by the Generalized Control Concept

The fineness of the control achieved by each scheme can be evaluated by a generalized control concept of the electric motor drives. To obtain that, the drive control inputs have to be expressed in terms of their controlling functions. Results obtained are general in nature.

### 4.3.1 Angle control scheme

From the Figure 2.2, the control inputs of the drive can be simplified as shown in Figure 4.1. Assuming $K_2$, $K_3$ and $K_5$ to be simple proportional controller gains, the inputs can be written after drawing the state diagram of the speed controller. The state diagram of the speed controller is shown in Figure 4.2. From this state diagram, the following equation is obtained:

$$Y_6 = K_1 T_1 [\delta\omega_{ref} - \delta\omega_m] + X_5 \qquad (4.13)$$

From Figure 4.1, the following are obtained:

$$Y_2 = K_5 Y_6 \qquad (4.14)$$

$$Y_3 = K_6 \frac{dy_6}{dt} \qquad (4.15)$$

$$= K_6 \frac{d}{dt} \{K_1 T_1 [\delta\omega_{ref} - \delta\omega_m] + X_5\} \qquad (4.16)$$
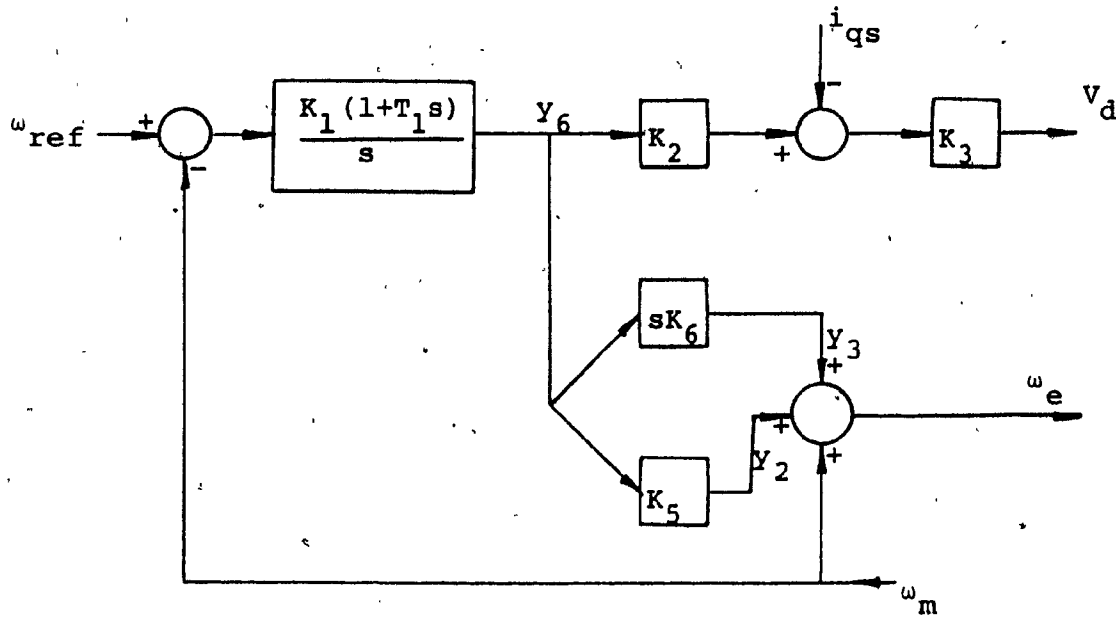
Figure 4.1  Control Inputs of the Angle Controlled Drive
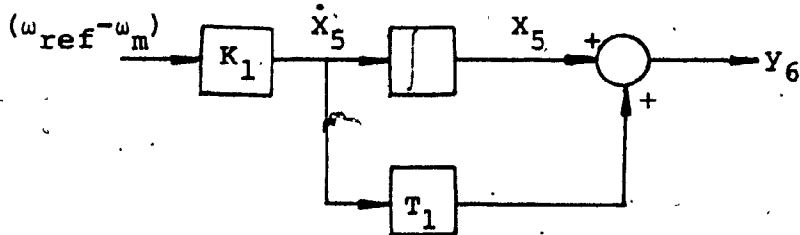


Figure 4.2  State-Diagram of the Speed Controller

$$= K_6 \frac{d}{dt} \{K_1 T_1 [\delta\omega_{ref} - \frac{(\delta T_e - \delta T_L)}{J}\}$$

$$+ K_6 K_1 (\delta\omega_{ref} - \delta\omega_m) \qquad (4.17)$$

$$= K_6 K_1 (\frac{-T_1 \delta T_e}{J} - \delta\omega_m) + K_6 K_1 (1 + T_1 \frac{d}{dt}) \delta\omega_{ref}$$

$$+ \frac{K_6 K_1 T_1}{J} \delta T_L \qquad (4.18)$$

And substituting for $\delta T_e$ from the electromechanical equation,

$$y_3 = K_6 K_1 (a_{41} \delta i_{qs} + a_{43} \delta i_{dr} - \delta\omega_m)$$

$$+ K_6 K_1 (1 + T_1 \frac{d}{dt}) \delta\omega_{ref} + \frac{K_6 K_1 T_1}{J} \delta T_L \qquad (4.19)$$

The stator incremental frequency is

$$\delta\omega_e = y_2 + y_3 + \delta\omega_m \qquad (4.20)$$

$$= [K_{21} \ K_{23} \ K_{24} \ K_{25}] \underline{X}$$

$$+ [K_6 K_1 + K_1 K_5 + K_6 K_1 T_1 \frac{d}{dt}] \delta\omega_{ref}$$

$$\qquad (4.21)$$

$$+ \frac{K_6 K_1 T_1}{J} \delta T_L$$

The link voltage, on the other hand, is

$$\delta V_d = K_3(Y_6 K_2 - \delta i_{qs}) \qquad\qquad (4.22)$$

$$= K_3 \delta i_{qs} - K_3 K_2 K_1 T_1 \delta \omega_m + K_3 K_2 X_5$$

$$+ K_3 K_2 K_1 T_1 \delta \omega_{ref}$$

$$= [K_{11} \ 0 \ 0 \ K_{14} \ K_{15}] \underline{X} + K_3 K_2 K_1 T_1 \delta \omega_{ref} \qquad (4.23)$$

The stator frequency and link voltage are not linear com-
binations of all the system states and particularly they are
totally independent of the rotor q-axis current. This
control scheme belongs to the category of incomplete state
feedback. The control consequence of this is clearly shown
in inadequate freedom of the pole-zero assignment explain-
ed in the following:

The closed-loop matrix $A_c$ is of the form

$$A_c = \begin{vmatrix} a^*_{11} & a_{12} & a_{13} & a_{14} & a^*_{15} \\ a^*_{21} & a_{22} & a^*_{23} & a^*_{24} & a^*_{25} \\ a^*_{31} & a_{32} & a^*_{33} & a^*_{34} & a^*_{35} \\ a_{41} & 0 & a_{43} & 0 & 0 \\ 0 & 0 & 0 & a^*_{54} & 0 \end{vmatrix} \qquad (4.24)$$

The asterisk denotes that the elements are modified by
the feedback. The sum of the closed-loop poles is,

$$a_p = -(a^*_{11} + a_{22} + a^*_{33}) \qquad (4.25)$$

where only two elements are modified by the feedback.
Similarly the zeros of the speed-load torque transfer function are computed using [57] and the sum is given by:

$$a_z = -(a^*_{11} + a_{22} + a_{33}) \qquad (4.26)$$

where only the element $a^*_{11}$ is under control. From equations (4.25) and (4.26), the curtailment of freedom of assignment of poles and zeros is evident.

If the disturbance matrix, $\underline{d}$, is examined, it is of the form:

$$
\begin{bmatrix}
d_{11} & 0 \\
d_{21}(1+T_a \frac{d}{dt}) & d_{22} \\
d_{31}(1+T_b \frac{d}{dt}) & d_{32} \\
0 & d_{42} \\
d_{51} & 0
\end{bmatrix}
\cdot
\begin{bmatrix}
\delta\omega_{ref} \\
\delta T_L
\end{bmatrix}
\qquad (4.27)
$$

The stator equation is not directly influenced by load torque and the electromechanical equation is not coupled directly to the reference speed. The former situation is effectively countered by adding the differentiated output of torque reference signal, $y_6$, into the current

reference. This brings in the element $d_{12}$, is shown by the equation (4.18).

## 4.3.2 Synchronous control scheme

Figure 4.3 shows the control input generation for the synchronous control scheme. Utilizing Figure 4.3 and the simplification, that for small torque angles;

$$\sin \delta\theta \simeq \delta\theta \qquad (4.28)$$

the following can be deduced:

$$\delta V_d = K_6 \{ K_2 y_6 + K_3 (\delta\omega_m - \delta|\psi|) - \delta i_{qs} \} \qquad (4.29)$$

$$\delta|\psi| = m_1 \delta i_{qs} + m_2 \delta i_{qr} + m_3 \delta i_{dr} \qquad (4.30)$$

and substituting for $y_6$ from equation (4.13),

$$\delta V_d = [K_{11} \ K_{12} \ K_{13} \ K_{14} \ K_{15}] \underline{X} + d_{11} \delta\omega_{ref} \qquad (4.31)$$

The stator incremental frequency is

$$\delta\omega_e = [(y_6 - \delta T_e) K_4 - \delta\theta] K_5 + \delta\omega_m \qquad (4.32)$$

Obtaining incremental electromagnetic torque from the machine equation,
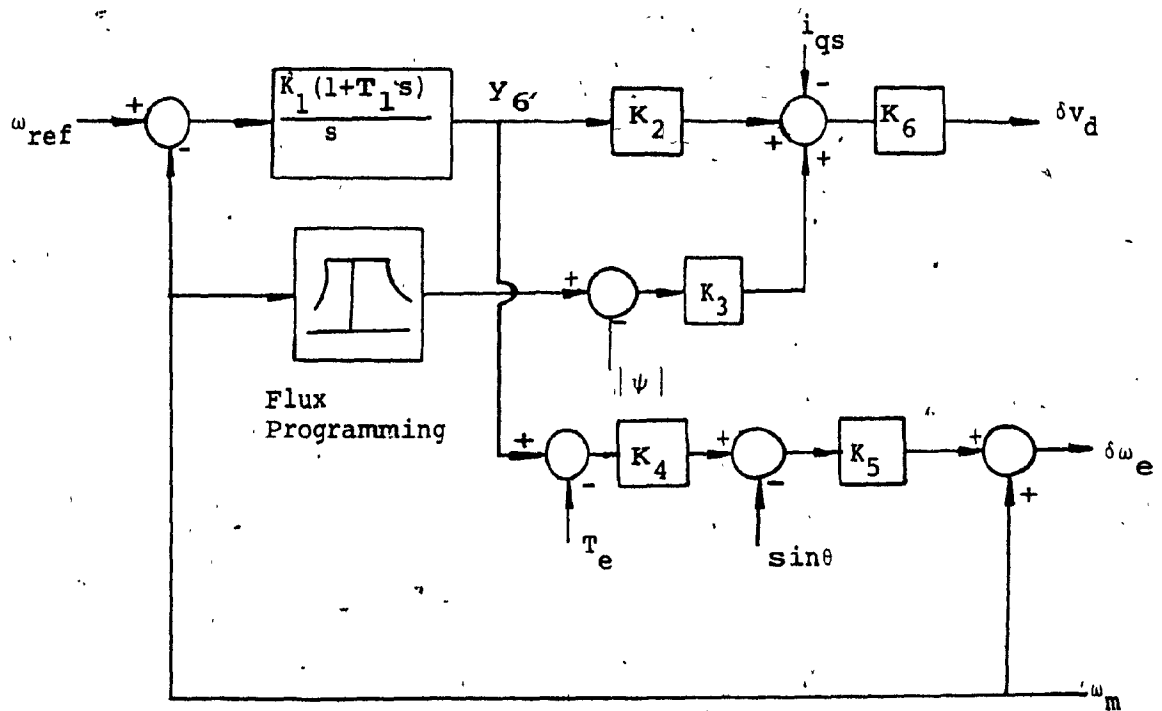
Figure 4.3  Generation of Inputs for Synchronous Control Scheme

$$\delta T_e = a_{41} \delta i_{qs} + a_{43} \delta i_{dr} \qquad (4.33)$$

$$\delta \theta = a \delta i_{qs} + b_1 \delta i_{qr} + c_1 \delta i_{dr} \qquad (4.34)$$

Substituting for $\delta T_e$ from equation (4.33) and $\delta \theta$ from equation (4.34) into equation (4.32),

$$\delta \omega_e = [K_{21} \ K_{22} \ K_{23} \ K_{24} \ K_{25}] \underline{X} + a_{ref} \delta \omega_{ref} \qquad (4.35)$$

From equations (4.31) and (4.35), it is seen that the inputs are linear combinations of all the system states and the synchronous control scheme constitutes a complete state feedback. Hence the poles and zeros are arbitrarily assignable and the freedom is unrestricted in such an endeavour.

The disturbance matrix is similar to that for the angle control scheme excepting that no time derivatives of reference speed are included.

### 4.3.3 Field-oriented control scheme

By the same procedure adopted for the synchronous control scheme, it is found that the field-oriented scheme is a complete state feedback system. Also the state feedback gain matrix $K$ is of the form

$$K = \begin{bmatrix} K_{11} & K_{12} & K_{13} & K_{14} & K_{15} \\ K_{21} & K_{22} & K_{23} & K_{24} & K_{25} \end{bmatrix} \qquad (4.36)$$

and the individual gains can be independently changed by such variables as controller gains. The rigidity of their inter-relationship in simple angle feedback scheme is overcome in this way.

### 4.4 Comparison of the Schemes

The comparison of the schemes can be obtained using the generalized control concept of the drives. It is noted that the angle control scheme is one of the incomplete state feedback category whereas the synchronous and field-oriented control schemes are of the complete state feedback category. Optimal control can be achieved in the synchronous and field-oriented control schemes because of this structural property. But only sub-optimal control is possible in the angle control scheme. Hence the superiority of the two schemes over the angle control scheme.

Summing up from the physical point of view, the following comments are in order:

Of the three schemes analyzed, the angle control scheme is conceptually simple and intuitively appealing. Instead of measuring the torque angle for dynamic positioning of the air-gap flux, the angle is constructed from the

torque reference signal. In this way, the complexity of processing a large number of signals is eliminated. However, by using only the motor slip speed to reconstruct the torque angle, the control circuit has no information about the actual value of the air-gap flux nor about its precise position. Since all these variables are obtained indirectly and also the drive controllers depend on machine constants, the drive performance normally deteriorates due to magnetic saturation, change in operating frequency and change in winding temperature.

The synchronous control scheme avoids these difficulties by providing almost complete information about the key motor variables. Although the torque and its angle are calculated, motor currents, air-gap flux and speed are measured. Furthermore, this scheme is less sensitive to variation in motor parameters than the angle control scheme. The air-gap flux can be programmed and precisely controlled during constant power operation. The unity gain frequency loop can also be obtained by using the flux linkages signal and the angle loop provides the slip and the sum of the two sets the stator frequency. Consequently the motor output speed may be controlled indirectly.

The field-oriented control is historically the oldest of the three schemes considered. This is the most complex scheme and has all the features of synchronous control in addition to a measurement of the flux producing component of the stator current. This enables a fast and accurate

positioning of the air-gap mmf phasor.

For ready reference, the comparison is listed in a tabular form and given in Table 4.1.

## Table 4.1
### Comparison of The Drive Schemes

| Item for Comparison | Angle Control Scheme | Synchronous Control | Field oriented Control |
|---|---|---|---|
| 1. Feedback Signals | Rotor speed and link current | Rotor speed, link current' Flux link-ages *Electromagnetic torque *Torque angle  *CALCULATED | Rotor speed  Link current  Flux linkages *Electromagnetic torque *torque angle *Field-oriented stator current components *CALCULATED |
| 2. Angle | Constructed from steady state charac-teristics | Instantaneous | Instantaneous Calculation |
| 3. Flux | Neither mea-sured nor cal-culated | Uses either mea-sured or a cal-culated one from terminal voltages and currents | Same as synchro-nous control |
| 4. Programming the flux | Possible but with no feed-back | Precisely imple-mented | Precisely implemented |
| 5. Control loops | Current loop unity gain speed loop An outer speed loop.Angle com-pensating loop (4 loops) | Inner current loop, unity gain speed loop Flux loop Torque loop Angle loop Outer speed loop (6 loops) | Inner current loop Unity gain speed loop Flux loop Torque loop Angle loop Field-oriented stator current component loop Outer speed loop (8 loops) |
| 6. Speed loop | Essential for operation | Optional but flux programming would suffer | Optional but flux programming would suffer |
| 7. Parameter dependence | Large | To an extent.Affects angle and electro-magnetic torque cal-culation. | To an extent. Af-fects electromag-netic torque and magnetizing current phasor calculation |
| 8. Design of Frequency compensator | Complicated due to dependence on machine para-meters and oper-ting conditions | Simple | Simple |

Table 4.1

| Item for Comparison | Angle Control Scheme | Synchronous Control | Field Oriented Control |
|---|---|---|---|
| 9. Nature of the Scheme | Conceptually Simple | More complex scheme | The most complex scheme |
| 10. Others | - | - | Fast positioning of flux space phasor is made possible due to the comparison with the neces- sary stator cur- rent component |

CHAPTER 5

TORQUE ANGLE AND ITS EFFECT ON DRIVE CHARACTERISTICS

5.1 Introduction

The central role played by the torque angle in the performance and stabilization of the drives has been covered in the previous chapters. An analysis of the various torque angle transfer functions and the time responses of the torque angle for various drive inputs is made. From the drive equations and the time response of the torque angle, it is shown that the change in the torque angle is associated with a change in speed of the magnetizing current phasor. In spite of the fact that torque angle is a linear combination of all electrical states, it is proved that it has a strong limitation in that its feedback alone cannot stabilize the drive system.

5.2 Torque Angle Transfer Functions

The transfer functions of torque angle for stator current magnitude, stator current frequency and load torque inputs are evaluated. The purpose for the evaluation of such transfer functions is:

(i)     To find whether the transfer functions are minimum phase or non-minimum phase. This particular property of the transfer function indicates the limitations placed on the

magnitude of the gain of the compensator.

(ii)     To compute the time responses.

The procedure for the computation of transfer functions and time responses is given in Appendix-IV.  The link filter is neglected in this study.  Note that even this extreme assumption is justifiable in the light of availability of converters with switching frequencies usually in the order of 5KHz for the front-end current source in a CSIM drive. Similar assumption is justified in the case of a fast acting PWM power converters for VSIM drives.  The drive details pertain to Appendix-III.  Stable operating points are chosen and torque angle transfer functions for both CSIM and VSIM drives are given in Table 5.1.  This table is for a machine model neglecting stator dynamics in the case of CSIM drive.

All the transfer functions relating to torque angle are minimum phase in both the drives excepting for voltage input case in the VSIM drive.  For frequency input, the CSIM drive has no steady-state gain in torque angle because the slip speed is the same and hence the relative angular positions of the stator and rotor fluxes remain the same.  But in the VSIM drive, the frequency increase weakens the stator flux and to generate the same torque as in steady-state, the torque angle increases thereby showing a certain amount of steady-state gain.

In the case of a CSIM drive, there is no pole-zero

## Table 5.1

### Torque angle transfer functions

| CSIM Drive | | | | | |
|---|---|---|---|---|---|
| Operating point:slip=0.005, $i_{qso}$=1.68 p.u., frequency=377 rad/sec, Electromagnetic torque=1.335 p.u. | | | | | |
| INPUT | | | | | |
| Stator current (Magnitude) | | Frequency | | Load Torque | |
| SSG | ZEROS | SSG | ZEROS | SSG | ZEROS |
| -7.69 | -3.70 <br> -20.0±j221.1 | 0.0 | -0.49E-12 <br> -1.938 | 4.844 | -1.94 |

POLES: -0.264, -1.89±j33.8

| VSIM DRIVE | | | | | |
|---|---|---|---|---|---|
| Operating point:slip=0.0125, $V_{qso}$=1.414, frequency=377 rad/sec, Electromagnetic torque=0.97 p.u. | | | | | |
| INPUT | | | | | |
| Voltage (Magnitude) | | frequency | | Load Torque | |
| SSG | ZEROS | SSG | ZEROS | SSG | ZEROS |
| -0.514 | -19.3 <br> -32.1±j65.7 <br> 138.2 | 0.71 | -3.78 <br> -24.82 <br> -1197.3 <br> -0.29E+17 | 0.374 | -23.76 <br> -26.93±j385.3 |

POLES: -12.44±j63.6, -46.99±j374.1, -24.4

cancellation for all the three inputs. For a closed-loop drive with simple angle feedback and slip speed current interface, the torque angle-frequency transfer function becomes non-minimum phase. When stator dynamics and link filter are included one after another, the CSIM torque angle transfer functions become non-minimum phase for frequency and load torque inputs and they are given in Table 5.2. Note then the drive has to be closed-loop to have a stable operation. And the closed-loop structure corresponds to the above description. Consideration of the link filter has affected both the nature of zeros and the location of both zeros and poles.

## 5.3 Relationship Between Torque Angle Change and Speed of Magnetizing Current Phasor

It has been stated in the second chapter that a change in torque angle is associated with a change in the speed of the magnetizing current phasor. The mechanism of torque angle change and its consequence is not explicit in the synchronously rotating reference frame model of the drive. But in space phasor modelling, the effect is discernible directly [60]. Neglecting the stator equations leads to the conclusion that $i_{SQ}$ and $i_{SD}$ are inputs at command, the remaining equations are then:

$$i_{SQ} = (\frac{d\phi_s}{dt} - \omega_m) i_m T_r \qquad (5.1)$$

## Table 5.2

CSIM drive torque angle transfer functions with stator dynamics

| ITEM | Operating point:Slip=0.0125, Stator current (Quadrature axis) = 1.68 p.u. Frequency=377 rad/sec, Electro.Torque=0.97 p,u. | | | | | |
|------|-------|-------|-------|-------|-------|-------|
| | INPUT | | | | | |
| | Link Voltage | | Frequency | | Load Torque | |
| | SSG | ZEROS | SSG | ZEROS | SSG | ZEROS |
| With no link filter | −0.097 | −2.89 −20.4±j81.5 | 0.186 | −1.51, −12.29, −45.53 | 0.0988 | 5.07, −40.2 |
| | POLES: −7.05, −28.5, −36.8±j300.3 | | | | | |
| with link filter | −0.98 | −2.9, −20.4±j81.5 | 0.186 | −1.52, 13.46, −62.9 | 0.099 | 5.43, −55.9 |
| | POLES: −7.09, −28.2, −9.92±j136.7 | | | | | |

$$i_{SD} = (1 + T_r \frac{d}{dt}) i_m \qquad (5.2)$$

where

$\phi_s$ is field angle

and $T_r$ is rotor time constant,

$$T_e = \frac{2}{3} \frac{L_m}{(1+\sigma_r)} i_m i_{SQ} \qquad (5.3)$$

$$J \frac{d\omega_m}{dt} = T_e - T_L \qquad (5.4)$$

Taking the small-signal increments of the variables, the equations become:

$$\delta i_{SQ} = [\frac{d}{dt}(\delta\phi_s) - \delta\omega_m] i_{mo} T_r + (\omega_{eo} - \omega_{mo}) T_r \delta i_{mo} \qquad (5.5)$$

$$\delta i_{SD} = (T_r \frac{d}{dt} + 1) \delta i_m \qquad (5.6)$$

$$\delta T_e = \frac{2}{3} \frac{L_m}{(1+\sigma_r)} [i_{mo} \delta i_{SQ} + i_{SQ0} \delta i_{mo}] \qquad (5.7)$$

$$\frac{d}{dt}(\delta\omega_m) = \frac{1}{J}[\delta T_e - \delta T_L] \qquad (5.8)$$

The phasor diagram is shown in Figure 5.1 for constant stator current magnitude and frequency. Note that $\frac{d}{dt}[\delta\phi_s]$ is the incremental speed of the magnetizing current phasor. With the following approximation, due to a large rotor time consant
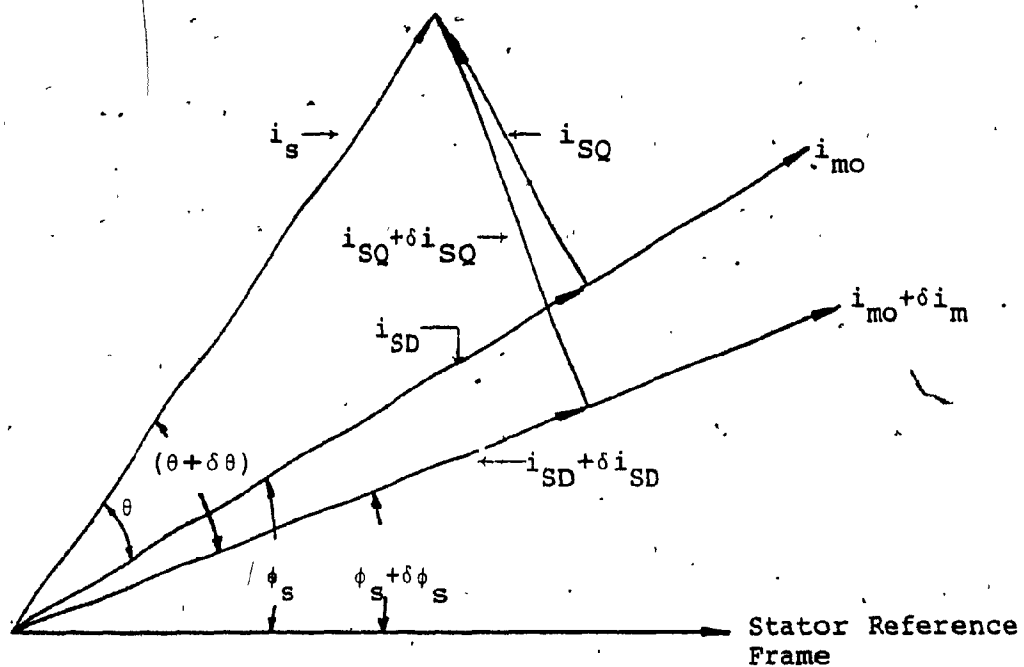
Figure 5.1   Phasor Diagram for Perturbation Around an Operating
Point with Constant Stator Current and Frequency

$$\delta i_m \simeq 0 \tag{5.9}$$

$$\delta i_{SQ} = [p\delta\phi_s - \delta\omega_m] i_{mo} T_r \tag{5.10}$$

$$p\delta\omega_m = \frac{1}{J}[\frac{2}{3}\frac{L_m}{(1+\sigma_r)} i_{mo}\delta i_{SQ}] - \frac{1}{J}\delta T_L \tag{5.11}$$

and integrating equation (5.11),

$$\delta\omega_m = \frac{1}{J}\frac{2}{3}\frac{L_m}{(1+\sigma_r)} i_{mo} \int (\delta i_{SQ}) dt - \frac{1}{J} \int (\delta T_L) dt \tag{5.12}$$

And combining equation (5.10) and (5.12),

$$p\delta\phi_s = [\frac{1}{i_{mo}T_r}] \delta i_{SQ} + \frac{1}{J}\frac{2}{3}\frac{L_m i_{mo}}{(1+\sigma_r)} \int (\delta i_{SQ}) dt$$

$$- \frac{1}{J} \int (\delta T_L) dt \tag{5.13}$$

It can be seen that $\delta i_{SQ}$ changes directly the torque angle and is shown in the following:

$$\tan\theta = \frac{i_{SQO}}{i_{SDO}} \tag{5.14}$$

$$\tan(\theta+\delta\theta) = \frac{i_{SQO}+\delta i_{SQ}}{i_{SDO}+\delta i_{SD}}$$

$$= \frac{\tan\theta + \tan\delta\theta}{1-\tan\theta\tan\delta\theta} \tag{5.15}$$

And treating $\tan\delta\theta \simeq \delta\theta$ $\tag{5.16}$

$$\frac{i_{SQO} + \delta i_{SQ}}{i_{SDO}} = \frac{\tan\theta + \delta\theta}{1 - \tan\theta\,\delta\theta} \tag{5.17}$$

$$\delta\theta[i_{SDO} + i_{SQO}\tan\theta] = \delta i_{SQ} \tag{5.18}$$

$$\delta i_{SQ} = [\frac{2i_{SQO}}{\sin 2\theta}]\,\delta\theta \tag{5.19}$$

$$= \ell_1\,\delta\theta \tag{5.20}$$

$$\text{where} \quad \ell_1 = \frac{2i_{SQO}}{\sin 2\theta} \tag{5.21}$$

$$p\delta\phi_s = [\frac{\ell_1}{i_{mo}T_r}]\,\delta\theta + \frac{1}{J}\,\frac{2}{3}\,\frac{L_m i_{mo}}{(1+\sigma_r)}\,\ell_1 \int (\delta\theta)\,dt$$

$$- \frac{1}{J}\int(\delta T_L)\,dt \tag{5.22}$$

From equation (5.22), the dependence of the incremental
speed of the magnetizing current phasor on load torque
perturbation and change in torque angle is demonstrated.
Note that the change in the incremental stator frequency is
absorbed in the incremental torque angle change itself.
An increase in load torque lowers the speed of magnetizing
current phasor if supply frequency is constant. An increase
in stator frequency causes an increase in torque angle
and hence increases the magnetizing current phasor speed.
The maintenance of magnetizing current phasor speed in the
face of load torque disturbance amounts to

$$p\delta\phi_s \doteq 0 \tag{5.23}$$

which in turn means,

$$\left\{ \left[\frac{\ell_1}{i_{mo}T_r}\right] + \frac{1}{J}\frac{2}{3}\frac{L_m i_{mo}}{(1+\sigma_2)}\ell_1 \frac{1}{p}\right\}\delta\theta = \frac{1}{JP}\delta T_L \tag{5.24}$$

where

$$p = \frac{d}{dt} \tag{5.25}$$

Hence,

$$[\ell_2 p + \ell_3]\delta\theta = \delta T_L \tag{5.26}$$

where

$$\ell_2 = \frac{J\ell_1}{i_{mo}T_r}$$

$$\tag{5.27}$$

$$\ell_3 = \frac{2}{3}\ell_1 \frac{L_m i_{mo}}{(1+\sigma_r)}$$

Note that change in torque angle is introduced by change in stator frequency and hence

$$p\delta\theta = \delta\omega_e \tag{5.28}$$

Substituting equation (5.28) into equation (5.26),

$$\left(\frac{\ell_2 p + \ell_3}{p}\right)\delta\omega_e = \delta T_L \tag{5.29}$$

$$\therefore \delta \omega_e = \frac{p}{(\ell_2 p + \ell_3)} \delta T_L \qquad (5.30)$$

This $\delta \omega_e$ is the incremental frequency to be added to the frequency of the stator currents to overcome the load torque disturbance without changing the speed of the air-gap mmf. It is interesting to observe that the frequency compensator in the angle control scheme described in Chapter 4 also has the form given by equation (5.30).

## 5.4 Time Responses of Torque Angle and Incremental Speed of Magnetizing Current Phasor

The torque angle controls the magnitude of the torque and the flux-producing component of the stator current. In a CSIM drive, the behaviour of the torque angle acquires an importance during dynamic conditions as normally, for a few milliseconds, the magnitude of current cannot be increased due to the time constants involved both in current reference controller and current controller. Consider a load being applied to the rotor while the stator frequency is constant. The position of the stator current phasor must also be fixed in position since this is taken as the reference axis. If the frequency is not changed, the only way that the machine can adjust to increased loading is by an increase in the torque angle, i.e., by the magnetizing current phasor losing its position. This crucial phenomenon is examined in detail for a CSIM drive

under dynamic conditions. Naturally this requires consideration of the torque angle responses for current, frequency and load torque inputs. The incremental input magnitude is assumed to be 0.02 p.u.. The operating point chosen is that given in Table 5.1 and the following discussion is with reference to this operating point.

### 5.4.1 Current input

An increase in stator current with constant load decreases the torque angle so as to maintain the torque producing component of stator current phasor the same, before and after perturbation. The torque angle reaches its steady-state with oscillations inherent for an open loop CSIM drive and is shown in Figure 5.2. The initial rate of change of incremental torque angle is small and for the first 80 msec, the plot of torque angle is almost a straight line of negative slope. The rate of change in this region is -0.345 rad/sec and the negative of this correponds to the incremental speed of the magnetizing current phasor. A point-by-point computation of incremental magnetizing current phasor speed is shown in Figure 5.3. Note that the time considered has been reduced to one tenth of that in Figure 5.2 as the effect during the first 100 msec is very critical and important. In addition, it is within this interval that corrective action is normally initiated. The corrective action would in this case be
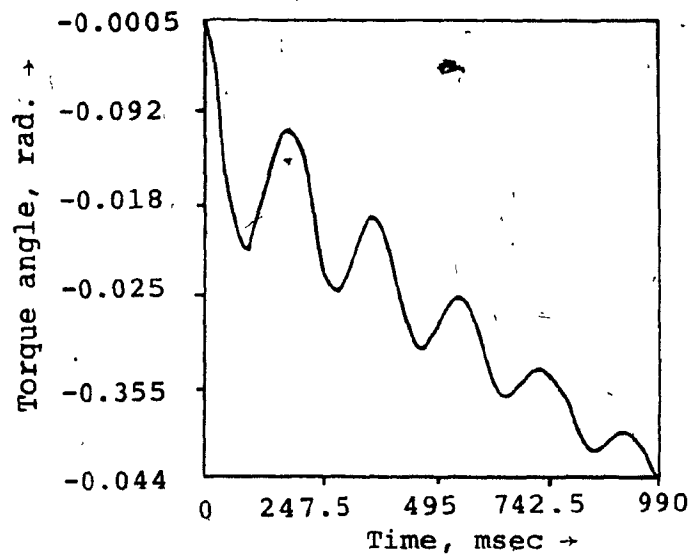
Figure 5.2   Torque Angle Response for Current Input
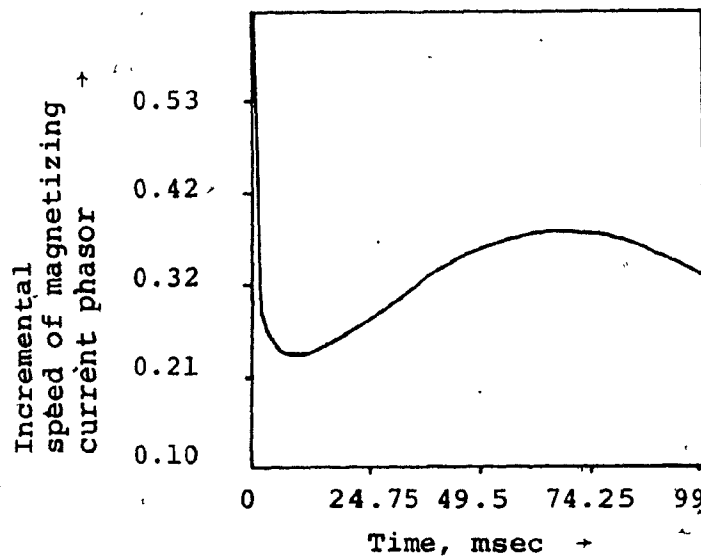


Figure 5.3   Incremental Magnetizing Current Phasor
Speed for Current Input

- 93 -

a slowing down of the stator current phasor transiently by decreasing the frequency of the stator current.

## 5.4.2 Frequency input

The incremental torque angle and incremental gain of speed of magnetizing current phasor for frequecy input are shown in Figures 5.4 and 5.5, respectively. It is observed that the incremental torque angle change may be considered linear for the first 40 msec. The magnetizing current phasor is speeded up and is done at a linear rate up to 100 msec with respect to the pre-disturbance speed. With respect to after disturbance speed, the magnetizing current phasor tries to catch up with the stator current phasor. The rate of change of incremental torque angle is 6.334 rad/sec and the rise time of it is zero because the steady-state gain is zero. But the rise time of frequency of magnetizing current phasor is around 80 msec. In a VSIM drive, the slope of the incremental torque angle is 48.22 rad/sec and rise time is 1.75 msec. There is a certain rise time for its torque angle because of a steady-state gain. Note that the salient difference in the incremental speed of the magnetizing current phasor between the two types of drives. This factor contributes to the dynamic problems of the CSIM drive.
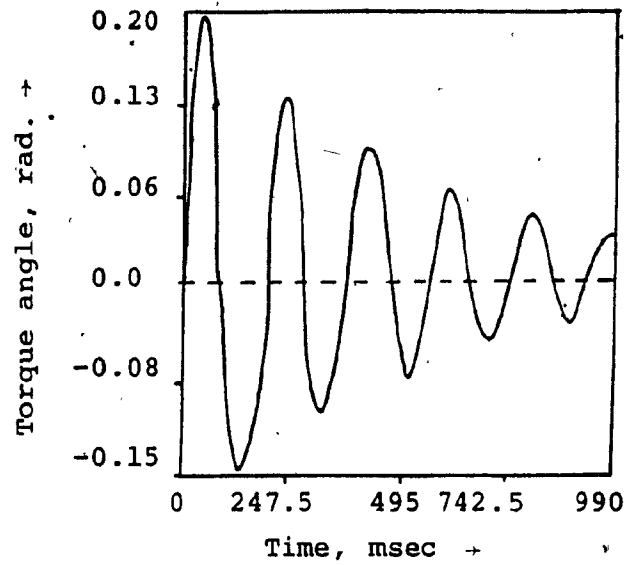
Figure 5.4  Torque Angle Response for Frequency Input
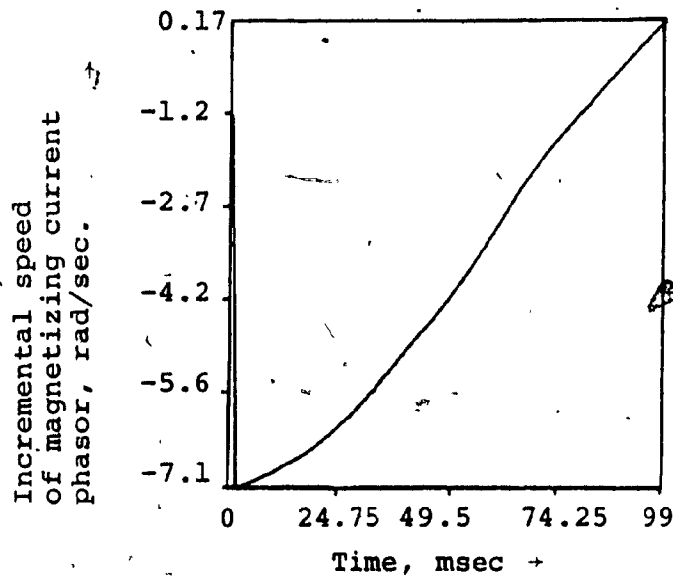


Figure 5.5  Incremental Speed of Magnetizing
Current Phasor for Frequency Input

### 5.4.3 Load torque input

The incremental torque angle and incremental speed of magnetizing current phasor are shown in Figures 5.6 and 5.7 respectively for a load torque input. The rate of rise of torque angle is 0.423 rad/sec and the rise time is large equalling the rotor time constant. This corresponds to the case of current input where the same slow response is comparable. A notable factor is the linearity of change of magnetizing current phasor speed over a period of the first 50 msec. This linearity in change points to the ease of compensation in a simple and direct manner.

In a VSIM drive, the slope of the incremental torque angle is the same as for a CSIM drive and the rise time is only 18.75 msec. The improvement in response time is due to the fact that there is no constraint to the change in the magnitude of stator current phasor in the form of controller time constants in a VSIM drive. The time constant associated with the torque angle can be identified as the rotor transient time constant. The difference in time constants of the two types of drives is proved using the drive equations as follows:

### Case (i): CSIM drive

Considering the rotor equations of the induction machine given in Appendix-I.
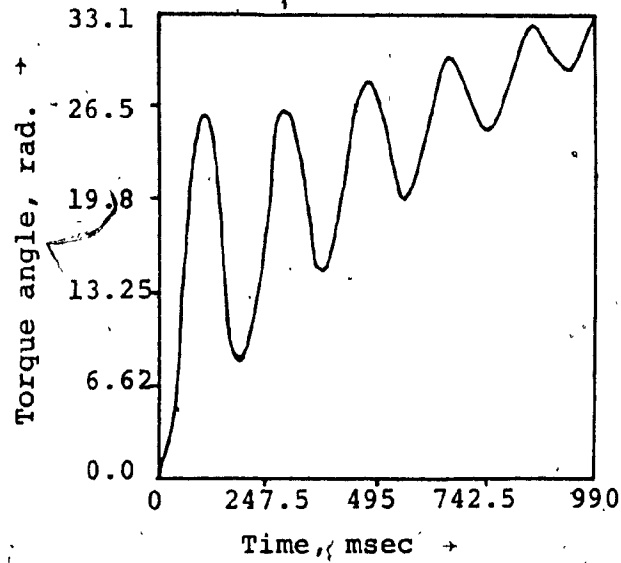
Figure 5.6   Torque Angle Response for Load Torque
             Input
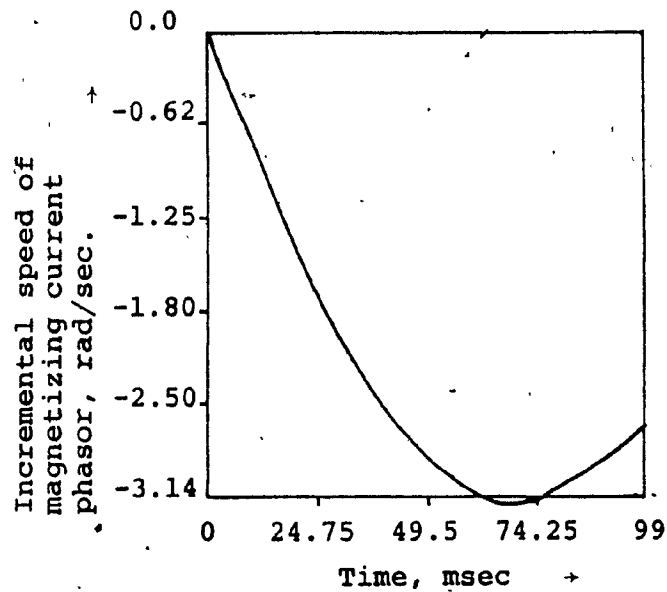


Figure 5.7   Incremental Magnetizing Current Phasor
             Speed for Load Torque Input .

$$\left(R_r + \frac{X_r}{\omega_b} p\right) i_{qr} + \frac{(\omega_e - \omega_r)}{\omega_b} X_r i_{dr} = -\frac{X_m}{\omega_b} i_{qs} - \frac{(\omega_e - \omega_r)}{\omega_b} X_m i_{ds}$$

(5.31)

$$\frac{-(\omega_e - \omega_r)}{\omega_b} X_r i_{qr} + \left(R_r + \frac{X_r}{\omega_b} p\right) i_{dr} = \frac{(\omega_e - \omega_r)}{\omega_b} X_m i_{qs} - \frac{X_m}{\omega_b} p i_{ds}$$

(5.32)

As $i_{ds} = 0$ due to the alignment of the axes, and perturbing the equations around an operating point, the equations (5.31) and (5.32) are arranged in the form given below:

$$\begin{bmatrix} p \delta i_{qr} \\ p \delta i_{dr} \end{bmatrix} = \begin{bmatrix} \dfrac{-R_r \omega_b}{X_r} & \omega_{s\ell o} \\ -\omega_{s\ell 0} & \dfrac{-R_r \omega_b}{X_r} \end{bmatrix} \begin{bmatrix} \delta i_{qr} \\ \delta i_{dr} \end{bmatrix}$$

(5.33)

$$+ \begin{bmatrix} \dfrac{X_m}{X_r} p & i_{dro} \\ \omega_{s\ell o} \dfrac{X_m}{X_r} & \left(i_{qro} + \dfrac{X_m}{X_r} i_{qso}\right) \end{bmatrix} \begin{bmatrix} \delta i_{qs} \\ \delta \omega_{s\ell} \end{bmatrix}$$

For the load torque input case, $\delta i_{qs}$ is constrained to be zero and treating the change in slip frequency $\delta \omega_{s\ell}$ as an input, the roots of the characteristic equation for (5.33) become,

$$\lambda_{1,2} = \frac{-R_r \omega_b}{X_r} \pm j \omega_{s\ell o}$$

(5.34)

and hence the time constant of the rotor currents is equal to

$$\frac{R_r}{L_r} \qquad\qquad (5.35)$$

= Rotor time constant

Note that the stator current magnitude and frequency are not disturbed and hence the change in rotor current alone affects the torque angle. Therefore, the time constant associated with incremental rotor current can be equated to that of the incremental torque angle.

Case (ii): VSIM drive

Neglecting the stator resistance and stator leakage inductances, the stator equations are given by:

$$L_m p i_{qs} + \omega_e L_m i_{ds} + L_m p i_{qr} + \omega_e L_m i_{dr} = V_{qs} \qquad (5.36)$$

$$-L_m \omega_e i_{qs} + L_m p i_{ds} - \omega_e L_m i_{qr} + L_m p i_{dr} = V_{ds} \qquad (5.37)$$

Taking the corresponding small-signal equations and with the following constraints imposed:

$$\delta V_{qs} = 0 \qquad\qquad (5.38)$$

$$\delta V_{ds} = 0 \qquad\qquad (5.39)$$

Rearranging the equations gives:

$$\begin{bmatrix} p & \omega_e \\ -\omega_e & p \end{bmatrix} \begin{bmatrix} \delta i_{qs} \\ \delta i_{ds} \end{bmatrix} = \begin{bmatrix} -p & -\omega_e \\ \omega_e & p \end{bmatrix} \begin{bmatrix} \delta i_{qr} \\ \delta i_{dr} \end{bmatrix} \qquad (5.40)$$

From equation (5.40),

$$\delta i_{qs} = -\delta i_{qr} \qquad (5.41)$$

$$\delta i_{ds} = -\delta i_{dr} \qquad (5.42)$$

Substituting equations (5.41) and (5.42) in the small-signal rotor equations, with the assumption that $\delta\omega_{s\ell}$ is an input, it is obtained:

$$\begin{bmatrix} p\delta i_{qr} \\ p\delta i_{dr} \end{bmatrix} = \begin{bmatrix} \dfrac{-R_r}{L_{\ell r}} & -\omega_{s\ell o} \\ -\omega_{s\ell o} & \dfrac{-R_r}{L_{\ell r}} \end{bmatrix} \begin{bmatrix} \delta i_{qr} \\ \delta i_{dr} \end{bmatrix}$$

$$+ \begin{bmatrix} -L_{\ell r} i_{dro} \\ L_{\ell r} i_{qro} \end{bmatrix} \delta\omega_{s\ell} \qquad (5.43)$$

and hence rotor currents' time constant is given by

$$\frac{R_r}{L_{\ell r}} \qquad (5.44)$$

As the change in rotor currents is reflected instantaneously in stator currents, the torque angle change is associated with the change in rotor currents. Hence the time constant of rotor currents can be directly related to the time constant of torque angle.

## 5.5 Stability Considerations with Torque Angle Feedback

The incremental torque angle is given as

$$\delta\theta = [a]\delta i_{qs} + [b_1]\delta i_{qr} + [c_1]\delta i_{dr} \tag{5.45}$$

where

$$b_1 = a \tag{5.46}$$

$$c_1 = \frac{-a}{\tan\theta} \tag{5.47}$$

The values $a$ and $c_1$ are calculated for various operating points and are shown in the Table 5.3. It is assumed that only torque angle is used for feedback and that too for determining the stator frequency. It corresponds to,

$$\delta\omega_e = \delta\omega_{ref} + K_1(\delta\theta_{ref} - \delta\theta)$$

$$= \delta\omega_{ref} + K_1\delta\theta_{ref} - K_2\delta i_{qr} - K_2\delta i_{qr} \tag{5.48}$$

$$+ \frac{K_2}{\tan\theta}\delta i_{dr}$$

## Table 5.3

### Coefficients of Incremental Torque Angle

Frequency = 377 rad/sec.,

Stator current (Magnitude) = 1.0 p.u.

| Ser. No. | Slip | Torque p.u. | Torque Angle,deg. | a | $c_1$ |
|---|---|---|---|---|---|
| 1 | 0.002 | 0.309 | 19.4 | −0.354 | 1.006 |
| 2 | 0.004 | 0.453 | 34.6 | −0.708 | 1.025 |
| 3 | 0.006 | 0.469 | 45.1 | −1.061 | 1.057 |
| 4 | 0.008 | 0.437 | 52.03 | −1.411 | 1.018 |
| 5 | 0.010 | 0.393 | 56.63 | −1.175 | 1.158 |
| 6 | 0.012 | 0.352 | 59.7 | −2.104 | 1.227 |
| 7 | 0.014 | 0.315 | 61.84 | −2.444 | 1.308 |
| 8 | 0.016 | 0.284 | 63.3 | −2.780 | 1.401 |
| 9 | 0.018 | 0.258 | 64.1 | −3.114 | 1.505 |
| 10 | 0.020 | 0.236 | 64.76 | −3.436 | 1.619 |

where

$$K_2 = K_1 a$$
$$= -K_3 \qquad\qquad (5.49)$$

The A and B matrices for the open loop CSIM drive are numerically computed in p.u. values for the following operating point and are given below:

The operating point: Stator frequency = 377 rad/sec, slip = 0.0125, electromagnetic torque = 0.97 p.u., stator current (quadrature axis) = 1.6826 p.u. The base values are defined in Appendix-III.

$$A = \begin{bmatrix} -10.88 & 5.04 & -927.9 & -545.2 \\ 10.35 & -6.81 & 878.3 & 737.6 \\ 4.48 & 4.71 & -2.02 & -93.87 \\ 1.21 & 0 & 3.53 & 0 \end{bmatrix} \qquad (5.50)$$

$$B = \begin{bmatrix} 285.91 & 0 \\ -272.0 & -218.75 \\ 0 & 93.87 \\ 0 & 0 \end{bmatrix} \qquad (5.51)$$

Substituting (5.48) in (5.51) and obtaining the closed-loop matrix

$$A_c = \begin{bmatrix} -10.88 & 5.04 & -927.9 & -545.2 \\ (10.35- \atop -218.75K_3 & (-6.81 \atop -218.75K_3 & (878.3+ \atop \frac{218.75K_3}{\tan\theta}) & 737.6 \\ (4.48+ \atop 93.87K_3) & (4.71+ \atop 93.8TK_3) & \{-2.02- \atop \frac{K_3}{\tan\theta}93.87\} & -93.87 \\ 1.21 & 0 & 3.53 & 0 \end{bmatrix}$$

$$\tag{5.52}$$

The characteristic equation of matrix $A_c$ is

$$\lambda^4 + a_p\lambda^3 + a_2\lambda^2 + a_3\lambda + a_4 = 0 . \tag{5.53}$$

Evaluating,

$$a_p = -(a_{11} + a_{22} + a_{33}) \tag{5.54}$$

$$a_2 = a_{14}a_{41} + a_{34}a_{43} + a_{11}a_{22} + a_{22}a_{33}$$

$$+ a_{33}a_{11} - a_{13}a_{31} - a_{12}a_{21} - a_{23}a_{32}$$

$$= \{-917.88 - 78606K_3 + \frac{630}{\tan\theta}K_3\} \tag{5.55}$$

For stability, one essential condition is that the coefficients of the characteristic equation must be positive. For a CSIM drive, the operating point must be on the statically unstable portion of the torque-speed

characteristic and thus the angle $\theta$ cannot approach zero and must be greater than at pull-out torque. For the machine whose properties are given in Table 5.3 this angle must then be greater than 45 degrees. Therefore there is no positive value of $K_3$ for which $a_2$ can be positive. Hence the system cannot be stabilized with only torque angle feedback. A slip speed current interface and or unity speed feedback loop have to be introduced along with torque angle loop for stabilization. Note in that case, the first and fourth columns of the closed-loop matrix are modified for such feedbacks and depending upon the values of feedback controllers, stabilization is achieved.

CHAPTER 6

CONTROL CHARACTERISTICS OF INVERTER-FED
INDUCTION MOTOR DRIVES

## 6.1 Introduction

Efficient use of an inverter-fed induction motor
drive necessitates a knowledge of the characteristics of
the induction motor from a control point of view. The
characteristics of both the VSIM and CSIM drives are
investigated, neglecting the filter time constants in the
link and in the feedback loops. Of particular interest
is the role of the voltage/current and frequency inputs
in the drive performance. Their effects on variables that
are not often discussed such as torque angle, stator real
power, air-gap flux-linkages and stator and rotor voltages/
currents are studied. They are useful in the independent
control of these variables and in the design of respective
feedback loops to control the same. A by-product of this
aspect of the study leads to the nature of feedback sig-
nals and their suitability for control purposes. The link
filter is incorporated in CSIM drive study and it has
little effect on the relative suitability of signals for
feedback control. To enhance the value of the results
arrived at for open-loop CSIM drives, a closed-loop CSIM
drive with torque angle feedback and a slip speed current
interface is included.

## 6.2 Transfer Functions of the Open-Loop Drives

The various transfer functions of the drives are computed following the procedure outlined in Appendix-IV. Table 6.1 lists the CSIM drive transfer functions and Table 6.2 contains the VSIM drive transfer functions. A glance at these transfer functions reveals a striking difference between the CSIM and the VSIM drive in their output speed behaviour for stator frequency input. The frequency input makes the CSIM drive's speed follow the input frequency without an error whereas for the VSIM drive, the rotor follows with an error on open-loop. This is explained in the following manner:

Frequency input does not change the steady-state value of the rotor current magnitude in a CSIM drive for constant load torque and stator current, as seen from the computed steady-state gain listed in Table 6.1. The inference is that the slip changes in a way that the magnetizing and rotor branch impedances maintain their relative magnitudes and hence the division of current amongst themselves is not changed. Therefore, the slope of the speed-torque characteristic for the new frequency will be the same as that of the previous operating frequency. Moreover, to generate the same electromagnetic torque, the slip speed has to remain the same and for increasing stator frequency the slip will decrease. Let subscripts 1 and 2 denote the variables before and after a frequency perturbation. If

Table 6.1

Transfer functions of the CSIM drive

Operating point description: slip=0.005, $i_{qso}$=1.6826 p.u.,

$\omega_{eo}$=377 rad/sec, $T_{eo}$=1.335 p.u.

| OUTPUT | INPUT | | | | | |
| | CURRENT (MAGNITUDE) | | FREQUENCY | | LOAD TORQUE | |
| | SSG | ZERO | SSG | ZERO | SSG | ZERO |
|---|---|---|---|---|---|---|
| Electromagnetic torque, $\delta T_e$ | 0 | $0.3\times10^{-11}$, $-2.022\pm j3.346$ | 0 | $-0.435\times10^{-10}$, $-0.265$ | 1.0 | -0.2651 |
| Rotor mechanical speed, $\delta\omega_m$ | 0.0282 | $-2.022\pm j3.346$ | 0.333 | -0.26513 | -0.0177 | $-2.02\pm j1.885$ |
| Torque angle, $\delta\theta$ | -7.688 | -3.7068, $-20.06\pm j221.1$ | 0 | $-0.493\times10^{-12}$, -1.9372 | 4.844 | -1.937 |
| $\delta v_{qs}$ | — | — | 1.586 | -0.264, -5.66 | 1.188 | -0.2676, 4006.6 |
| Rotor current magnitude | -9.249 | $-8.75\pm j14.21$, 15.47 | 0 | $0.29\times10^{-11}$, -2.02 | 6.2374 | -2.02 |

POLES: -0.26436, -1.89±j33.81

*SSG - Steady-state gain

## Table 6.2

Transfer functions of the VSIM drive

Operating point: slip = 0.0125, POLES: -12.442+j63.613, -46.999±j374.157, -24.393

$V_{qso}$ =1.414, $T_{eo}$ =0.97, $\omega_{eo}$ =377 rad/sec

| OUTPUT | CURRENT (MAGNITUDE) | | INPUT FREQUENCY | | LOAD TORQUE | |
|---|---|---|---|---|---|---|
| | SSG | ZEROS | SSG | ZEROS | SSG | ZEROS |
| Electromagnetic torque | 0 | 0.12x10^-5, -11.7±j26.6, -111.9 | 0 | -0.5x10^-8, -24.196, 2123.3, -0.35x10^17 | 1.0 | -24.74, -24.8+j374.4 |
| Rotor mechanical speed | 0.00657 | -11.748±j26.6, -111.9 | 0.3242 | -24.196, 2123.3, -0.252x10^17 | -0.00479 | -25.29±j7.6, -46.34±j374.0 |
| Stator power | -0.0922 | 2.01, -13.23±j32.06, -112.69, -2320.3 | 3.038 | -2.1, -24.05, 1037.15, -1154.3 | 3.1547 | -24.93, -22.9±j378.8 |
| Stator current real comp. | -1.01 | 47.72, -45.06, -38.16±j39.9 | 1.4321 | -2.1, -24.05, 1037.1, -1154.28 | 1.487 | -24.934, -22.94±j378.8, |
| Air-gap flux linkages | 0.5134 | -41.0, -13.72±j64.65, 6.49x10^3 | 0.7157 | -31.49, -51.84±j53.36, -81.75 | -0.03 | -51.24, -87.28±j60.14 |
| Torque angle | -0.5135 | -19.322, -32.145±j65.75, 138.2 | 0.7112 | -3.783, -24.82, -1197.3, -0.288x10^17 | 0.374 | -23.76, -26.93±j385.3 |
| Rotor current (Magnitude) | -1.16 | 30.51, -18.76±j40.3, -129.3 | 1.608 | -2.36, -23.286, 2152.2 | 1.604 | -26.16, -24.58±j374.9 |

$\omega_e$ is the electrical stator frequency in rad/sec

$\omega_r$ is the electrical rotor speed in rad/sec

$s_o$ is the slip

the equal slip speed condition is given by

$$s_{01}\omega_{e1} = s_{02}\omega_{e2} \tag{6.1}$$

then,

$$\omega_{r1} = (1.0 - s_{01})\omega_{e1} \tag{6.2}$$

$$\omega_{r2} = (1.0 - s_{02})\omega_{e2} \tag{6.3}$$

Change in rotor speed = $\delta\omega_r$

$$= (1.0 - s_{02})\omega_{e2} - (1.0 - s_{01})\omega_{e1}$$

$$= \omega_{e2} - \omega_{e1} + s_{01}\omega_{e1} - s_{02}\omega_{e2}$$

$$= \omega_{e2} - \omega_{e1} \tag{6.4}$$

= change in stator frequency

It may be seen that the rotor follows the stator frequency without an error in the CSIM drive.

In a VSIM drive, frequency input decreases the flux and hence the slope of the speed-torque characteristic decreases. To generate the same electromagnetic torque, the slip is bound to increase over the previous value. Hence there is a tracking error in rotor speed in the steady-state for stator frequency changes.

## 6.3  Time Responses of the CSIM Drive

An input of magnitude 0.02 p.u. is applied. The transient responses of the variables are normalized for plotting. The rise time of the variable is the time taken to rise to 90% of the new steady-state value and the rate of change of variable is the time derivative of the variable in the first 100 msec. The transient responses due to current/voltage (magnitude) are not considered in detail due to the fact that they are not independent inputs in a drive scheme and are related to frequency and load torque inputs.

Frequency input produces similar responses of electromagnetic torque, torque angle and stator quadrature axis voltage as shown in Figure 6.1. As the steady-state gains of the electromagnetic torque and torque angle are zero, rise time has no meaning whereas the rise time for stator voltage (magnitude) is in the order of 2 to 3 msec. The responses for load torque input are similar for electromagnetic torque and stator voltage (magnitude) and in the case of torque angle, the response is identical only for first 100 msec, as shown in Figure 6.2. The rise time for stator voltage (magnitude) and electromagnetic torque are nearly equal, whereas the rise time of torque angle is very large and exceeds three seconds. In contrast is the 8 msec rise time of mechanical rotor speed. It is to be noted that there is no linear relationship between the electromagnetic torque and incremental rotor speed beyond
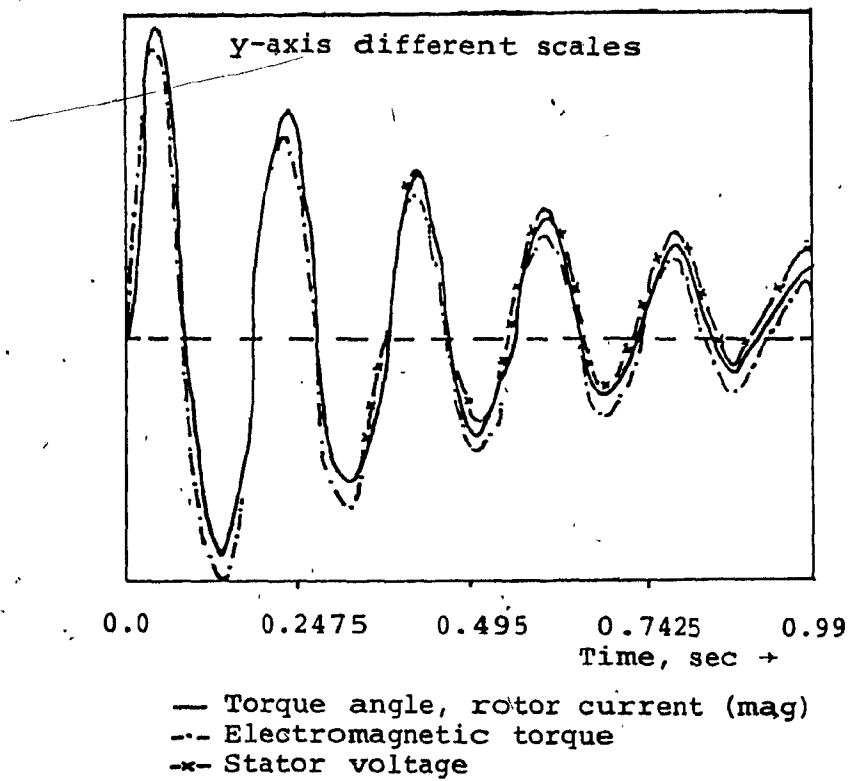
Figure 6.1  CSIM Responses for Frequency Input.

y-axis different scales

| 0.0 | 0.2475 | 0.495 | 0.7425 | 0.99 |

Time, sec →

——  Torque angle, rotor current (mag)
---- Electromagnetic torque
—x— Stator voltage (mag)
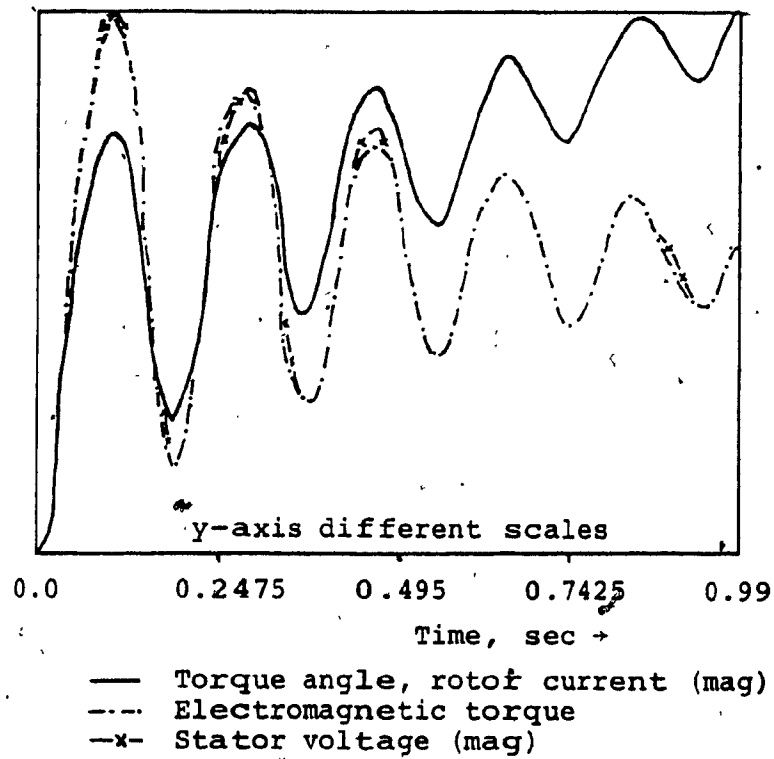
Figure 6.2  CSIM Responses for Load Torque Input

100 msec, and hence one cannot be substituted for the other in the feedback. The rise times and rate of change of variables are given in Table 6.3.

## 6.4 Time Responses of VSIM Drive

The steady-state operating point is that given in Table 6.2. Figures 6.3 and 6.4 show the time responses of the variables in a VSIM drive for frequency and load torque inputs, respectively. For the first 99 msec, the responses of stator power, real component of stator current, magnitude of rotor current and electromagnetic torque for the frequency input are almost identical with the torque angle leading in response by 3 to 5 msec. This trend is repeated by these variables for load torque input, shown in Figure 6.4. The change in rotor speed, the negative of which is the instantaneous slip, is plotted in Figure 6.4 and on comparison with electromagnetic torque, it is observed that there is no linear relationship between them. The rise times and their initial rates of change are given in Table 6.4.

## 6.5 Superiority of Frequency Input Over Current/Voltage Input

The stator dynamics were neglected in the CSIM drive and therefore no time delay was involved in the change of

## Table 6.3

### CSIM drive:  open loop response characteristics

(Magnitude of each input = 0.02 p.u.)

Note: $t_r$ - rise time, msec

$\frac{d}{dt}$ (output) - rate of change in p.u. quantities/sec.

| OUTPUT | INPUT | | | | | |
| --- | --- | --- | --- | --- | --- | --- |
| | CURRENT (MAGNITUDE) | | FREQUENCY | | LOAD TORQUE | |
| | $t_r$,msec | $\frac{d}{dt}$ (output) | $t_r$,msec | $\frac{d}{dt}$ (output) | $t_r$,msec | $\frac{d}{dt}$ (output) |
| Electromagnetic torque | 0 | 0.4657 | 0 | 9.861 | 45.0 | 0.591 |
| Rotor mechanical speed | 17.0 | 0.0068 | 48.0 | 0.194 | 8.0 | -0.01328 |
| Torque angle | >1000 | -0.345 | 0 | 6.334 | >1000 | 0.423 |
| Stator voltage magnitude ($\delta V_{qs}$) | - | - | 2.5 | 11.745 | 48.5 | 0.6833 |
| Rotor current magnitude | >1000 | -0.355 | 0 | 6.736 | >1000 | 0.453 |
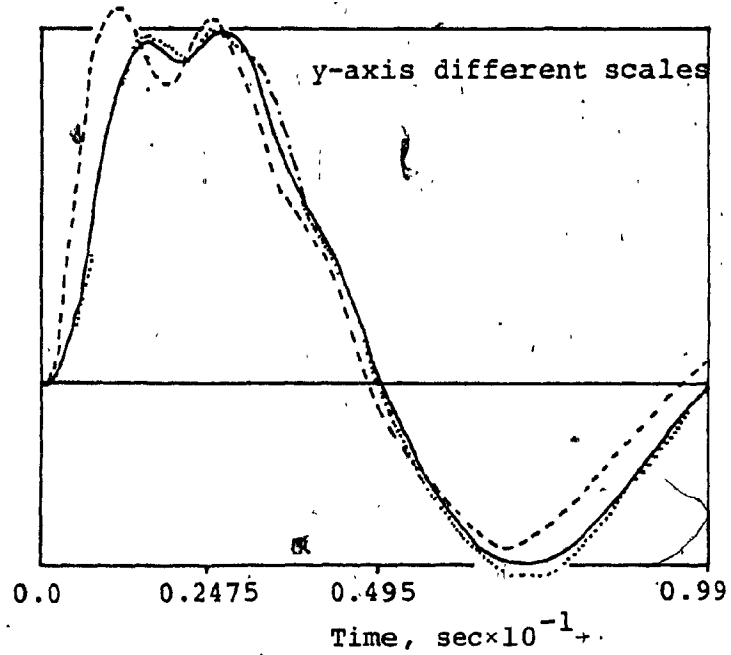
- Stator power, stator real current
-- Torque angle,
-.. Rotor current (mag)
.... Electromagnetic torque

Figure 6.3  VSIM Responses for Frequency Input

y-axis different
scales

0        0.2475        0.495        0.7425        0.99

Time, sec×10$^{-1}$ →

— Electromagnetic torque, stator power,
  stator real current
-- Torque angle,
--- Rotor current (mag)
-×-Negative of rotor speed
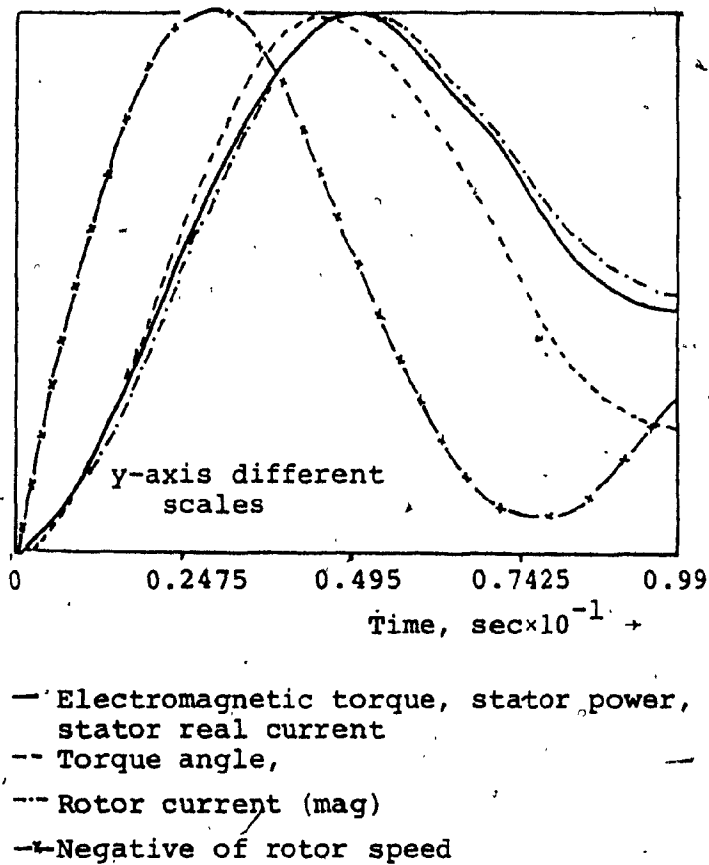
Figure 6.4   VSIM Responses for Load Torque Input

Table 6.4

VSTM drive on open loop:
Response characteristics

| OUTPUT | INPUT | | | | | |
| | VOLTAGE (MAGNITUDE) | | FREQUENCY | | LOAD TORQUE | |
| | $t_r$ msec | $\frac{d}{dt}$ (output) | $t_r$ msec | $\frac{d}{dt}$ (output) | $t_r$ msec | $\frac{d}{dt}$ (output) |
|---|---|---|---|---|---|---|
| Electromagnetic torque | 0 | 2.7345 | 0 | 42.86 | 25.67 | 0.9783 |
| Rotor mechanical speed | 4.0 | 0.0426 | 27.5 | 0.3284 | 6.5 | -0.01379 |
| Stator power | 0 | 60.92 | 3.0 | 153.2 | 26.4 | 2.772 |
| Stator current, real component | 0 | 28.68 | 3.5 | 53.5 | 27.0 | 1.2619 |
| Air-gap flux-linkages | 7.0 | 1.722 | 5.75 | -0.2978 | 38.5 | 0.0189 |
| Torque angle | 2.5 | 16.379 | 1.75 | 48.22 | 18.75 | 0.424 |
| Rotor current (magnitude) | 0.5 | 30.976 | 3.5 | 63.26 | 27.0 | 4.049 |

current magnitude.  It is to be observed that their input
magnitudes are the same, i.e., 0.02 p.u.  In spite of all
these, the frequency input produces greater rate of change
of variables than the current magnitude input is clearly
demonstrated from the Tables 6.3 and 6.4.  It is true for
both the VSIM and CSIM drives.  To evaluate in full the
superiority of frequency input over the current/voltage
(magnitude) input, the steady-state gains and the rate of
change of variables are normalized in terms of the  cor-
responding load torque produced steady-state gain and rate
of change of variables.  These are given in Tables 6.5 and
6.6.  In both types of drives, a lower p.u. frequency
input than current/voltage (magnitude) input will produce
a specified level of response of major output variables
such as rotor speed.


## 6.6  Control Characteristics of Drive Signals and Their
### Suitability for Feedback Control

The control characteristic of a drive signal is asses-
sed from its rise time.  It indicates the speed with which
the particular drive signal is capable of portraying the
true state of the drive under all conditions.  From Tables
6.3 and 6.4 it is seen that load torque change is identi-
fied in the shortest time by rotor mechanical speed.  Torque
angle gives the quickest indication of frequency change.
This applies to both CSIM and VSIM drives.  Hence for both

## Table 6.5

Magnitudes of rate of change of variables expressed in p.u. basis, with reference to load torque input produced rate of change.

| OUTPUT | CSIM INPUT | | VSIM INPUT | |
|---|---|---|---|---|
| | CURRENT (MAGNITUDE) | FREQUENCY | VOLTAGE (MAGNITUDE) | FREQUENCY |
| Electromagnetic torque | 0.787 | 16.68 | 2.795 | 43.81 |
| Rotor mechanical speed | 0.511 | 14.60 | 3.089 | 23.81 |
| Torque angle | 0.815 | 14.97 | 38.62 | 113.72 |
| Stator voltage (magnitude) | - | 17.18 | - | - |
| Stator power | - | - | 21.97 | 55.26 |
| Stator current real component | - | - | 22.72 | 42.39 |
| Rotor current (magnitude) | 0.7836 | 14.869 | 7.65 | 15.62 |
| Air-gap flux-linkages | - | - | 91.11 | 15.75 |

Table 6.6

Magnitudes of steady-state gains expressed with
reference to load torque input steady-state gains

| OUTPUT | CSIM INPUT | | VSIM INPUT | |
|---|---|---|---|---|
| | CURRENT (MAGNITUDE) | FREQUENCY | VOLTAGE (MAGNITUDE) | FREQUENCY |
| Electromagnetic torque | 0 | 0 | 0 | 0 |
| Rotor mechanical speed | 1.59 | 18.83 | 1.371 | 67.68 |
| Torque angle | 1.587 | 0 | 1.372 | 1.90 |
| Stator voltage (magnitude) | - | 1.335 | - | - |
| Stator power | - | - | 0.029 | 0.963 |
| Stator current, real component | - | - | 0.699 | 0.963 |
| Rotor current (magnitude) | 1.482 | 0 | 0.723 | 1.002 |
| Air-gap flux-linkages | - | - | 17.113 | 23.856 |

load torque disturbance and reference change, there is no
single drive variable that could indicate them in the mini-
mum time possible. For instance, if rotor mechanical speed
is used to meet the two types of changes, it would be bene-
ficial in the case of load torque change. But for a fre-
quency input change, this is the least desirable signal for
feedback. The second best signal to indicate load torque
change is torque angle in the case of VSIM drive and elec-
tromagnetic torque in the CSIM drive. Similarly, for the
reference frequency change, the second best signal is rotor
current magnitude or stator power.

From the transient responses shown in Figures 6.1, 6.2,
6.3 and 6.4, it is observed that magnitude of rotor cur-
rent follows closely the torque angle. Hence the magnitude
of rotor current can be substituted for torque angle in
feedback. This simplifies the measuring and or calculating
circuit in comparison to the torque angle measuring and
calculating circuit.

In all the fast response drive schemes such as syn-
chronous control scheme and field-oriented control scheme,
it is noticed that both rotor mechanical speed and torque
angle are utilized for control. Therefore, the load tor-
que and reference frequency changes are fastly detected and
accordingly good dynamic control is exercised.

## 6.7  Closed-Loop CSIM Drive

An open-loop CSIM drive is unstable for desired opera-
ting points and hence all CSIM drives have closed-loop
operation.   Therefore, it becomes necessary to verify the
results of the above sections for a closed-loop CSIM drive.
For this purpose a closed-loop scheme given in Figure 6.5
is chosen.   The torque angle reference  $\theta_{ref}$,  may be either
generated by slip speed signal or any other suitable sig-
nal.   The model considered for this study is simple and a
change of slip speed will alter the current reference
instantaneously.  Stator dynamics and link filter are neg-
lected.

For a controller gain of  K=0.1, the transfer functions
are given in Table 6.7.   Their time responses are shown in
Figures 6.6 and 6.7 for reference frequency change and
load torque disturbance, respectively.   The improvement in
responses and stabilizing effect is obvious.   From these
transient responses of the variables, it is seen that the
results of the section 6.6 is in agreement for the closed-
loop drive too.   Note the close similarity between the
torque angle and rotor current magnitude responses, re-
gardless of the input.   It is very important to realise
that torque angle and electromagnetic torque cannot be
substituted for one another in a feedback scheme as they
have different control characteristics.
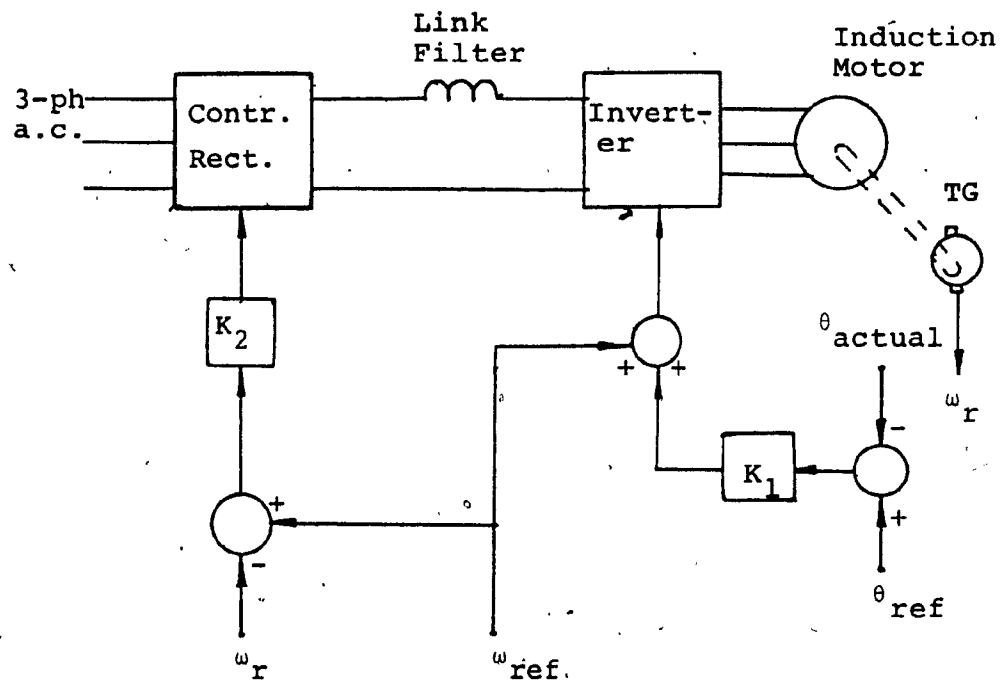
Figure 6.5  Angle Feedback Strategy for CSIM Drive

Table 6.7

CSIM drive with the angle feedback and a slip speed-current interface

$K_1 = 0.1$, $T_{eo} = 0.97$, $I_{qso} = 1.6826$ p.u.

| OUTPUT | INPUT | | | | | |
| --- | --- | --- | --- | --- | --- | --- |
| | CURRENT (MAGNITUDE) | | FREQUENCY | | LOAD TORQUE | |
| | SSG | ZEROS | SSG | ZEROS | SSG | ZEROS |
| Electromagnetic torque | 0.832 | -4.28,-36.89, -61.03 | 0 | $0.35 \times 10^{-11}$, -4.26 | 0.278 | -4.26 |
| Rotor mechanical speed | 0.0096 | -4.28, -36.89 | 0.333 | -2.48, -44.1 | -0.00832 | -2.11, -37.35 |
| Torque angle | -0.283 | -3.21, $-50.8 \pm j82.39$ | 0 | $0.8 \times 10^{-11}$ -2.28 | 0.2456 | -2.28 |
| Stator voltage magnitude | - | - | 1.152 | -2.11, -11.6 | 0.298 | -4.62 1170.9 |
| Rotor current magnitude | 0.699 | -2.25, -43.85, -54.09 | 0 | $+0.8 \times 10^{-11}$ -2.14 | 0.152 | -2.14 |

Poles: -2.495,
-49±j16.678
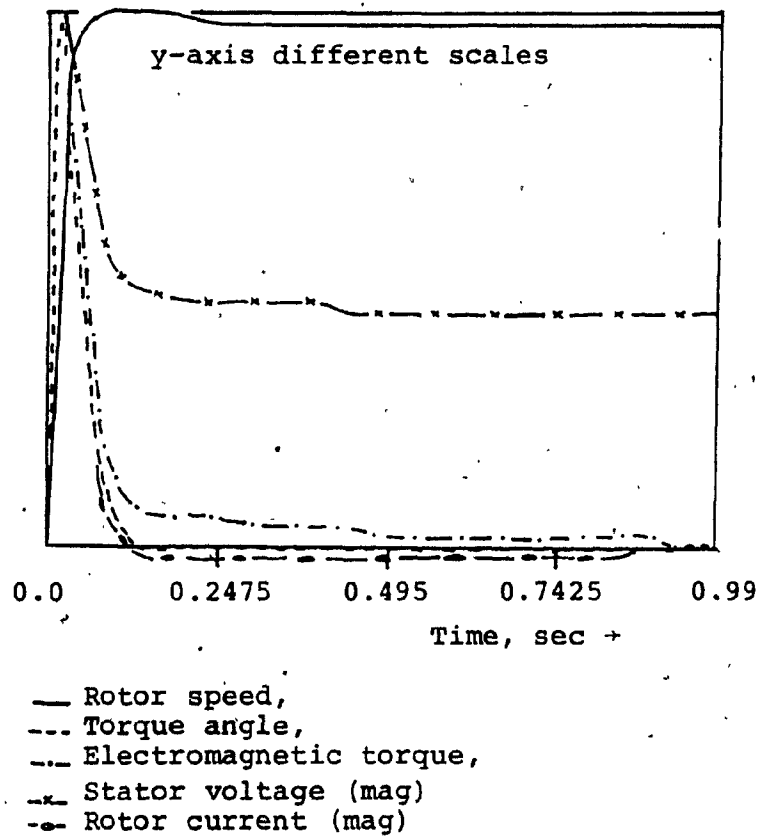
Figure 6.6   Closed Loop Responses of CSIM for
            Frequency Input

y-axis different scales

0.0          0.2475          0.495          0.7425    0.99
                               Time, sec →

——— Negative of rotor speed
—.. Torque angle
—.— Electromagnetic torque
—::- Stator voltage (mag)
—•— Rotor current (mag)
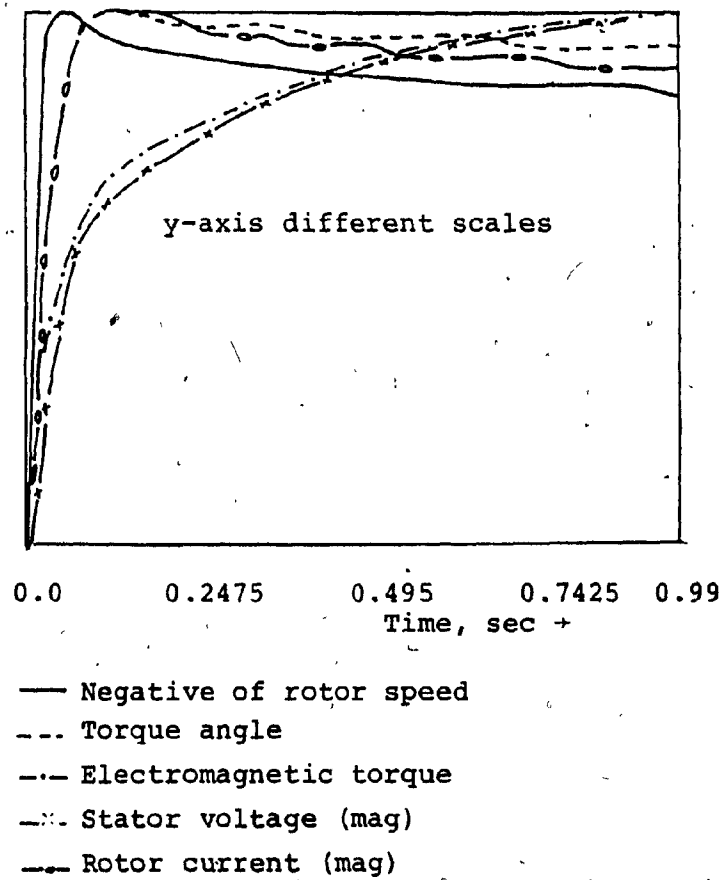
Figure 6.7   Closed Loop CSIM Responses for Load Torque
             Input

## 6.8  Effect of Link Filter

Conventional CSIM drives have a D.C. link filter and hence the validity of the results must be verified by a model including the D.C. link filter.  Along with the link filter, stator dynamics are also included in the model. The rise times of variables and the rate of change of variables with and without link filter are given in Tables 6.8 and 6.9 respectively.  They adequately reinforce the results of the previous sections.  To illustrate the results in the case of a CSIM drive with D.C. link filter included, the results are normalized with respect to corresponding load torque produced steady-state gains and rate of change of variables.  This is listed in Table 6.10 and it clearly demonstrates the superiority of frequency input over link voltage input.  Hence the incorporation of the link filter has little effect on the superiority of frequency input and on the suitability of a feedback signal.

## Table 6.8

Rise times and rate of change of variables
for the CSIM drive without D.C. link filter

| OUTPUT | INPUT | | | | | |
|---|---|---|---|---|---|---|
| | Link Voltage | | Frequency | | Load Torque | |
| | Rise time, ms | Rate of change | Rise time, ms | Rate of Change | Rise time, ms | Rate of Change |
| Electromagnetic Torque | 575 | 0.01 | 0.0 | 2.1 | 643.5 | 0.0864 |
| Rotor Mechanical Speed | 680 | 0.005 | 40.0 | 0.243 | 24.3 | 0.007 |
| Torque Angle | 325 | 0.099 | 0.0 | 3.20 | 58.2 | 0.081 |
| Stator voltage (magnitude) | - | - | 9.2 | 2.91 | 693.0 | 0.077 |
| Rotor current (magnitude) | 0 | 0.039 | 0.0 | 2.12 | 55.8 | 0.100 |

## Table 6.9

Rise times and rate of change of variables for the
CSIM drive with the D.C. link filter

| OUTPUT | INPUT | | | | | |
|---|---|---|---|---|---|---|
| | Link Voltage | | Frequency | | Load Torque | |
| | Rise time, ms | Rate of Change | Rise time, ms | Rate of Change | Rise time, ms | Rate of Change |
| Electromagnetic Torque | 0.0 | 2.85 | 0.0 | 88.0 | 35.71 | 1.86 |
| Rotor Mechanical Speed | 9.7 | 0.018 | 21.6 | 0.80 | 16.66 | 0.008 |
| Torque angle | 7.28 | 0.28 | 0.0 | 6.1 | 73.8 | 0.266 |
| Stator Voltage (Magnitude) | 600 | 0.41 | 2.0 | 28.6 | >500 | 0.60 |
| Rotor Current (Magnitude) | 24.76 | 2.67 | 0.0 | 131.7 | 17.85 | 6.0 |

## Table 6.10

CSIM drive with D.C. link filter

(Expressed in p.u. basis, with reference

to load torque produced changes)

| OUTPUT | STEADY-STATE GAIN | | RATE OF CHANGE | |
|---|---|---|---|---|
| | INPUT | | | |
| | Link voltage | Frequency | Link voltage | Frequency |
| Electromagnetic Torque | 0.0 | 0.0 | 1.54 | 47.31 |
| Rotor Mechanical Speed | 0.983 | 65.32 | 2.27 | 96.78 |
| Torque angle | 0.983 | 1.87 | 1.04 | 22.97 |
| Stator voltage (Magnitude) | 0.058 | 1.88 | 1.37 | 95.40 |
| Rotor current (Magnitude) | 0.273 | 0.52 | 0.89 | 43.91 |

## CHAPTER 7

## ANALYSIS AND DESIGN OF ANGLE CONTROLLED CSIM DRIVE

### 7.1 Introduction

Literature is available to design both the synchronous control scheme [44] and the field-oriented control scheme [61],[63],[66]. The systematic design of an angle control-led CSIM has to be started from scratch as there is not enough published material on this scheme. A step-by-step design procedure for the angle controlled CSIM drive is given in this chapter. The design of the inner current loop, linear relationship between reference and output of electromagnetic torque, maximum torque per ampere, speed controller and finally the frequency compensator constitute the core of the angle control scheme. For designing the frequency compensator, the commutation delay encountered in the inverter is modelled. Incorporation of this time delay into transfer function design techniques by a rational transfer function of Pade second order approximation is accurate. The effect of the commutation delay on drive dynamics is assessed in terms of the drive bandwidth. Experimental results of the drive are included to corroborate the design procedure.

## 7.2 Design of Current Control Loop

Synthesis of the current loop is made difficult due to:

    (i)    The input impedance of the induction motor varies with load condition.

    (ii)    The operating point is dependent upon many factors such as load torque, stator frequency and machine saturation.

The operating equations, even for a small-signal disturbance, will become four and hence a straight forward approach is ruled out. A simple and direct design of the current loop is possible by considering the physical insight provided by the steady-state equivalent circuit. The following assumptions are made:

    (i)    Airgap flux is constant

    (ii)    Change in load condition is reflected in the equivalent rotor resistance.

Then the load and D.C. link with the current loop is of the form given in Figure 7.1. The D.C. link filter and the stator can be represented by a block diagram and its transfer function is given by:

$$G_1(s) = \frac{1}{(R+sL)} \tag{7.1}$$

where
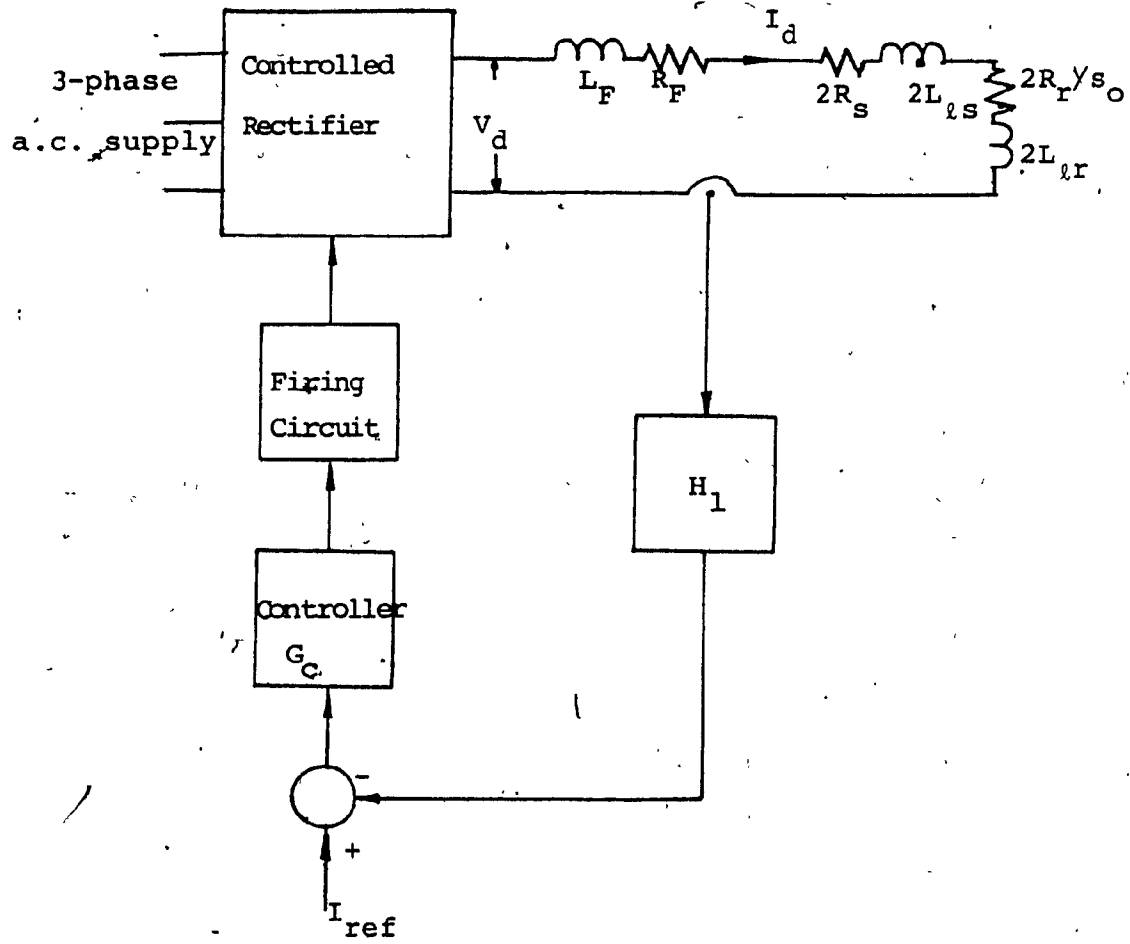
Figure 7.1 Current Control Loop with Load

$$R = R_F + 2R_s \tag{7.2}$$

$$L = L_F + 2L_{\ell s} \tag{7.3}$$

$$S_o = \text{slip}$$

The delay in the converter firing is represented by a transfer function of first order Pade approximation given as:

$$G_{dc}(s) = \frac{1-bs}{1+bs} \tag{7.4}$$

where

$2b=T$ = statistical average of delay = 1/12 of the

period of a.c. input waveform

= $(1/2)*(1/60)$ seconds $\tag{7.5}$

The first order approximation has errors in phase less than 4.7% upto 570 rad/sec and 7.8% upto 750 rad/sec. Also the irrational $e^{-Ts}$ is replaced by a rational transfer function suited to linear design techniques. The overall block diagram of the current loop is given in Figure 7.2 and let,

$$G_{d\ell}(s) = G_\ell(s) \; G_{dc}(s) \tag{7.6}$$
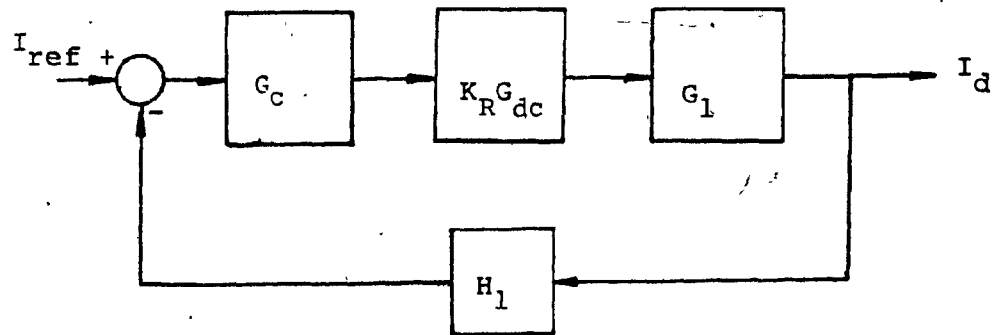
Figure 7.2

Overall block diagram of the current control loop



$$K_c = \frac{1}{R_i C_f}$$

$$T_c = R_f C_f$$
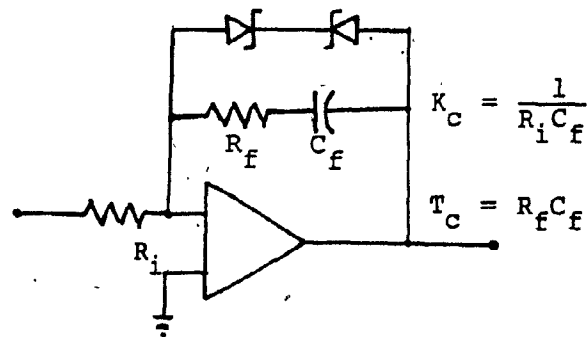
Figure 7.3

Current controller realization

### 7.2.1 Design of current controller

The current controller is chosen to be a proportional and integral controller of the form:

$$G_c(s) = K_c \frac{(1+sT_c)}{s} \qquad (7.7)$$

The transfer function of the link current and its reference is,

$$\frac{I_d}{I_{ref}}(s) = \frac{\frac{K_c(1+sT_c)}{s} \cdot K_R G_{dc} \cdot \frac{1}{R(1+s\frac{L}{R})}}{1+H_1 K_c \frac{(1+sT_c)}{s} \cdot K_R G_{dc} \frac{1}{R(1+s\frac{L}{R})}} \qquad (7.8)$$

Let

$$T_c = \frac{L}{R} \qquad (7.9)$$

Substituting equation (7.9) in (7.8),

$$\frac{I_d}{I_{ref}}(s) = \frac{\frac{K_c K_R G_{dc}}{R}}{s + \frac{H_1 K_c K_R G_{dc}}{R}} \qquad (7.10)$$

$$= \frac{K_a}{s+K_b} \qquad (7.11)$$

where

$$K_a = \frac{K_c K_R}{R} G_{dc} \qquad (7.12)$$

$$K_b = H_1 K_a \qquad (7.13)$$

Depending on the value of the gain of the current controller $K_c$, the rise time of the link current is controlled. The delay time in the converter can be overcome by adding a derivative of the current error singal to the control signal. The controller given in equation (7.7) is realized as shown in the Figure 7.3. The zener clamps are to limit the control signal on the lower and higher levels. For safe operation during inversion, the maximum triggering angle of the controlled rectifier is limited to 155°. A linear relationship between control signal and the output link voltage in the converter is obtained with cosine inverse firing of the converter

### 7.3 Strategy for Maximum Torque per Ampere and the Design of Current Reference Controller

For some applications of the drive, it is mandatory that maximum torque per ampere is extracted from the drive. The implementation criterion for such a strategy is developed from the steady-state operation of the induction motor. The electromagnetic torque of the induction motor is:

$$T_e = \frac{K_t}{R_r} \cdot \frac{\omega_{s\ell}}{1+(\omega_{s\ell} T_r)^2} \cdot [I_r^2 + I_m^2] \tag{7.14}$$

where

$$T_r = \frac{(L_m + L_{\ell r})}{R_r} \tag{7.15}$$

$$\omega_{s\ell} = s\omega_e \tag{7.16}$$

For maximum torque per ampere, the criterion is

$$I_m = I_r \tag{7.17}$$

In this case, then the drive has a variable air-gap flux for varying load conditions. From a practical point of view, it is desirable to have the motor operating with a certain minimum level of flux even under no load condition.

This is to enable the fast generation of electromagnetic torque upto the value corresponding to the minimum level of flux. Therefore, the minimum level of flux upto some load is chosen on the basis of load and dynamic requirements of the drive. For the present, this will be fixed at 0.25 p.u. Hence the magnetizing current vs rotor current relationship is slightly modified from equation (7.17) and is shown in Figure 7.4. From this figure, the stator current reference is obtained as:

$$I_{s,ref} = \sqrt{(0.25^2 + I_r^2)} \qquad , \; 0 < I_r < 0.25 \; p.u.$$

$$= \sqrt{2} \, I_r \qquad , \; 0.25 \leq I_r \leq 1.00 \qquad (7.18)$$

$$= \sqrt{1 + I_r^2} \qquad , \; I_r > 1.00 \; p.u.$$

## 7.4 Design of Linear Relationship Between Reference Input and Output of Electromagnetic Torque

Linearity in input-output relationship of electromagnetic torque is a necessity for torque regulated drives. This relationship is enforced by co-ordinating the stator current reference and slip frequency. Considering the outer speed loop and slip frequency loop of the angle control scheme, shown in Figure 7.5, the blocks to be inter-related are $G_2$ and $G_5$. Writing the outputs, $\omega_{s\ell}$, $I_r$ as functions of the torque reference,
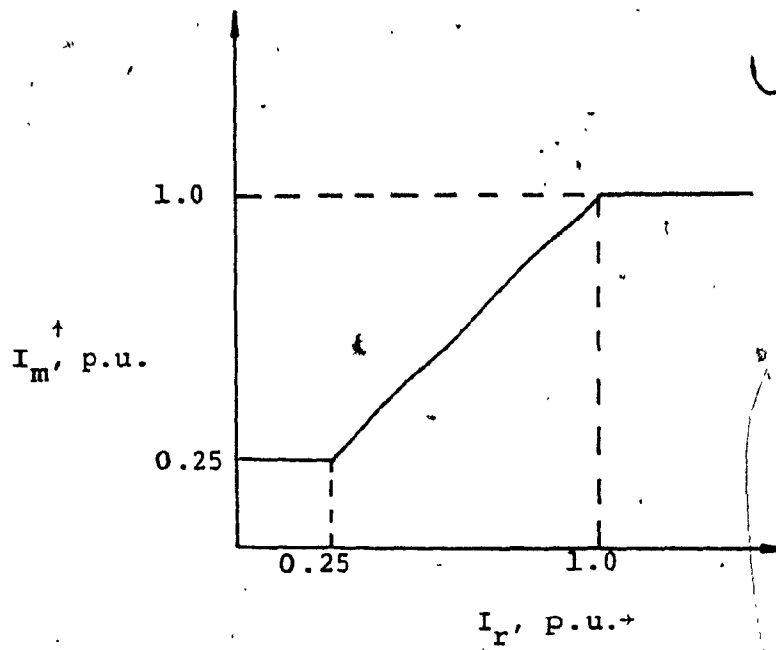
Figure 7.4  Modified  $I_m$  vs  $I_r$  Relationship
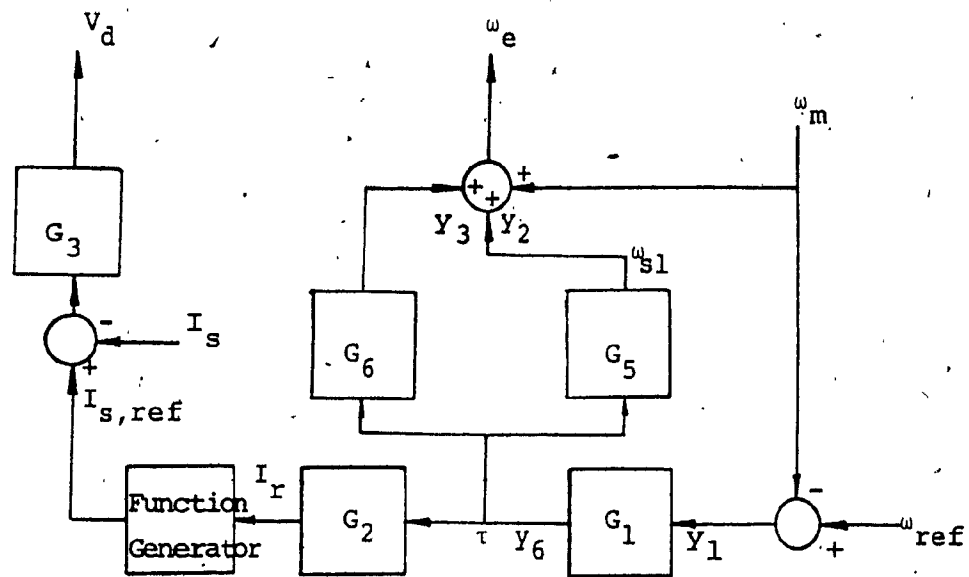
Figure 7.5  Outer Speed Loop and Slip Speed Loop of
the CSIM Drive

$$\omega_{s\ell} = K_5 \tau \qquad\qquad (7.19)$$

$$I_r = K_2 \tau = I_m \qquad\qquad (7.20)$$

Substituting equations (7.19) and (7.20) in (7.14),

$$T_e = \frac{K_t}{R_r} \; \frac{K_5 \tau}{1 + (K_5 \tau T_r)^2} \; 2K_2^2 \tau^2 \qquad\qquad (7.21)$$

For $T_e$ vs $\tau$ linearity, let

$$1 + (K_5 \tau T_r)^2 = K_5 K_2^2 \tau^2 \qquad\qquad (7.22)$$

i.e. $K_5^2 [T_r^2 \tau^2] - K_5 [K_2^2 \tau^2] + 1 = 0 \qquad\qquad (7.23)$

$$K_5 = \frac{K_2^2 \tau^2 \pm \sqrt{K_2^4 \tau^4 - 4T_r^2 \tau^2}}{2\tau^2 T_r^2} \qquad\qquad (7.24)$$

$$\omega_{s\ell} = K_5 \tau$$

$$= [\frac{K_2^2}{2T_r^2}]\tau \pm \sqrt{[\frac{K_2^2}{2T_r^2}]^2 \tau^2 - \frac{1}{T_r^2}} \qquad\qquad (7.25)$$

The flow-chart for the computation of slip frequency $\omega_{s\ell}$ is given in Figure 7.6. Note that this could be implemented with available analog components.

Substituting the value of (7.23) in (7.21),

$$\tau$$

$$\boxed{\text{Gain}=K_2^2/2T_r^2}$$

$$\boxed{\text{SQUARER}}$$

$$1./T_r^2 \longrightarrow \boxed{-\quad \text{ADDER}}$$

$$\boxed{\begin{array}{c}\text{SQUARE-}\\ \text{ROOTER}\end{array}}$$

$$\boxed{\begin{array}{c}+\\ \text{ADDER} \quad +\end{array}}$$

$$\omega_{S\ell}$$
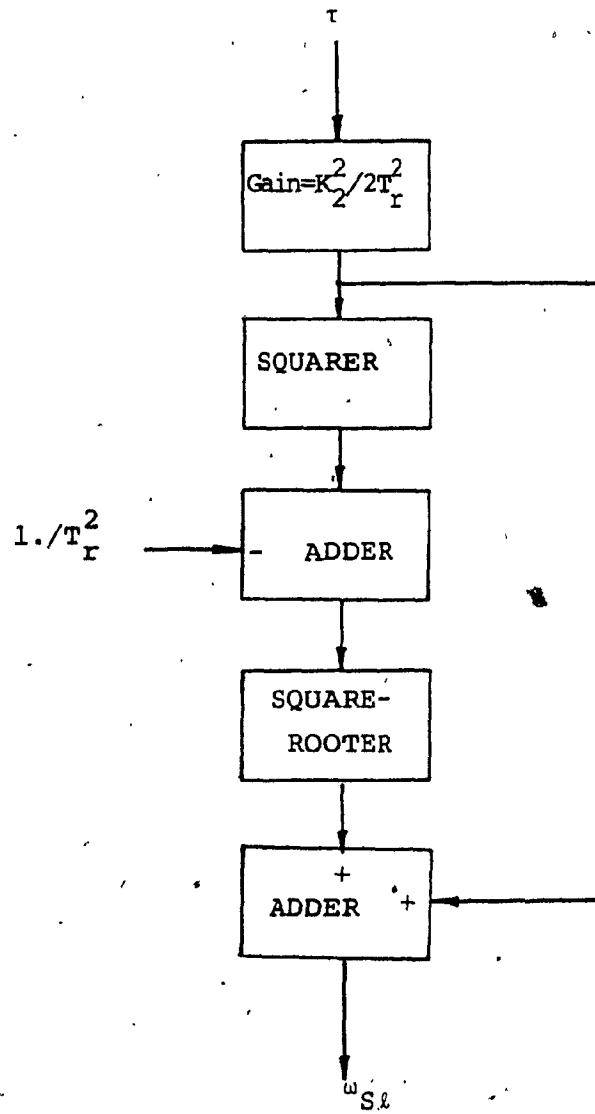
Figure 7.6. Flow-Chart for the Computation of Slip
Frequency

$$T_e = [2\frac{K_t}{R_r}]\tau \qquad\qquad (7.26)$$

Using equation (7.22) in (7.28),

$$T_{e,max} = \frac{2K_t}{R_r} \cdot \frac{I_r}{K_2} = \frac{2K_t}{R_r} \cdot \frac{I_m}{K_2} \qquad (7.27)$$

$$= K_{ta}I_r \qquad\qquad (7.28)$$

$$= K_{ta}I_m$$

where

$$K_{ta} = \frac{2K_t}{K_2 R_r} \qquad\qquad (7.29)$$

The equation (7.28) corresponds to a D.C. motor drive with either a constant field excitation or with constant armature current.

## 7.5  Design of Frequency Compensator and the Speed Controller

The frequency compensator supplies the incremental stator frequency to move the stator current phasor in phase, during load torque disturbance and frequency reference changes.  The design of this block then needs an understanding of the crucial phenomenon in the current source inverter, i.e., of the commutation delay.  A numerical quantification of commutation delay for an

operating point from the simple steady-state equivalent
of the induction motor and its incorporation in the design
via a second-order Pade approximation of $e^{-T_d s}$ is ac-
complished.

## 7.5.1 Commutation delay in the inverter

Hitherto, it is assumed that the inverter output fre-
quency follows the frequency input command without a time
delay. In an actual motor drive system there is a delay
dependent on motor operating point.

The current source inverter in Figure 7.7 with thyris-
tors T5 and T6 conducting is considered. The phase se-
quence is assumed to be A-B-C. At $t=t_1$ a signal is
given to increase motor frequency. For this purpose, the
current has to be transferred from the conducting phase
C to phase A. Firing of T1 at $t=t_1$ commutates T5. But
the current continues to flow into phase C, through T1
and D5 charging the commutation capacitors. As far as the
motor is concerned, nothing has changed. The current
starts to be transferred to phase A at $t=t_2$, only after
the diode D1 is forward biased. The transfer of current
from phase C to phase A is complete when diode D5 is
reverse biased, i.e., at $t=t_3$. In the current source
literature time $[t_2-t_1]$ is known as charging time and
interval $[t_3-t_2]$ is the transfer time. The sum of
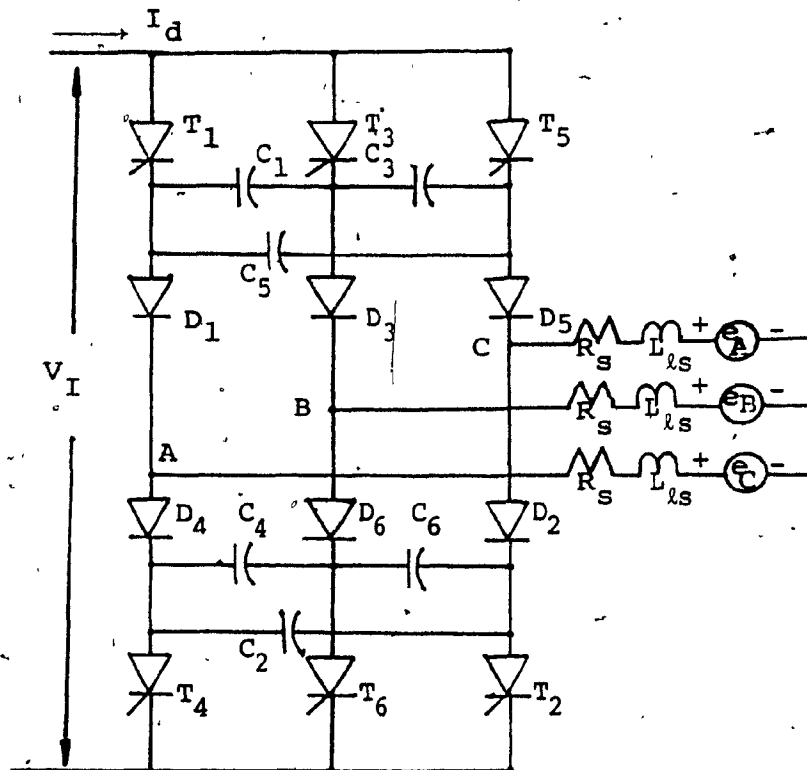charging and transfer time constitutes the commutation

Figure 7.7   Current Source Inverter with Motor Load

time. This is the time delay involved between the frequency
change request and the actual change of frequency. The
transfer time is constant whereas the charging time is both
load and frequency dependent [75]. The simulation of the
drive model is concerned with the ideal 120 degrees rectan-
gular current waveforms and hence the transfer time is also
included in the commutation delay time. Because of this,
the results of stability studies will be conservative.

·Around a steady-state operating point, the commutation
time is calulcated either numerically, solving the system
transcendental equations of the CSIM drive [75], [76], or
using the simplified expression given in [75]. The maxi-
mum error involved in using the simplified expression is
less than 2% in comparison with the rigorous solution [75].
This expression for commutation delay time is given below:

$$T_d = 5.73 \omega_e L_b C + \sqrt{3 L_\ell C} \cdot (1 + \pi/2) \qquad (7.30)$$

where

$$T_d = \text{commutation delay time}$$

$$L_b = \frac{(\frac{R_r}{\omega_{s\ell}})^2 (L_m - L_{\ell r}) - L_{\ell r}^2 (L_m + L_{\ell r})}{(\frac{R_r}{\omega_{s\ell}})^2 + (L_m + L_{\ell r})^2} \qquad (7.31)$$

$$L = L_{\ell s} + L_{\ell r}$$

$$\omega_e = \text{stator frequency, rad/sec}$$

$$\omega_{s\ell} = \text{slip frequency, rad/sec}$$

$$C = \text{commutation capacitance, Farads}$$

## 7.5.2  Modelling of commutation delay

Commutation effects have been incorporated into an analog computer simulation of CSIM drives [36] and a simplified representation of the drive in average values has been formulated [37]. In the past it has been reported that the commutation has no effect on drive dynamic performance. But in the light of [75], [76] this conclusion seems to be highly improbable. A common aspect of these studies is that they are useful in analysis. When it is desired to include the commutation delay in the synthesis of CSIM drives via the frequency domain approach, no ready made model is available.

Delay time is modelled as a transfer function of the form $e^{-T_d s}$ where $T_d$ is the delay time in control systems [77]. Since this transfer function is irrational, it is not possible to incorporate this directly into the linearised system equations. Hence a suitable linearised approximation has to be found for this transfer function.

It is known that when the commutation delay time corresponding to a commutation angle of 120 electrical degrees is exceeded, then it is impossible to recover the inverter to normal operation. Therefore for a very good design, the maximum commutation angle is assumed to be 120 electrical degrees. Then the guiding factor in modelling of commutation delay is this constraint put on engineering practice.

The closest approximation to the original transfer function $e^{-T_d s}$ is the second order Pade approximation [78] and is given by

$$e^{-T_d s} \simeq \frac{12 - 6T_d s + T_d^2 s^2}{12 + 6T_d s + T_d^2 s^2} \qquad (7.32)$$

It is found that the second-order Pade approximation follows the original transfer function in phase till 120 electrical degrees with a maximum of 2% error, and in gain with no error at all. Table 7.1 shows the comparison of the first and second-order Pade approximations with the original transfer function.

The commutation delay model with its limitation is still the better alternative to the actual model in the sense that:

(i) Minimum complexity is involved

(ii) Time-hallowed frequency domain techniques are used when this model is incorporated in the design of CSIM drives.

### 7.5.3  Design of frequency compensator

The frequency compensator supplies an incremental frequency at the time of load torque disturbance and reference frequency change. Its output is proportional to the rate of change of torque angle. In the angle controlled scheme, the torque angle is not measured. Therefore,

## Table 7.1

Comparison of first and second-order Pade

approximations with the original function

| $\omega T_d$, rad. | Original Phase, deg. | First Order Pade | Second Order Pade | % error First-order Pade | % error Second-order Pade |
|---|---|---|---|---|---|
| 1 | -57.29 | -53.13 | -57.22 | 7.26 | 0.12 |
| 1.5 | -85.94 | -73.73 | -85.41 | 14.20 | 0.61 |
| 2.0 | -114.6 | -90.00 | -112.6 | 21.45 | 1.72 |
| 2.0943 | -120.0 | -92.63 | -117.5 | 22.80 | 3.02 |

the torque angle change is to be reconstructed from other available measurements. One such variable normally available is the torque reference signal generated through the slip speed. The torque angle change can be written in terms of the other variables:

$$\frac{d\theta}{dt} = (\frac{d\theta}{ds_s}) \cdot (\frac{ds_s}{dt}) \tag{7.33}$$

where

$$s_s = \text{slip speed, rad/sec}$$

The relationship between the torque angle and slip speed is fixed regardless of the magnitude of current for a particular value of rotor resistance. The value of the rotor resistance used is that at the average operating temperature. Writing,

$$\frac{d\theta}{dt} = K(s_s) \cdot \frac{ds_s}{dt} \tag{7.34}$$

where

$$K(s_s) = \frac{d\theta}{ds_s} \tag{7.35}$$

$K(s_s)$ vs $s_s$ can be programmed in the form of function generator or in the read only memory of the digital circuit. For the drive given in Appendix III, the value of the $K(s_s)$ varies by 8 times within zero to full-load torque region, as seen from the Table 7.2.

## Table 7.2

Slip speed vs $K(s_s)$

| Slip-speed rpm | $K(s_s)$ |
|---|---|
| 1.0 | 8.399 |
| 3.0 | 7.297 |
| 5.0 | 5.551 |
| 7.0 | 3.982 |
| 9.0 | 2.819 |
| 11.0 | 2.006 |
| 13.0 | 1.440 |
| 15.0 | 1.040 |
| 17.0 | 0.752 |
| 19.0 | 0.539 |

To compute equation (7.34), the rest that is needed is to compute the time derivative of slip speed. The realization of the rate of change of torque angle is given in Figure 7.8.

The gain $K_a$ in the time derivative loop is used to offset the effect of inverter commutation delay, $T_d$. Keeping,

$$K_a \; \alpha \; \overset{o}{T_d} \qquad\qquad (7.36)$$

gives a flexibility to assign the desired level of compensation for the commutation delay. $T_d$ from equation (7.30) is seen to be the sum of a constant term and a variable term. The variable term is proportional to the product of load dependent $L_b$ and the stator frequency $\omega_e$. The realization of $T_d$ is shown in Figure 7.9. $L_b$ vs $s_s$ can be programmed in a read only memory or obtained through a function generator. The relevant information is shown in Table 7.3. Then the final step is to incorporate the computed gain $K_a$ into Figure 7.8 to evaluate the rate of change of torque angle. It is given in the Figure 7.10.

Both $K(s_s)$ and $L_b$ are dependent upon the rotor resitance, which is quite sensitive to temperature variation. To account for rotor resistance sensitivity, parameter adaption scheme [65] may be used to estimate the rotor time constant. Then the estimated value can be

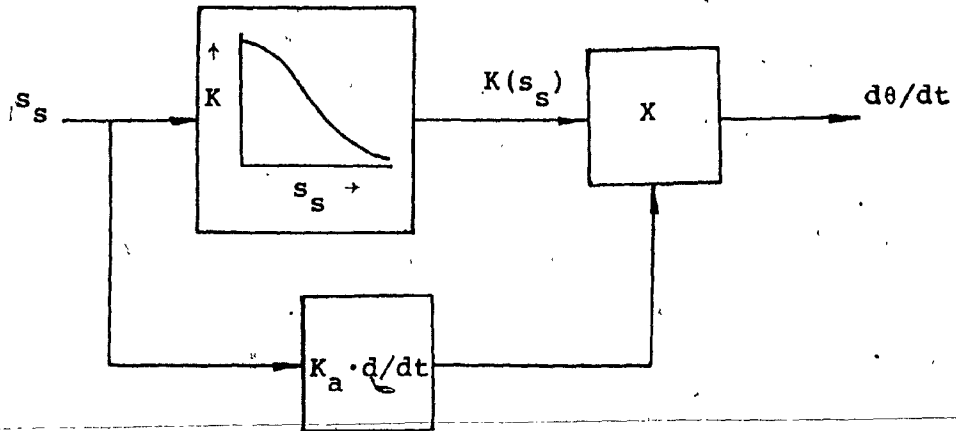Figure 7.8   Realization of Rate of Change of Torque Angle
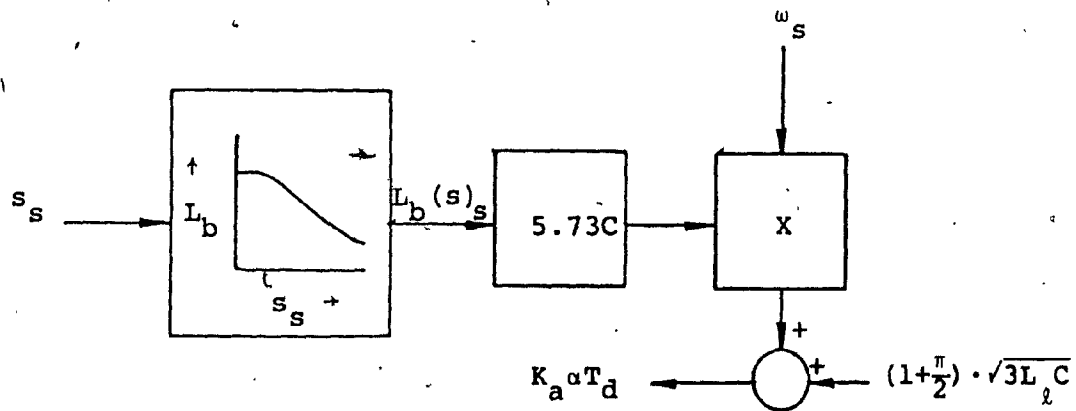


Figure 7.9   Realization of Time Delay

## Table 7.3

Slip speed vs $L_b$

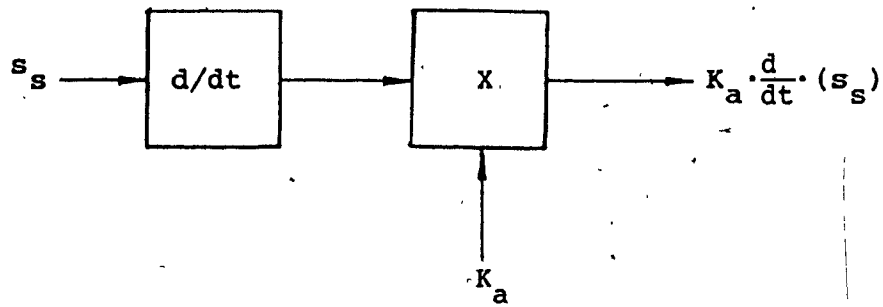| Slip-speed, rpm | $L_b$, Henry |
|---|---|
| 1.0 | 0.047 |
| 3.0 | 0.039 |
| 5.0 | 0.030 |
| 7.0 | 0.022 |
| 9.0 | 0.017 |
| 11.0 | 0.013 |
| 13.0 | 0.010 |
| 15.0 | 0.008 |
| 17.0 | 0.006 |
| 19.0 | 0.005 |

Figure 7.10   Incorporation of   $K_a$   in the slip speed
Derivative Loop.

employed to modify both $K(s_s)$ and $L_b$.

### 7.5.4 Design of speed controller

With the design of current controller, current reference controller, slip speed controller and frequency compensator completed, the remaining things to be considered are the design of the speed controller and the unity speed feedback loop. In the unity speed loop, the filter is to be carefully chosen with a view to minimise the time delay and as well as to keep the ripple in the tacho-generator feedback to an acceptable level.

The speed controller, $G_1$, is designed by obtaining the open-loop transfer function between $y_1$ and $y_6$ and using the Bode-plot, the values of the controller gain and time constants are evaluated. This approach takes into account both the frequency control channel and current channel effect, in contrast to simplified design method [79].

### 7.5.5 Effect of commutation delay on drive dynamics

To assess the drive dynamics, the drive shown in Figure 2.2 is modelled on the lines of [52]. The transfer functions of the control blocks are given in Appendix V. The drive equations are written in the state-space form of

$$\underline{\dot{X}} = A\underline{X} + B\underline{U} \qquad\qquad (7.37)$$

where  A  and  $'B$  are implied by context.  If the desired output is expressed as

$$y = C\underline{X} + D\underline{U} \qquad\qquad (7.38)$$

then

$$y(s) = [C(sI-A)^{-1}B+D]\ u(s) \qquad\qquad (7.39)$$

For a specific input and output, the Bode plot can be generated by substituting

$$s = j\omega \qquad\qquad (7.40)$$

in equation (7.39) and varying  $\omega$  over the required range.

For illustration, the operating point considered is for rated current, 0.97 p.u. torque and rated stator frequency.  A lead-lag compensator is chosen with break frequencies  of 0.175 and 100 rad/sec for the zero and pole. The closed-loop frequency response of speed-input reference without commutation delay in the drive model and with commutation delay is shown in Figures 7.11 and 7.12 respectively.  The model with commutation delay indicates the occurrence of instability with increasing gain and also a reduction in bandwidth of ten percent over that without

Figure 7.11  Closed-Loop Speed-Input Reference Frequency Response
(No Commutation Delay)
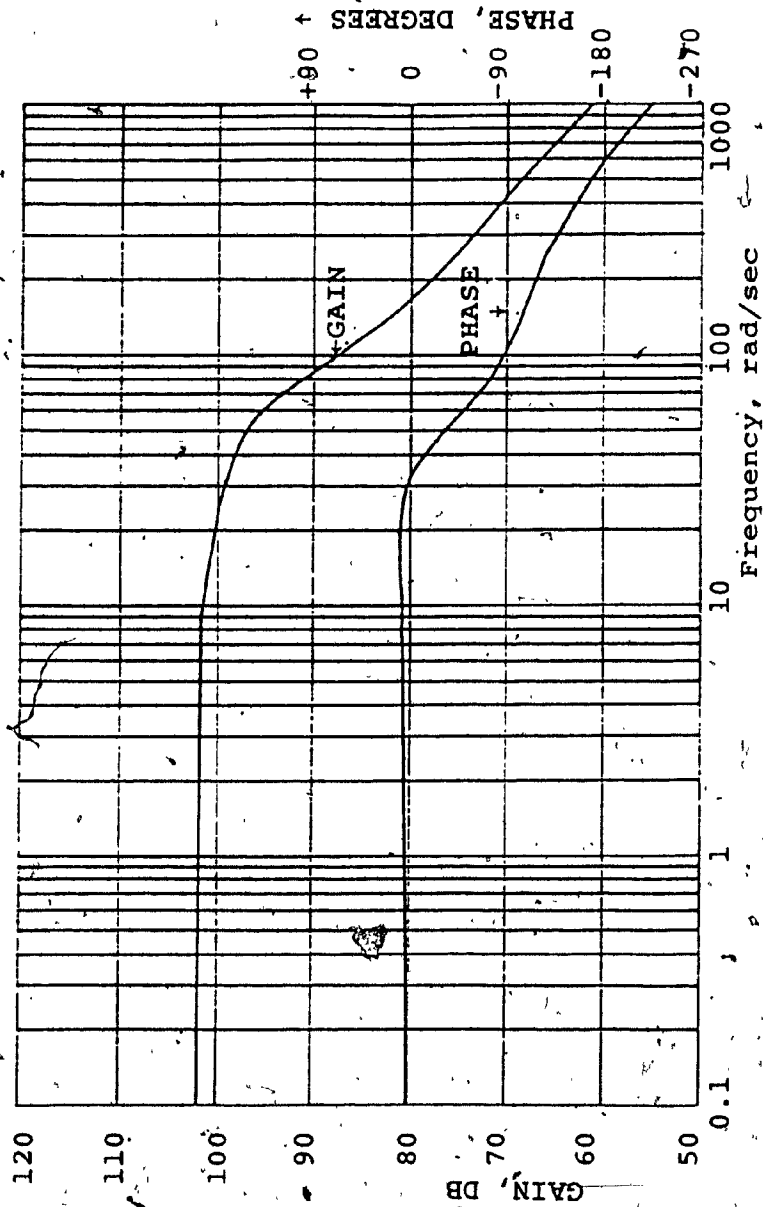
Figure 7.12   Closed-Loop Speed-Input Reference Response
(with Commutation Delay)

commutation delay. This points out the necessity for exhaustive modelling of the drive to assess dynamic performance both in terms of response and stability.
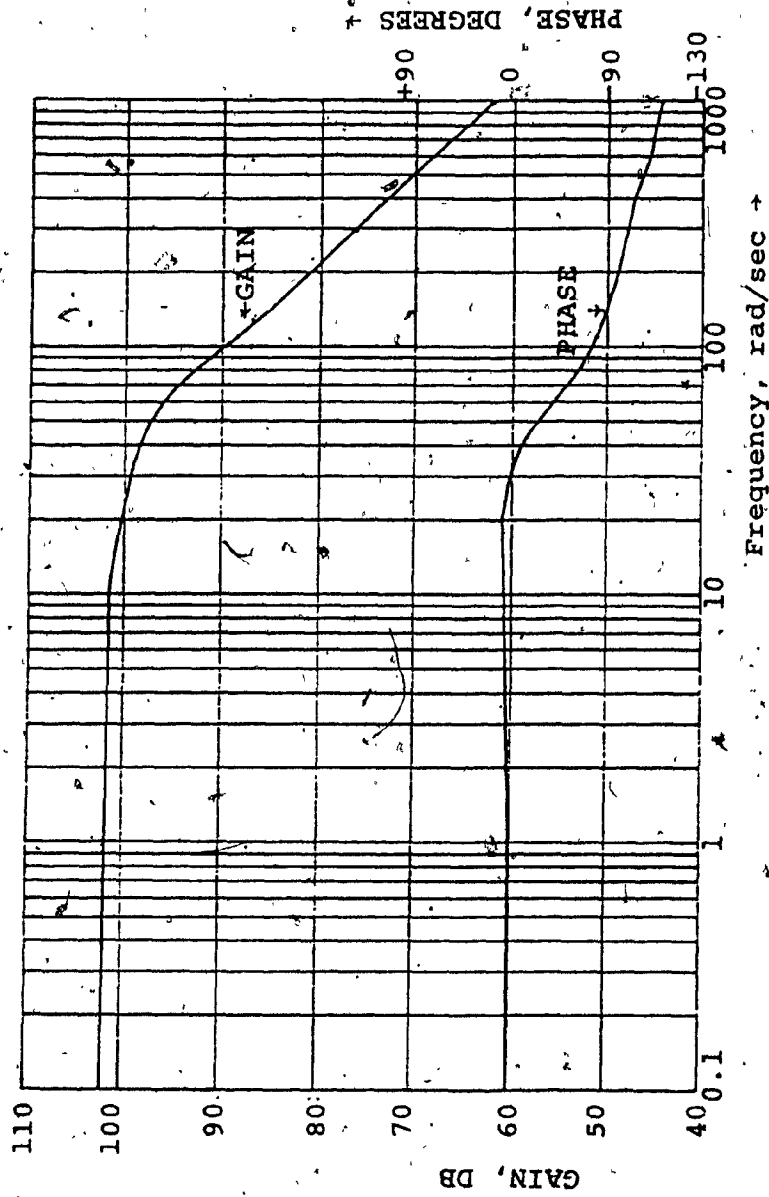
The drive data given in Appendix III, representing a typical CSIM drive, is used to illustrate the design procedure.

## 7.6 Experimental Results

The data of the experimental CSIM drive is given in Appendix VI. It is noted that the experimental machine does not represent a typical CSIM drive. The machine's flux is programmed as follows:

$$
\begin{aligned}
I_m &= 0.324 \text{ p.u.} & 0<\tau<0.2 \\
&= 0.682\ I_r & 0.2\leq\tau<0.4 \\
&= 1 \text{ p.u.} & 0.4\leq\tau\leq1.5
\end{aligned}
\tag{7.41}
$$

where $\tau$ is the torque reference in p.u. For the experimental induction motor, it is found that linearization of torque reference to electromagnetic torque output cannot be implemented. It is because the value of the mutual inductance is large and hence magnetizing current is far below the value of the torque producing component of stator current. The experimental drive has the characteristics shown in Figure 7.13.

Time responses for a change in reference speed were measured using a strip chart recorder and have been
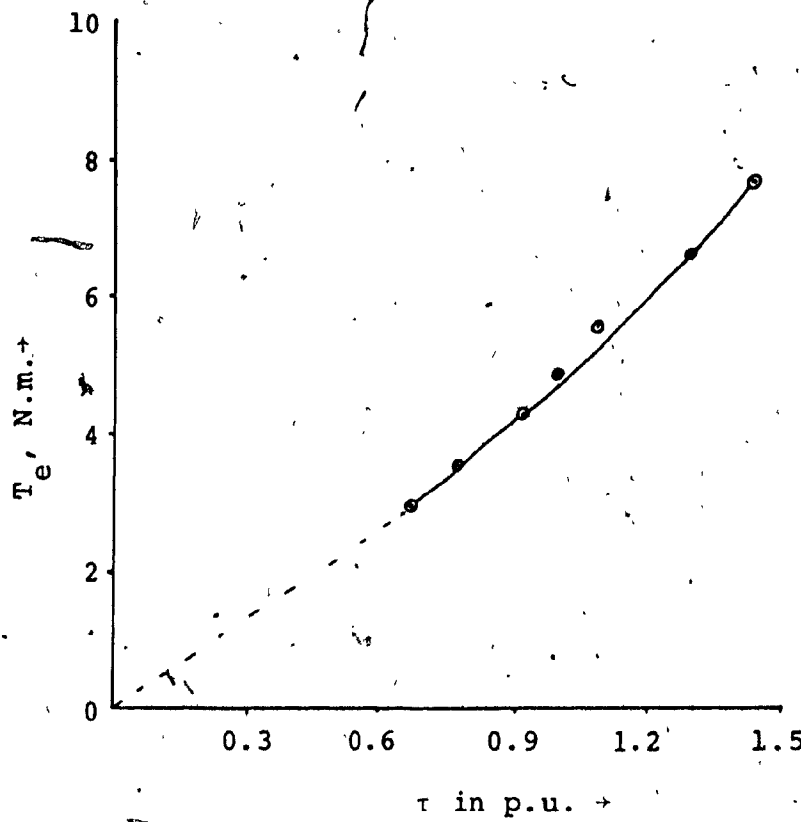
Figure 7.13

Input reference to output electromagnetic torque
relationship in the experimental drive

transcribed for clarity in Fig. 7.14. The step input of speed reference is 240 rpm and the machine is in the steady-state at 480 rpm. The load that is presently on the machine is proportional to speed. The link current reference and slip frequency command change in a very short time whereas the link current follows its reference in 25 msec. This is due to the fact that the value of link filter and the stator, leakage inductance is very high and amounts to 128 mH. Also the voltage available to force the current in the link filter is limited to 280V. The slow response in speed is the consequence of large inertia of the machine, its load, variable flux operation of the machine and the limited voltage available in the d.c. link.

The step responses for the load torque input are shown in Figure 7.15. The steady-state operating speed of the machine is 720 rpm. The magnitude of step load torque applied is 0.4 p.u., over the steady-state operating torque of 0.367 p.u. The drive operates in stable condition over its entire designed speed region of 0 to 2400 rpm.

The tuning of speed controller requires minimum effort. It is made possible due to the presence of the angle look. Experimental results corroborate this aspect in the CSIM drive.

The responses were uniform over the entire speed-torque region. Oscillatory response was not present for all possible loading conditions. The dynamic performance improved by a factor of more than six, in comparison to uncontrolled deceleration of the machine system. The removal of frequency compensator in the drive scheme led to sustained oscillations around no load operating points and oscillatory response for other operating points.
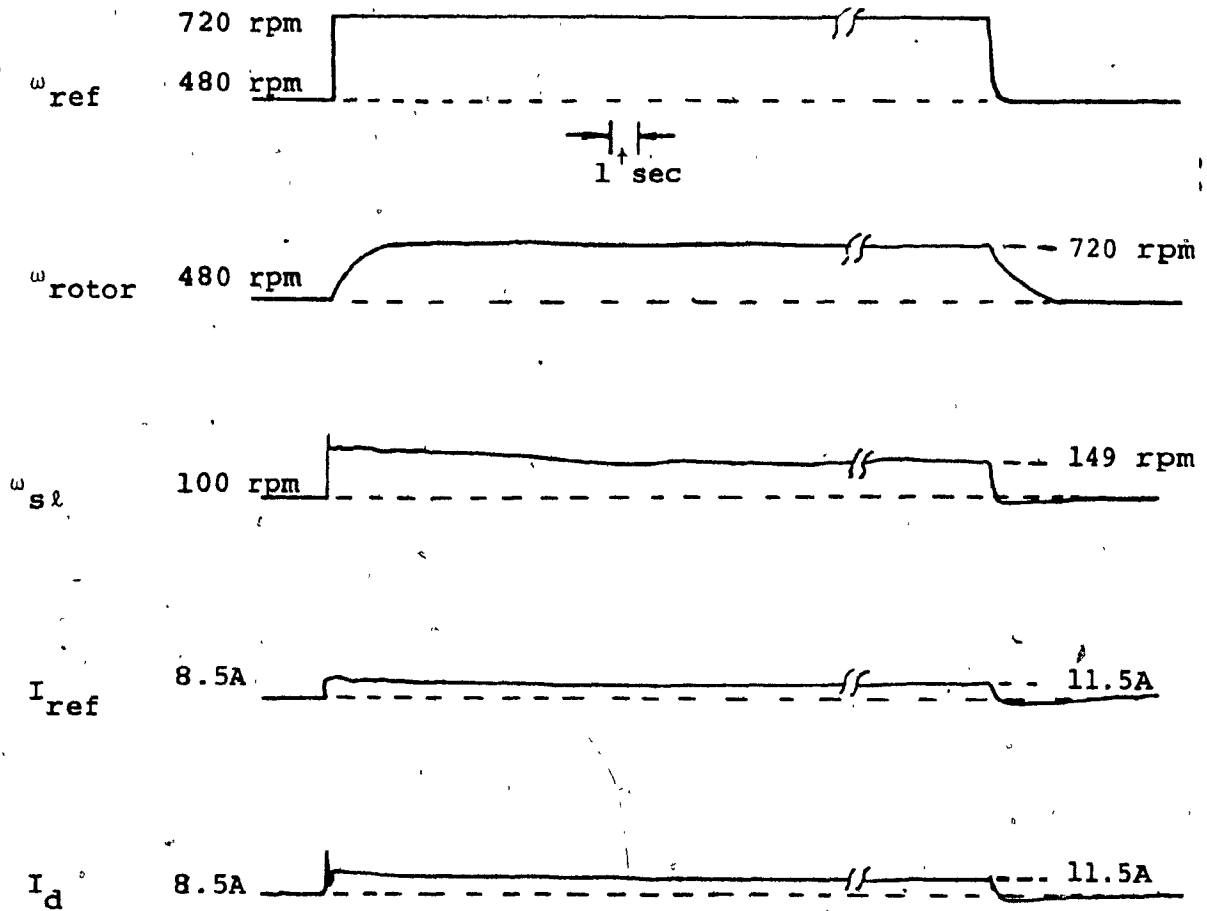
Figure 7.14

Step responses for speed reference input with
load proportional to speed
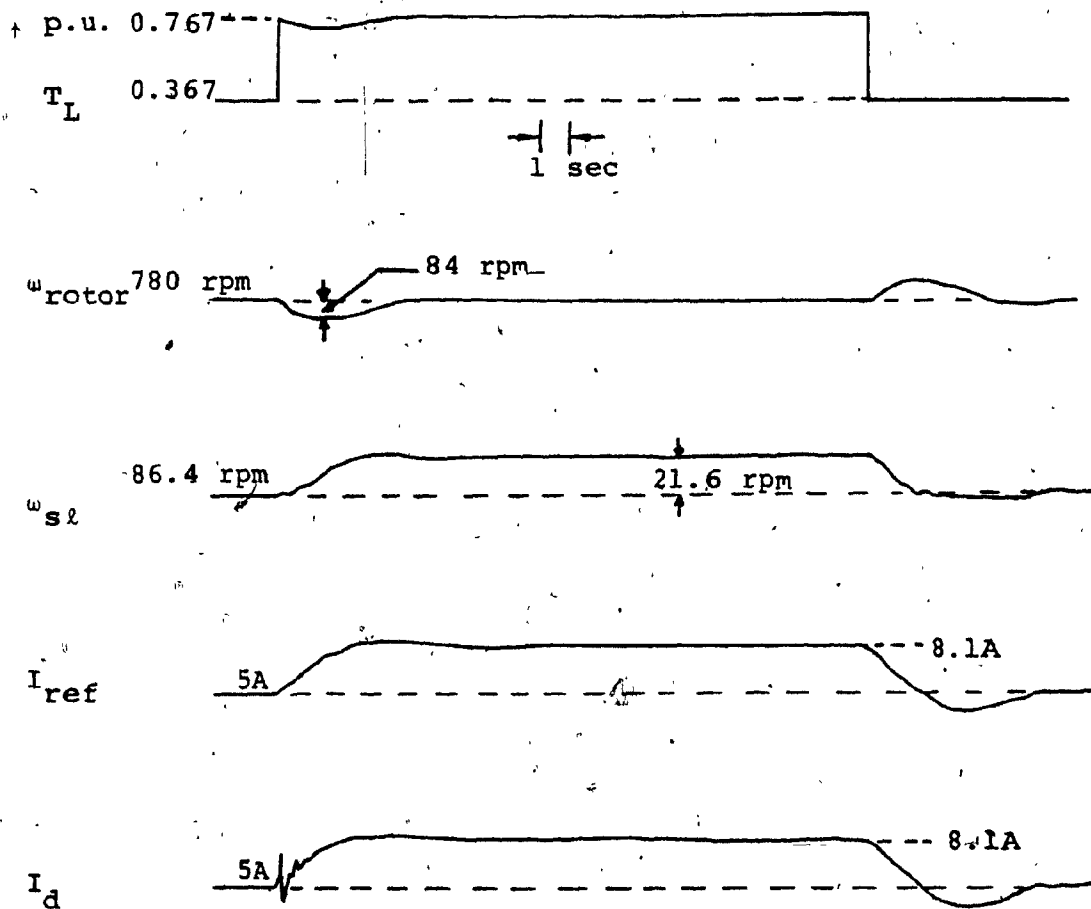
Figure 7.15

Step responses for load torque

input

CHAPTER 8

CONCLUSION

## 8.1 Conclusions

Control and dynamics of inverter-fed induction motor drives were investigated. The following conclusions resulted from the study:

(i)  The heart of all the three fast response drive strategies is the simultaneous control of torque angle and the stator current magnitude. This principle is known as 'frequency compensation'. The inner relationship of one scheme to another is evident with the understanding of this aspect.

(ii)  Incremental torque angle is a linear combination of drive electrical states only. Its feedback alone cannot stabilize a CSIM drive system. Arbitrary pole-zero assignment is possible in a drive scheme with torque angle, stator current and rotor speed feedbacks.

(iii)  The speed of the magnetizing current phasor changes with the onset of either a load torque disturbance or a change in reference frequency, even though the frequency of the stator current is maintained constant.

(iv)   A generalized control concept of electric motor
       drive classifies the drive schemes into either
       one of complete or incomplete state feedback
       categories.  The implications of each category
       are obtained from modern control theory.
       Further, the generalized control concept rela-
       tively evaluates the different drive schemes.
       The developed concept is applicable to any
       electric motor drive.

(v)    The angle control scheme has an incomplete
       state feedback whereas the synchronous and
       field-oriented control schemes have complete
       state feedback.  The consequence of this is
       that the angle control scheme is machine para-
       meter dependent and the others are not.  The
       comparison of the drive schemes has been given.

(vi)   Frequency input is superior to voltage/current
       (magnitude) input for both the steady-state
       and dynamic control of the inverter-fed induc-
       tion motor drives.

(vii)  There is no single drive variable to identify
       both the load torque disturbance and reference
       frequency change in the shortest time.  For
       load torque disturbance, rotor speed is the
       best feedback signal.  Torque angle is the
       suitable signal for reference frequency change.

For load torque change, torque angle is the
second best signal for feedback. For the CSIM
drive, rotor current magnitude can be substitu-
ted for the torque angle in a feedback without
affecting the dynamics. The link filter has
little effect on the above conclusions regard-
ing the suitability of feedback signals.

(viii) A step-by-step design of the angle controlled
CSIM drive is given. The design consists of
the following:

Inner current loop

Unity speed loop

Slip speed loop

Outer speed loop and

Frequency compensation loop

The frequency compensation loop is designed taking into
account the commutation delay of the current source inver-
ter. For the purpose of incorporating the commutation
delay in the design using frequency response methods, a
second order Pade approximation of the delay is used.
Consideration of the commutation delay indicates a 10%
reduction in bandwidth of the drive for reference frequency
change.

The design incorporates a linear relationship between
the reference input and output of electromagnetic torque
and a strategy to obtain maximum torque per ampere.

## 8.2   Recommendation for Future Work

There are two areas where further investigation may be of interest and value.  The first is the application of linear multi-variable control design techniques for non-interactive control in inverter-fed induction motor drives. The other is the implementation of optimal control of inverter-fed drives.

## APPENDIX I

### Induction Motor Equations in Synchronously Rotating Reference Frames

The pertinent differential equations of the induction motor in synchronously rotating reference and in p.u. are given below:

$$
\begin{bmatrix} V_{qs} \\ V_{ds} \\ 0 \\ 0 \end{bmatrix} =
\begin{bmatrix}
R_s + \dfrac{X_s}{\omega_b}p & \dfrac{\omega_e}{\omega_b}X_s & \dfrac{X_m}{\omega_b}p & \dfrac{\omega_e}{\omega_b}X_m \\[2ex]
\dfrac{-\omega_e}{\omega_b}X_s & R_s + \dfrac{X_s}{\omega_b}p & \dfrac{-\omega_e}{\omega_b}X_m & \dfrac{X_m}{\omega_b}p \\[2ex]
\dfrac{X_m}{\omega_b}p & \dfrac{(\omega_e - \omega_r)}{\omega_p}X_m & R_r + \dfrac{X_r}{\omega_b}p & \dfrac{(\omega_e - \omega_r)}{\omega_b}X_r \\[2ex]
\dfrac{-(\omega_e - \omega_r)}{\omega_b}X_m & \dfrac{X_m}{\omega_b}p & \dfrac{-(\omega_e - \omega_r)}{\omega_b}X_r & R_r + \dfrac{X_r}{\omega_b}p
\end{bmatrix}
\begin{bmatrix} i_{qs} \\ i_{ds} \\ i_{qr} \\ i_{dr} \end{bmatrix}
$$

$$\text{(AI.1)}$$

$$T_e = \frac{X_m}{2}(i_{qs}i_{dr} - i_{ds}i_{qr}) \tag{AI.2}$$

$$Jp\omega_r = T_e - T_L \tag{AI.3}$$

Note that the base current and base voltage are the rms values.

## APPENDIX II

### CSIM Drive Matrices

The elements of the matrices are in SI units

$$
A = \begin{bmatrix}
\dfrac{-R_o L_r}{D_a} & \dfrac{L_m R_r}{D_a} & \dfrac{-(1-s)\omega_{eo} L_m}{D_a} & \dfrac{-n L_r L_m i_{dro}}{D_a} \\[3ex]
\dfrac{M R_o}{D_a} & \dfrac{-L_o R_r}{D_a} & \dfrac{\omega_{eo}(L_m^2 - s L_r L_o)}{D_a} & \dfrac{n L_r L_o i_{dro}}{D_a} \\[3ex]
\dfrac{s\omega_{eo} L_m}{L_r} & s\omega_{eo} & \dfrac{-R_r}{L_r} & \dfrac{-n}{L_r}(L_m i_{qso} + L_r i_{qro}) \\[3ex]
\dfrac{3}{2}\dfrac{n L_m}{J} i_{dro} & 0 & \dfrac{3}{2} n L_m i_{qso} & 0
\end{bmatrix}
$$

$$\text{(AII.1)}$$

$$
B = \begin{bmatrix}
\dfrac{L_r}{D_a} & 0 \\[3ex]
\dfrac{-L_m}{D_a} & -i_{dro} \\[3ex]
0 & \dfrac{(L_m i_{qso} + L_r i_{qro})}{L_r} \\[3ex]
0 & 0
\end{bmatrix}
$$

$$\text{(AII.2)}$$

Where

$$D_a = L_o L_r - L_m^2 \qquad\qquad (AII.3)$$

$$L_o = L_s + (\frac{\Pi^2}{18}) L_F \qquad\qquad (AII.4)$$

$$R_o = R_s + (\frac{\Pi^2}{18}) R_F \qquad\qquad (AII.5)$$

## APPENDIX III

CSIM Drive Parameters

MACHINE DETAILS

30 H.P., 460V, 3-ph, $\lambda$-connected

Base Quantities: 460V, 22.38 kW

| SI Units | p.u. |
|---|---|
| $R_s$ = 0.189 Ohm | $R_s$ = 0.0199 |
| $R_r$ = 0.106 Ohm | $R_r$ = 0.0112 |
| $n$ = 3 | |
| $f$ = 0.0145 N-m sec/rad | $H$ = 0.2367 |
| $J$ = 0.6709 Kgm.m | $X_s$ = 2.054 |
| $L_s$ = 0.05151 Henry | $X_r$ = 2.088 |
| $L_r$ = 0.05155 Henry | $X_m$ = 1.987 |
| $L_m$ = 0.04983 Henry | |

FILTER DATA

| | |
|---|---|
| $R_F$ = 0.05218 Ohm | $R_F$ = 0.0055 |
| $L_F$ = 0.029 Henry | $L_F$ = 1.156 |

## APPENDIX IV

### Computation of Transfer Functions and Time Responses
### Computation of Transfer Functions

The transfer function between an output and input of voltage/current, stator frequency or load torque can be obtained on the lines of [73]. The steps involved are briefly given below:

$$\dot{\underline{X}} = A\underline{X} + B\underline{U} \qquad \text{(AIV.1)}$$

$$\underline{y} = C\underline{X} + D\underline{U} \qquad \text{(AIV.2)}$$

where $y$ denotes the output, and A,B,C and D are matrices of appropriate dimensions, then

$$y(s) = [C(sI - A)^{-1}B + D]\underline{u}(s) \qquad \text{(AIV.3)}$$

where I is the identity matrix of pertinent dimensions. Computation of equation (AIV.3) is described in [73],[74].

### Computation of Time Response

Substituting $\underline{X} = P\underline{Z}$ in equation (AIV.1),

$$P\dot{\underline{Z}} = AP\underline{Z} + B\underline{U} \qquad \text{(AIV.4)}$$

$$\dot{\underline{Z}} = P^{-1}AP\underline{Z} + P^{-1}B\underline{U}$$

$$= M\dot{\underline{Z}} + H\underline{U} \qquad \text{(AIV.5)}$$

where M is a diagonal matrix with distinct eigenvalues and

$$M = P^{-1}AP \qquad\qquad \text{(AIV.6)}$$

$$H = P^{-1}B$$

solving for $z_1, z_2, \ldots, z_q$ from equation (AIV.5),

$$z_n(t) = (\sum_{j=1}^{m} H_{nj} U_j)(-1.+\exp(\lambda_n))/\lambda_n \qquad \text{(AIV.7)}$$

where $\lambda_n$ is the nth eigenvalue and $m$ is the number of inputs. Once vector Z is evaluated by equation (AIV.7), the output y is obtained from equation (AIV.8).

$$y = C\underline{X} + D\underline{U} \qquad\qquad \text{(AIV.8)}$$

$$= CP\underline{Z} + D\underline{U}$$

## APPENDIX V

### Transfer Functions of the Controllers in the Angle Controlled CSIM Drive

$$G_1(s) = \frac{K_1}{s} (1+T_1 s)$$

$$G_2(s) = K_2$$

$$G_3(s) = \frac{K_c(1+T_c s)}{s}$$

$$G_5(s) = K_5$$

$G_6(s)$ = Transfer function of frequency compensator discussed in the section 7.5.3.

$$G_7(s) = K_7$$

$$G_D(s) = \frac{12-6T_d s+T_d^2 s^2}{12+6T_d s+T_d^2 s^2}$$

$$G_{10}(s) = K_{10}$$

$$G_{11}(s) = \frac{K_{11}}{1+T_{11}s}$$

$$G_{12}(s) = K_{12}$$

$$H_1(s) = K_{H1}$$

$$H_2(s) = K_{H2}$$

## APPENDIX VI

EXPERIMENTAL CSIM DRIVE PARAMETERS

240V, 4H.P., 3-ph, $\Delta$-connected semi-squirrel cage rotor

| | |
|---|---|
| $R_s$ = 1.85 ohms | $K_R$ = 56.16 |
| $R_r$ = 2.128 ohms | $K_C$ = 10 |
| $n$ = 1 | $K_1$ = 1 |
| $L_{\ell r}$ = $L_{\ell s}$ = 9.104 mH | $K_{10}$ = 1 |
| $R_m$ = 9569.38 ohms | $K_{11}$ = 1 |
| $J$ = 0.1546 kg.m$^2$ | $K_{12}$ = 0.004 |
| $R_F$ = 0.4 ohm | $K_{H1}$ = 0.7235 |
| $L_F$ = 120 mH | $K_{H2}$ = 1 |
| $L_m$ = 637.9 mH | $T_1$ = 1 |
| $C$ = 30 $\mu$F | $T_C$ = 0.0312 |
| | $T_{11}$ = 0.023 |

Machine parameters were measured with 60Hz sinusoidal supply.

# REFERENCES

1. D.A. Paice, "Induction Motor Speed Control by Stator Voltage Control", IEEE Transactions on Power Apparatus and Systems, Vol. PAS-87, pp. 585-590, Feb. 1968.

2. T.A. Lipo, "The Analysis of Induction Motors with Voltage Control by Symmetrically Triggered Thyristors", IEEE Transactions on Power Apparatus and Systems, Vol. PAS-89, pp. 558-596, May 1969.

3. M.S. Erlicki, J. Ben Uri and Y. Wallach, "Switching Drive of Induction Motors", Proceedings of Institution of Electrical Engineers (London), Vol. 110, No. 8, pp. 1441-1450, Aug. 1963.

4. P.C. Sen and K.H.J. Ma, "Rotor Chopper Control for Induction Motor Drive: TRC Strategy", IEEE Transactions on Industry Applications, Vol. IA-11, No. 1, pp. 43-49 Jan./Feb. 1975.

5. A. Lavi and R.J. Polge, "Induction Motor Speed Control with Static Inverter in the Rotor", IEEE Transactions on Power Apparatus and Systems, Vol. PAS-85, pp. 76-84, Jan. 1966.

6. D.A. Paice, "Speed Control of Large Induction Motors by Thyristor Converters", IEEE Transactions on Industry and General Applications, Vol. IGA-5, pp. 545-551, Sept./Oct. 1969.

7.   D.A. Bradley, C.D. Clarke, R.M. Davis and D.A. Jones,
     "Adjustable Frequency Inverters and Their Application
     to Variable Speed Drives", Proceedings of Institution
     of Electrical Engineers (London), Vol. 111, No. 11,
     pp. 1833-1846, Nov. 1964.

8.   A.H. Mittag, "Electric Valve Converting Apparatus",
     U.S. Patent 1,946,292., 1934.

9.   F. Harashima and K. Uchida, "Analysis of Inverter
     Induction Motor System by State Transition Method",
     Electrical Engineering in Japan, Vol. 89, No. 12,
     pp. 27-34, 1969.

10.  W. Charlton, "Matrix Method for the Steady-State
     Analysis of Inverter-Fed Induction Motors", Proceed-
     ings of Institution of Electrical Engineers (London),
     Vol. 120, No. 3, pp. 363-364, March 1973.

11.  W. Charlton, "Matrix-Approach to Steady-State Analysis
     of Inverter-Fed Induction Motors", Electronics Letters,
     No. 6, pp. 451-452, 1970.

12.  T.A. Lipo and F.G. Turnbull, "Analysis and Comparison
     of Two Types of Square Wave Inverter Drives", Conf.
     Record, IEEE-IAS Annual Meeting, Philadelphia,
     pp. 127-136, Oct. 1972.

13.  R. Magureanu, "A State Variable Analysis of Inverter-
     Fed A.C. Machines", Rev. Roum. Sci. Techn.-Electrotechn
     et. Energ., Vol. 18, No. 4, pp. 663-678, Bucarest,
     1973.

14. D.W Novotny; "Switching Function Representation of Polyphase Invertors", Conf. Record, IEEE-IAS Annual Meeting, pp. 823-831, Oct. 1975.

15. D.W. Novotny, "Steady-State Performance of Inverter Fed Induction Machines by Means of Time Domain Complex Variables", IEEE Transactions on Power Apparatus and Systems, Vol. PAS-95, No. 3, pp. 927-935, May/June 1976.

16. J. Lessene and F. Notelet, "Simplification by use of Ku's transformation, of the Analytical Study of an Asynchronous Motor Fed by Stepped Voltages", Proceedings of Institution of Electrical Engineers (London), Vol. 124, No. 6, pp. 554-556, June 1977.

17. M. Ramamoorty and M.F. Samek (Correspondence), "Matrix Method for the Steady-State Analysis of Inverter-Fed Induction Motors", Proceedings of Institution of Electrical Engineers (London), Vol. 120, No. 9, pp. 1015-1016, Sept. 1973.

18. M. Ramamoorty, "Steady-State Analysis of Inverter Driven Induction Motor Having Harmonic Equivalent Circuits", Conf. Record, IEEE-IAS Annual Meeting, pp. 437-440, Oct. 1973.

19. F. Blaschke, H. Ripperger and H. Steinkonig, "Regelung umrichtergespeister Asynchronmaschinen mit eingepragtem Standerstrom", Siemens-Zeitschrift, Vol. 42, No. 9, pp. 773-777, Aug. 1968.

20. L.D. Beer, "Static Induction Motor Drive: An Ideal Drive for the Paper Industry", Conf. Record, IEEE-Puls and Paper Conference, Georgia, pp. 35-40, April 21, 1971.

21. R.B. Maag, "Characteristics and Application of Current Source/Slip Regulated AC Induction Motor Drives", Conf. Record, IEEE-IGA Annual Meeting, Cleveland, pp. 411-416, Oct. 1971.

22. K.P. Phillips, "Current Source Converter for AC Motor Drives", IEEE Transactions on Industry Applications, Vol. IA-8, No. 6, pp. 679-683, Nov./Dec. 1972.

23. W. Farrer and D. Miskin, "Quasi-Sine Wave Fully Regenerative Inverter", Proceedings of Institution of Electrical Engineers (London), Vol. 120, No. 9, pp. 969-976, Sept. 1973.

24. T.A. Lipo, "State Variable Steady-State Analysis of a Controlled Current Induction Motor Drive", IEEE Transactions on Industry Applications, Vol. IA-11, pp. 704-712, Nov./Dec. 1975.

25. V. Subrahmanyam, D. Subbarayadu and M.V.C. Rao, "On the Utility of Signal Flow Graphs in the Analysis of Current Controlled Induction Motor", Proceedings of the Second IFAC Symposium, Dusseldorf, FRG, pp. 455-462, Oct. 1977.

26. PH.. Lataire, G. Maggetto, D. Van Goethem and J. Wambacq, "Analysis and Simulation of the Working of a Current-Fed Induction Motor Drive Using

Symmetrical Components of Instantaneous Potentials and Currents", Conf. Record, IEEE-IAS Annual Meeting, pp. 844-852, Oct. 1978.

27.  G.C. Jain, "The Effect of Voltage Waveshape on the Performance of a 3-Phase Induction Motor", IEEE Transactions on Power Apparatus and Systems, Vol. PAS-83, pp. 561-566, June 1964.

28.  E.A. Klingshirn and H.E. Jordan, "Polyphase Induction Motor Performance and Losses on Nonsinusoidal Voltage. Source", IEEE Transactions on Power Apparatus and Systems, Vol. PAS-87, pp. 624-631, March 1968.

29.  V.B. Honsinger, "Induction Motor Operating From Inverters", Conf. Record, IEEE-IAS Annual Meeting, Cincinnati, pp. 1276-1285, Oct. 1980.

30.  K. Venkatesan and J.F. Lindsay, "Comparative Study of the Losses in Voltage and Current Source Inverter Fed Induction Motors", Conf. Record, IEEE-IAS Annual Meeting, Philadelphia, pp. 644-649, Oct. 1981.

31.  M. Abbas and D.W. Novotny, "Stator Referred Equivalent Circuits for Inverter Driven Electric Machines", Conf. Record, IEEE-IAS Annual Meeting, pp. 828-835, Oct. 1978.

32.  P.C. Krause and T.A. Lipo, "Analysis and Simplified Representations of a Rectifier-Inverter Induction Motor Drive", IEEE Transactions on Power Apparatus and Systems, Vol. PAS-88, No. 5, pp. 588-596, May 1969.

33. P.C. Krause and L.T. Woloszyk, "Comparison of Computer and Test Results of a Static AC Drive System", IEEE Transactions on Industry and General Applications, Vol. IGA-4, pp. 583-588, Nov./Dec. 1968.

34. P.C. Krause and J.R. Hake, "Method of Multiple Reference Frames Applied to the Analysis of a Rectifier-Inverter Induction Motor Drive", IEEE Transactions on Power Apparatus and Systems", Vol. PAS-88, No. 11, pp. 1635-1641, Nov. 1969.

35. E.P. Cornell and T.A. Lipo, "Modeling and Design of Controlled Current Induction Motor Drive Systems", Conf. Record, IEEE-IAS Annual Meeting, pp. 612-620, Oct. 1975.

36. T.A. Lipo, "Simulation of a Current Source Inverter Drive", IEEE Transactions on Industrial Electronics and Control Instrumentation, Vol. IECI-26, No. 2, pp. 98-103, May 1979.

37. S.S. Abd-el-Hamid and D.P. Carroll, "Analysis and Simplified Representation of a Current Source Inverter-Induction Motor Drive", IEEE Transactions on, Industrial Electronics and Control Instrumentation, Vol. IECI-27, No. 4, pp. 284-290, Nov. 1980.

38. T.A. Lipo, P.C. Krause and H.E. Jordan, "Harmonic Torque and Speed Pulsations in a Rectifier-Inverter Induction Motor Drive", IEEE Transactions on Power Apparatus and Systems, Vol. PAS-88, No. 5,

pp. 579-587, May 1969.

39. S.D.T. Robertson and K.M. Hebbar, "Torque Pulsations in Induction Motors With Inverter Drives", IEEE Transactions on Industry General Applications, Vol. IGA-7, pp. 318-323, March/April 1971.

40. T.V. Avadhanlu and R.B. Saxena, "Torque Pulsation Minimization in a Variable Speed Inverter-Fed Induction Motor Drive System", IEEE Transactions on Power Apparatus and Systems, Vol. PAS-98, No. 1, pp. 13-18, Jan./Feb. 1979.

41. T.H. Chin and H. Tomita, "Analysis of Torque Behaviour of Squirrel Cage Induction Motors Driven by Controlled Current Inverter and Evaluation Method for Torque Ripple", Electrical Engineering in Japan, Vol. 97, No. 6, pp. 127-133, 1977.

42. T.H. Chin and H. Tomita, "The Principles of Eliminating Pulsating Torque in Current Source Inverter-Induction Motor Systems", Conf. Record, IEEE-IAS Annual Meeting, pp. 910-917, Oct. 1978.

43. J. Zubek, "Evaluation of Techniques for Reducing Shaft Cogging in Current Fed AC Drives", Conf. Record, IEEE-IAS Annual Meeting, pp. 517-524, Oct. 1978.

44. L.H. Walker and P.M. Espelage, "A High Performance Controlled Current Inverter Drive", Conf. Record, IEEE-IAS Annual Meeting, pp. 928-936, Oct. 1979.

45. W. Lineau, "Torque Oscillations in Traction Drives With Current-Fed Asynchronous Machines", Conf. Publication, IEE Conference on Electrical Variable Speed-Drives, No. 179, pp. 102-107, 1979.

46. R. Palaniappan, J. Vithayathil and S.K. Datta, "Principle of a Dual Current Source Converter for AC Motor Drives", IEEE Transactions on Industry Applications, Vol. IA-15, No. 4, pp. 445-452, July/Aug. 1979.

47. T. Nakagawa, A. Hirata, S. Saito and M. Miyazaki, "New Application of Current-Type Inverters", Conf. Record, IEEE-IAS Annual Meeting, pp. 891-896, Oct. 1980.

48. T.A. Lipo, "Analysis and Control of Torque Pulsations in Current Fed Induction Motor Drives", Conf. Record, Power Electronics Specialists Conference, pp. 89-96, 1978.

49. G.K. Creighton, "Current-Source Invertor-Fed Induction Motor Torque Pulsations", Proceedings of the IEE (London), Vol. 127, Pt.B, No. 4, pp. 231-239, July 1980.

50. T.A. Lipo, and P.C. Krause, "Stability Analysis of a Rectifier-Inverter Induction Motor Drive", IEEE Transactions on Power Apparatus and Systems, Vol. PAS-88, No. 1, pp. 55-66, Jan. 1969.

51. N. Sato, M. Ishida and N. Sawaki, "Some Characteristics of Induction Motor Driven by Current Source Inverter";

Conf. Record, IEEE-IAS International Semiconductor
Power Converter Conference, pp. 477-482, 1977.

52.  E.P. Cornell and T.A. Lipo, "Design of Controlled
Current AC Drive Systems Using Transfer Function
Techniques", Conf. Record, IFAC Symposium on Control
in Power Electronics and Electrical Drives, Dusseldorf,
Vol. I, pp. 133-147, Oct. 7-9, 1974.

53.  F. Fallside and A.T. Wortley, "Steady-State Oscillation
and Stabilization of Variable-Frequency Inverter-Fed
Induction Motor Drives", Proceedings of the IEE
(London), Vol. 116, No. 6, pp. 991-999, June 1969.

54.  E.R. Laithwaite and S.B. Kuznetsov, "Development of
an Induction Machine Commutated Thyristor Inverter
for Traction Drives", Conf. Record, IEEE-IAS Annual
Meeting, Cincinnati, pp. 580-585, Oct. 1980.

55.  B. Mokrytzki, "The Controlled Slip Static Inverter
Drive", IEEE Transactions on Industry General Applica-
tions, Vol. IGA-4, No. 3, pp. 312-317, May/June 1968.

56.  A. Schonung and H. Stemmler, "Static Frequency Chan-
gers with 'Subharmonic' Control in Conjunction with
Reversible Variable-Speed AC Drives", The Brown
Boveri Review, Vol. 51, pp. 555-577, Aug/Sept. 1964.

57.  V.R. Stefanovic, "Variable Frequency Induction Motor
Drive Dynamics", Ph.D. Thesis, McGill University,
Aug. 1975.

58. C.E. Rettig, "U.S. Patent No. 3,962,614", June 1976.

59. A.B. Plunkett, J.D. D'Atre and T.A. Lipo, "Synchronous Control of a Static AC Induction Motor Drive", Conf. Record, IEEE-IAS Annual Meeting, pp. 609-615, Oct. 1977.

60. F. Blaschke, "Das Verfahren der Feldorientierung zur Regelung der Asynchronmaschine", Siemens. Forsch.-u. Entwickl.-Ber. Bd. 1, Nr.1, pp. 184-193, 1972 (in German).

61. W. Floter and H. Ripperger, "Field Oriented Closed-Loop Control of an Induction Machine with the New TRANSVEKTOR Control System", Siemens-Z. 45, pp. 761-764, 1971.

62. W. Leonhard, "Introduction to AC Motor Control Using Field Coordinates", Conf. Record, Simposia Sulla Evoluzione Nella Dinamica Delle Machine Elettriche Rotanti, Tirrania, pp. 370-376, 1975.

63. R. Gabriel, W. Leonhard and C. Nordby, "Field Oriented Control of a Standard AC-Motor Using Microprocessors", Conf. Record, IEEE-IAS Annual Meeting, pp. 910-916, Oct. 1979.

64. K.H. Bayer and F. Blaschke, "Stability Problems with the Control of Induction Machines Using the Method of Field Orientation", Conf. Record, IFAC Symposium on Power Electronics, pp. 483-492, 1977.

65. L.J. Garces, "Parameter Adaption for the Speed Controlled Static Drive with Squirrel Cage Induction

Motor", Conf. Record, IEEE-IAS Annual Meeting, pp. 843-850, Oct. 1979.

66. M. Akamatsu, K. Ikeda, H. Tomei and S. Yano, "High Performance IM Drive by Co-ordinate Control Using a Controlled Current Inverter", Conf. Record, IEEE-IAS Annual Meeting, Philadelphia, pp. 562-571, Oct. 1981.

67. A. Nabae, K. Otsuka, H. Uchino and R. Kurosawa, "An Approach to Flux Control of Induction Motors Operated With Variable Frequency", Conf. Record, IEEE-IAS Annual Meeting, pp. 890-896, Oct. 1978.

68. C.D. Schauder and R. Caddy, "Current Control of Voltage Source Inverters for Fast Four-Quadrant Drive Performance", Conf. Record, IEEE-IAS Annual Meeting, Philadelphia, pp. 592-599, Oct. 1981.

69. R. Krishnan, W.A. Maslowski and V.R. Stefanovic, "Control Principles in Current Source Induction Motor Drives", Conf. Record, IEEE-IAS Annual Meeting, Cincinnati, pp. 605-617, Oct. 1980. (Also accepted for publication in IEEE Transactions on Industry Applications).

70. R. Krishnan, V.R. Stefanovic and J.F. Lindsay, "Control Characteristics of Inverter-Fed Induction Motor", Conf. Record, IEEE-IAS Annual Meeting, Philadelphia, pp. 548-561, Oct. 1981. (Also accepted for publication in IEEE Transactions on Industry Applications).

71. P.C. Krause and C.H. Thomas, "Simulation of Symmetrical Induction Machinery", IEEE Transactions on Power Apparatus and Systems, Vol. PAS-84, No. 11, pp. 1038-1053, Nov. 1965.

72. V.H. Quintana, M.A. Zohdy and J.H. Anderson, "On the Design of Output Feedback Excitation Controllers of Synchronous Machines", IEEE Transactions on Power Apparatus and Systems, Vol. PAS-95, No. 3, pp. 954-961, May/June 1976.

73. T.A. Lipo and A.B. Plunkett, "A New Approach to Induction Motor Transfer Functions", Conf. Record, IEEE-IAS Annual Meeting, pp. 1410-1418, Oct. 1973.

74. Myung J. Youn and Richard G. Hoft, "Variable Frequency Induction Motor Bode Diagrams", Conf. Record, IEEE-IAS-ISPC, pp. 124-136, 1977.

75. Avinash Joshi, "A.C. Traction Drives Using Current Source Inverter", Ph.D. Thesis submitted to University of Toronto, Feb. 1979.

76. M. Showleh, W.A. Maslowski and V.R. Stefanovic, "An Exact Modeling and Design of Current Source Inverters", Conf. Record, IEEE-IAS Annual Meeting, pp. 439-459, Oct. 1979.

77. R.C. Dorf, "Modern Control Systems", Second Edition, Addison-Wesley Publishing Company, Reading, Massachusetts, 1974 (Book).

78. Arthur Hausner, "Analog and Analog/Hybrid Computer Programming", Prentice-Hall, Englewood Cliffs, N.J., 1971 (Book).

79. B. Ramaswami, R. Venkataraman and J. Holtz, "Design of Variable Speed Induction Motor Drive with a Current-Fed Inverter", Electric Machines and Electromechanics, No. 5, pp. 523-542, 1980.